CHARACTERIZATION OF SMALL SCALE ROUGHNESS ELEMENTS ON A WATER SURFACE

A DISSERTATION SUBMITTED IN PARTIAL FULFILLMENT
OF THE REQUIREMENTS FOR THE DEGREE OF
DOCTOR OF PHILOSOPHY

Serhad S. Ataktürk
Department of Atmospheric Sciences AK-40
UNIVERSITY OF WASHINGTON
Seattle, WA 98195

March, 1991

TECHNICAL REPORT
NASA GRANT NAGW-1322

CHARACTERIZATION OF SMALL SCALE ROUGHNESS ELEMENTS ON A WATER SURFACE

FOREWORD

This report is the doctoral thesis of Serhad S. Ataktürk. It is one of the major accomplishments under grant NAGW-1322 to the University of Washington from the Ocean Processes Branch of the National Atmospheric and Space Administration. The objective of the work was to relate variations in atmospheric wind stress and water surface roughness characteristics to radar backscatter. The radar measurements were obtained by colleagues from the University of Kansas while we obtained measurements of the hydrodynamic properties of the water surface, the wind stress, sensible heat and water vapor fluxes and mean environmental variables. Relationships between radar backscatter, the water surface and atmospheric quantities will be published jointly with Professors P. Gogineni, R. K. Moore and their collaborators at the University of Kansas. In this thesis the air-sea interaction processes for wind speeds less than 10 m/sec are analyzed.

Two important findings of this work are that the growth parameter, α, in our water wave spectra is substantially different from α's obtained for waves on Lake Ontario and on the Sea of Bothina, which in turn differ from each other. The explanation for the differences which we believe are real (and not due to measurement errors) is not yet in hand. Explanations include effects due to differences in the configuration of the water body and stratification effects on the source function of momentum transfer to the water. The role of viscosity which depends on water temperature, the spreading of the water waves which could depend on the gustiness of the wind, and other ideas are also being considered.

Effects of sheltering in wave troughs on the transfers of scalar properties as wind speed increases had been suggested by work from our group (Liu, Katsaros and Businger, 1979: Bulk parameterization of air-sea exchanges of heat and water vapor including the molecular constraints at the interface. *J. Atmos. Sci.*, **36**, 1722-1735). This thesis shows constant exchange coefficient for heat and water vapor rather than decreasing ones for wind speeds greater than 6 ms^{-1}. Beyond this wind speed evaporation of the aerosol due to breaking waves may counteract any sheltering effects. Fluxes of water vapor and sensible heat in white cap sea states is the subject of another Ph.D. thesis from our group by J. DeCosmo (1991: *Air-Sea Exchange of Momentum, Heat and Water Vapor over Whitecap Sea States).*

Further studies of the role of slicks and wave breaking on the wave spectrum and on wind stress are possible with these data. Some of the work on slicks produced in this thesis were also reported by Katsaros, Gucinski, Ataktürk and Pincus (1988: Effects of Reduced Surface Tension on Short Waves at Low Wind Speeds in a Fresh Water Lake. In *Radar Scattering from Modulated Wind Waves,* G.J. Komen and W.A. Oost, eds.. Kluwer Academic Publications, The Netherlands, pgs. 61-74). Preliminary work on wave breaking is gathered in two reports with slightly different emphasis: *A Video-Aided Study of Sea Spikes in Radar Backscatter at Moderate Incidence,* by D.A. Bush, S.P. Gogineni, R.K. Moore, K.B. Katsaros and S.S. Ataktürk, 1991; and *Dependence of Wave Breaking Statistics on Wind Forcing,* by K.B. Katsaros and S.S. Ataktürk to be presented at IUTAM, Sydney, Australia, July 19-23, 1991.

Further measurements on the directional spread of the wind driven water waves on Lake Washington, their fetch dependence and the high wave number tail of the water wave spectrum (out to 20 m^{-1}) are being planned. Several articles based on this thesis are in preparation.

March, 1991

Kristina B. Katsaros
Principal Investigator

University of Washington

Abstract

Characterization of Roughness Elements
on a Water Surface

by Serhad S. Ataktürk

Chairperson of the Supervisory Committee: Professor Kristina B. Katsaros
Department of Atmospheric Sciences

Air–water exchanges of momentum, heat and water vapor were investigated from a tower on a fresh water lake at low to moderate wind speeds, $3 < U_{10} < 8\ m/s$. The tower is located 15 m offshore where water depth is about 4 m. For this purpose, surface fluxes were determined directly from atmospheric turbulence measurements using the eddy correlation technique and water surface elevations due to long gravity and short gravity–capillary waves were measured by a resistance wire wave gauge. The observed wave field was generated purely by the local winds over a well–defined fetch of 7 km.

Experimental results showed that for the conditions of light winds and nonneutral atmospheric stratification encountered in this study, atmospheric turbulence statistics could not provide an estimate of the surface fluxes with great accuracy. For similar environmental conditions the neutral drag coefficient, C_{DN}, and the surface roughness length parameter, z_o, determined from flux–profile relationships were found to show large scatter mainly due to the significant variations in the contribution to total covariances by the low–frequency atmospheric phenomena. However, on the average they were found to be in good agreement with other independent estimates of C_{DN} and z_o obtained from the wave measurements. The technique of determining C_{DN} and z_o from wave spectra, devised in this study, was successfully used not only during steady state but also during rapidly changing wind speed conditions. The increase in

C_{DN} with U_{10} was typical of the results from other studies conducted in the marine environment. The experimental findings indicated that $z_o \propto \zeta(U_{10}/C_p)$, where ζ is the rms wave height and C_p is the phase speed of the dominant waves.

The neutral bulk transfer coefficients and the characteristic roughness lengths for heat and water vapor were found to be independent of wind speed for the conditions observed. Their magnitudes could be approximated by constants whose values depended on the atmospheric stratification such that they were larger in the unstable regime than in the stable regime. Sudden changes in the magnitudes of these parameters in near neutral conditions could be better described by the air–water temperature difference than by the atmospheric stratification parameter, z/L. It was shown that the characteristic roughness lengths for heat and water vapor do not decrease with growing sea state due to shadowing effects in the wave troughs as suggested by Liu *et al* (1979).

The shape of the frequency spectra of the observed long gravity waves (with an average dominant wavelength of about 5 m) could be adequeately described by the model of Donelan *et al* (1985). Hence, a spectral slope of -4 is appropriate for the range $1.5 < \omega/\omega_p < 3$ where ω_p is the frequency of the dominant waves. However, the experimental results on the relationships between fetch, total wave–height variance, equilibrium range parameter and the U_{10}/C_p ratio deviated significantly from those suggested by Donelan *et al* (1985). No definite explanation could be offered but it is suspected that these deviations are due to the differences in fetch and duration between the two experiments.

Measured frequency spectra of short gravity–capillary waves (3 to 38 cm in wavelength) were corrected for the Doppler frequency shifts. For the present experimental conditions, these corrections were small. Stronger distortions in the measured spectra were caused by wave breaking events therefore, the portions of the data affected by breaking waves were excluded from the analyses. Within

the limited range of wind speeds encountered, the spectral amplitudes of these short wave were observed to increase with increasing U_{10} as expected. However, the spectral slope at the high frequency tail of the wave spectra was not well defined and it varied between -4 and -5. When the spectra were represented in a nondimensional form, these variations in the spectral slope were noted to depend on ω_p and ω/ω_p. A parameterization of this dependency requires further experimental evidence.

It was also noted that these short wave components were strongly suppressed in the presence of surface films. Such surface films were observed mostly during periods of stable stratification when intermittent nature of atmospheric turbulent transport is pronounced.

TABLE OF CONTENTS

LIST OF FIGURES

LIST OF TABLES

ACKNOWLEDGMENTS

I wish to express sincere appreciation to my advisor, Professor Kristina B. Katsaros, for her constant support, friendship and endless encouragement. Her involvement and influence in the national and international arena of air–sea interaction have greatly aided my success as a graduate student.

I acknowledge with gratitude the constructive criticisms of Professors Robert G. Fleagle and Robert A. Brown. Particular thanks are also due to other members of my supervisory committee, Professors Michael Gregg and Eric D'Asaro, for their interest in this dissertation.

Special acknowledgments are due to Drs. Gary Geernaert and Janice DeCosmo for their motivating and helpful discussions on various aspects of air–sea interaction. The research conducted by Stu Smith and Mark A. Donelan as well as their comments on this investigation have been the most useful. Particular credits for the success of the field experiments are additionally due to Dick Lind, Noel Cheney and Bob Sunderland.

During my years as a graduate student, I had great pleasure in exchanging thoughts with cooperative and friendly students, faculty and staff in the Department of Atmospheric Sciences. I learned much about remote sensing with microwave radiometers and the tricks in UNIX through conversations with my office–mates, Dr. Grant Petty and Mr. Doug Miller. Finally, I wish to thank the members of my family both in Turkey and the U.S.A. for their endless support, patience and love. In particular, I am deeply indebted to my wife, Jane J. Hunter, without whom my achievement could not have been realized.

This work was supported by the National Aeronautics and Space Administration under Grants NAGW–736 and NAGW–1322.

CHAPTER 1: INTRODUCTION

The goal of this dissertation is to advance the state of knowledge and analysis techniques for evaluating air–sea exchanges of momentum, heat and water vapor during both transitional and steady state environmental conditions. To meet this goal, the scientific objectives include characterization of the roughness elements on a water surface and assessments of the variability of the bulk transfer coefficients and of the role of surfactants in wind stress–wave interaction. In the following section, the importance of this investigation for a better understanding of the energetics of the air–sea interaction, and its relevance to various areas of research and application are described. The specific questions to be addressed in this study are stated in Section 1.2.

1.1 Water Surface Waves: Importance and Relation to Air–Sea Interaction and Microwave Remote Sensing

Dynamic processes occurring in the planetary boundary layer and the oceanic mixed layer are important to a variety of fields including climatology, weather and wave forecasting, urban planning, environmental pollution control, fisheries, agriculture, marine construction and transportation. Interaction of the atmosphere and ocean is of particular importance. For example, the wind stress acting on the sea surface disturbs the water mass by producing waves and currents; these waves and currents govern the characteristics of the surface roughness which in turn modifies the wind stress. Steady winds, even if light, are responsible for the wind-driven circulations in the oceans. Strong storms can generate large surface waves that generate turbulence when they break. Therefore, breaking waves can cause vigorous vertical mixing in both the atmosphere and the ocean. This results in transport of momentum, heat

and salt stored in the upper layer to either the lower depths or to the atmospheric boundary layer. Evaporation cools the ocean surface and the resulting upward flux of water vapor gives rise to formation of clouds and rainfall.

In the atmosphere, temperature and humidity often change rapidly with height. During unstable convective conditions, vertical motions of the warm, moist surface air can generate strong turbulence in the boundary layer. The latent heat released upon condensation of the water vapor and the sensible heat flux from the surface provide the atmosphere with internal thermal energy that is vital for formation and intensification of cyclones and thunderstorms as well as for the general atmospheric circulation.

A variety of phenomena can be best described if the atmosphere and the oceans are treated as a coupled system. Coupling occurs through the exchange of momentum, heat and matter across the air–sea interface where the atmosphere and the oceans physically interact. Since air–sea fluxes, their magnitude and variability govern the dynamics of both atmospheric and oceanic boundary layers, much can be inferred about the nature of atmospheric and oceanic phenomena from the knowledge of the exchange processes at the surface.

Surface fluxes of momentum, τ, sensible heat, H_S, and latent heat, H_L, can be directly determined by the eddy correlation technique (Busch, 1973),

$$\left.\begin{aligned} \tau &= -\rho\overline{u'w'} \\ H_S &= \rho C_p\overline{w'T'} \\ H_L &= \rho L_e\overline{w'q'} \end{aligned}\right\} \qquad (1.1.1)$$

where u', w', T' and q' are the turbulent fluctuations of horizontal and vertical components of wind, air temperature and specific humidity, respectively, ρ is the air density, C_p is the specific heat of air at constant pressure and L_e is the latent heat of evaporation; the overbars denote a space average. One often applies the ergodicity principle which assumes that stationarity is achieved over

a long enough averaging time such that the space average is equivalent to a time average.

Measurements of turbulent fluctuations require delicate instruments. Such data, particularly from the open ocean, are extremely limited. Therefore, parameterizations of surface fluxes in terms of routinely observed variables have been widely investigated (see review by Geernaert, 1990). The outcome of such efforts is the bulk aerodynamic method;

$$\left.\begin{aligned} \tau &= \rho C_D (U_{10} - U_s)^2 \\ H_S &= \rho C_p C_H (U_{10} - U_s)(T_s - T_{10}) \\ H_L &= \rho L_e C_E (U_{10} - U_s)(q_s - q_{10}), \end{aligned}\right\} \qquad (1.1.2)$$

where C_D, C_H and C_E are, respectively, the drag coefficient, Stanton number and Dalton number; the subscripts 10 and s indicate the values at a reference height of 10 m and at the surface, respectively. Over land, U_s is zero, but over the oceans, it is the along-wind component of the surface currents. Intercomparisons by Blanc (1985, 1987) of ten bulk transfer schemes using the same one–year–long data set show that differences in schemes may result in variations from 15% to 30% in the mean fluxes and the maximum variations of about 80%. Differences may get even larger at low and very high wind speeds due to the paucity of data used in determining the coefficients of a particular scheme in these ranges.

The magnitude and behavior of bulk transfer coefficients are still under investigation, but they are known to be functions of wind speed, surface roughness and atmospheric stratification. Although C_H and C_E are less well known (Smith *et al*, 1983; Smith, 1988), it has been suggested that they are similar in magnitude (Kitaigorodskii *et al*, 1973; Bunker, 1976; Masagutov, 1981) and decrease with increasing stable stratification (Deardorff, 1968; Businger *et al*, 1971; Kondo, 1975) with a slight (Liu *et al*, 1979; Wu, 1980; DeCosmo *et al*, 1988) or no dependence on wind speed (Garratt and Hyson, 1975; Friehe and

Schmitt, 1976; Hasse *et al*, 1978b; Large and Pond, 1982). On the other hand, C_D shows a clear trend of increase with wind speed (see reviews, Brown and Liu, 1982; Blanc, 1985; Huang *et al*, 1986a; Geernaert *et al*, 1986; Geernaert, 1990). Since the effect of atmospheric stratification on C_D is relatively well known (for example, Liu *et al*, 1979; Brown and Liu, 1982; Geernaert and Katsaros, 1986; Smith, 1988), the large scatter in C_D is believed to be due to the differences in sea state, i.e. surface roughness, between various experiments as well as intermittency governing the total flux during a predetermined averaging period (Kitaigorodskii, 1973; Hsu, 1974, 1986; Huang *et al*, 1981,1986a; Donelan, 1982, 1990; Graf *et al*, 1984; Geernaert *et al*, 1986).

The roughness elements of the air-sea interface are the water surface waves that may cover a broad range of wavelengths from tens of meters (long gravity waves) to fractions of a centimeter (short gravity-capillary and capillary waves). There is a strong controversy on the scales of waves that determine the sea surface roughness. Drag coefficients measured over the open oceans (Smith, 1980; Large and Pond, 1981) are lower than those over shallow or coastal waters (Garratt, 1977; Wu, 1980; Donelan, 1982; Graf *et al*, 1984; Geernaert *et al*, 1986; DeCosmo *et al*, 1988; DeCosmo, 1991). It is believed that these differences are caused by the effects on surface roughness of the long gravity waves (e.g. Donelan, 1990; Geernaert, 1990). On the other hand, when surface slicks or films are present, small scale waves are immediately suppressed due to reduced water surface tension and increased surface dilational elasticity (Hühnerfuss and Garrett, 1981; Katsaros *et al*, 1989; Wu, 1989). If the slicks cover a large area, the long gravity waves may also become subject to some damping (Hühnerfuss *et al*, 1983). This indicates a reduction in momentum flux to long waves in the absence of small scale waves (Geernaert *et al*, 1988) because, the large scale waves are governed by gravity and not surface tension (e.g. Phillips, 1977). Furthermore, drag coefficients parameterized in terms of short wave features

have been found to be good predictors of the wind stress (Kitaigorodskii, 1973; Huang *et al*, 1986a; Geernaert *et al*, 1986). These considerations have led to the formulations of a composite drag coefficient which includes the effects of both large and small scale waves (Kitaigorodskii, 1973; Donelan, 1982). The relative importance of long and short water surface waves for momentum flux from air to sea is thought to be a function of the mean wind stress itself, but the details are poorly known (e.g., Stewart, 1961; Deardorff, 1967; Dobson, 1971; Valenzuela, 1976; Plant and Wright, 1977; Snyder *et al*, 1981; Hsu *et al*, 1982; Mitsuyasu, 1985).

Recently, with the recognition of the active and passive microwave instruments as the tools of the future for remote sensing of the vast oceans (Ulaby *et al*, 1981), the issues discussed above have become the primary target of many theoreticians and experimentalists. Microwave radiometers, such as SSM/I, Special Sensor Microwave Imager (Hollinger *et al*, 1987), or SMMR, Scanning Multichannel Microwave Radiometer (Gloersen and Barath, 1977), sense the surface brightness temperature which depends on wind speed or stress through the effects of surface roughness on the emissivity and reflectivity of the sea. Microwave radars, such as SASS, Seasat A Satellite Scatterometer (Pierson, 1983), and SAR, Synthetic Aperture Radar (Alpers, 1983), operate mainly on the principle that the electromagnetic radiation with wavenumber vector $\mathbf{k}_e$ is backscattered by the surface wave component whose wavenumber, $\mathbf{k}$, satisfies the Bragg resonance condition, $\mathbf{k}_e = 2\mathbf{k}\sin\phi$, where ϕ is the angle of incidence (see Plant, 1990). The most commonly used model of sea surface backscatter is the two-scale model: the coherent backscattered power, measured in terms of normalized radar cross section σ°, is directly proportional to the wavenumber spectrum, $E(\mathbf{k})$, of the short gravity-capillary waves. The long waves are involved indirectly by tilting and shadowing parts of the surface and by modulating the short wave spectra through hydrodynamic interactions (Rice, 1951;

Wright, 1968; Bass *et al*, 1968; Brown, 1978; Wright *et al*, 1980; Ulaby *et al*, 1981; Keller *et al*, 1985). While determination of the average wind vector over the ocean with microwave radars require the absolute value of the average σ°, ocean imagery with SAR relies on the MTF, Modulation Transfer Function (Plant *et al*, 1983; Plant, 1988), which is a dimensionless complex quantity describing variation of σ° about its average along the long wave phase. Remote sensing techniques have been succesfully employed in various atmospheric and oceanic studies. However, whether the scatterometer signal should be interpreted in terms of wind speed or wind stress (see O'Brien *et al*, 1982; Brown, 1983, 1986; Pierson, 1983; Donelan and Pierson, 1984) or, whether the SAR imaging of the ocean surface is related to orbital velocities or to phase speeds of the long waves (Hasselmann and Alpers, 1986), are fundamental questions that require further clarification.

Until now, discussions of the surface roughness have focussed on random water waves. However, as wind speed increases, characterization of the sea surface is further complicated by breaking waves of different scales, such as micro–, spilling– and large–scale breaking (Weissman *et al*, 1984). Although intermittent in nature, wave breaking can have significant effects on a wide class of processes. For example, Melville *et al* (1985) have shown that during one breaking event 30% of the high-frequency energy of a wave packet can be dissipated. This energy produces the turbulent mixing of the oceanic surface layer. Studies on air flow over water waves indicate that small–scale breaking increases the local drag of the wind and enchances the local momentum flux from wind to surface waves (Banner and Melville, 1976; Banner, 1986, 1990a). Whitecapping, foam, air bubbles and spray associated with breaking waves increase with wind speed (Monahan *et al*, 1983; Ó Muircheartaigh and Monahan, 1986) and affect the heat and gas exchange between air and sea (Blanchard and Woodcock, 1957; Thorpe, 1982; Monahan and Niocaill, 1986). Microwave

radars receive strong backscattered signals from breaking waves (Banner and Fooks, 1985; Keller *et al*, 1986; Phillips, 1988) due to high levels of roughness associated with such events (Weissman *et al*, 1984; Ataktürk, 1984; Ataktürk and Katsaros, 1987). Microwave radiometers respond to surface foam through its emission effect on brightness temperature (Wisler and Hollinger, 1977). Subsurface bubble clouds require special attention in remote sensing of sea surface from below by sonars (Thorpe, 1982). Despite its importance, breaking is the least understood wave phenomenon (e.g. Longuet-Higgins and Cokelet, 1978; Melville, 1982, 1983; McLean, 1982; Su *et al*, 1982). Generally, the only quantitative information comes from the statistics established through observations of breaking events detected by some sort of threshold mechanism (for example, Snyder and Kennedy, 1983; Weissman *et al*, 1984).

This review indicates that there is a close association between air–sea interaction processes and the sea surface roughness. Water surface waves due to their role in defining the sea state, are an integral part of these processes. Advancement in this field of research requires better parameterization of the relationship between water surface waves and surface roughness. Also, proper interpretations of the signals from microwave remote sensors may be possible only after a complete theory of water waves is devised. However, despite its importance and the great deal of progress made in the last two decades, there is still much to be done to fully understand the evolution of ocean waves as revealed by the following outline of the present state of knowledge.

For deep water in the absence of currents, changes in wave spectral energy propagating with the group velocity, $\mathbf{C}_g$, can be described by the radiative energy transfer equation (Hasselmann, 1960; Willebrandt, 1975),

$$\frac{\partial E(\mathbf{k})}{\partial t} + \mathbf{C}_g \cdot \nabla E(\mathbf{k}) = I + W + D, \qquad (1.1.3)$$

where I, W and D represent input from wind, wave—wave interactions and dissipation, respectively.

Various field and laboratory experiments have been conducted to measure the growth rates of surface waves due to wind forcing (Dobson 1971; Elliott, 1972; Larson and Wright, 1975; Snyder *et al*, 1981; Mitsuyasu and Honda, 1982; Hsiao and Shemdin, 1983; Hasselmann *et al*, 1986). Theories on the initiation and growth of waves through turbulent resonance (Phillips, 1957) or shear flow instability mechanisms (Miles, 1957; Valenzuela,1976; Kawai, 1979) predict rates that are somewhat smaller than experimental findings and are therefore in need of further considerations. In addition, it is not yet clear whether wind forcing should be scaled with the friction velocity, u_*, or the wind speed at an elevation such as 10 m or at a height that is related to the length of the waves considered (Donelan and Pierson, 1987).

The nonlinear energy transfer between waves due to resonant third–order wave–wave interactions has been formulated by Hasselmann (1962). The theory has succesfully explained the growth of long gravity waves with increasing fetch. Studies have shown that this process controls the shape and rate of evolution of a wave spectrum (Mitsuyasu, 1968, 1969; Hasselmann *et al*, 1973). With recent improvements in the computational time required to evaluate the Boltzmann integrals, incorporation of nonlinear transfer in operational wave models have become feasible (Hasselmann and Hasselmann, 1985; Hasselmann *et al*, 1985). However, the overall performance of different schemes strongly depends on the assumed shape of the wave spectrum (e.g. Hasselmann *et al*, 1985).

Dissipation of wave energy occurs mainly by breaking. Viscous forces (Lamb, 1932) and formation of parasitic capillaries in front of steep gravity waves (Longuet–Higgins, 1963) are other sinks of energy which become significant at high wavenumbers only. As mentioned before, dynamics of wave breaking is little understood. In Equation 1.1.3, it is generally represented by

an empirical function of convenient form which depends on the wavenumber of the breaking wave and some integral spectral parameter, such as average wave steepness (Komen *et al*, 1984) or wave energy (Donelan and Pierson, 1987).

Consequently, prediction of the wave evolution by operational wave models is limited due to sensitivity of the nonlinear wave–wave interactions to spectral shape which depends on the rather poorly known functions I and D in Equation 1.1.3. This has led scientists to study the form and evolution of wave spectra (after initial and transitional stage of growth) under different conditions.

Wave spectra obtained in the JONSWAP, Joint North Sea Wave Project (Hasselmann *et al*, 1973), experiment show remarkably similar shapes with increasing fetch: the front face rises sharply to a maximum then decreases; after an overshoot the rear face seems to approach an equilibrium condition. Empirical functions describing the behavior of the spectral peak such as migration to lower frequencies, enhancement over the Pierson–Moskowitz (1964) spectrum and width, are now available (Hasselmann *et al*, 1973). However, characterization of the rear face at frequencies above the spectral peak is still unresolved. For example, Phillips (1958) spectrum which has been widely used, is defined by a universal constant β and a -5 power law in frequency. But the JONSWAP mean spectrum (Hasselmann *et al*, 1973) which assumes the same power law, clearly indicates that Phillips' constant β is not a universal parameter and must be replaced by a function that includes the effects of the wind, fetch and duration. Theories on the nature of the equilibrium range (Kitaigorodskii, 1983; Phillips, 1985) are not in agreement however, they produce the same result: the energy containing part of the rear face where energy is greater than 1% of the spectral maximum, is the universal part of a wind–wave spectrum. In this region a spectral form $\propto \omega^{-4}$ is more appropriate. This result is supported by measurements of Toba (1973), Kahma (1981), Forristal (1981), Donelan *et al* (1985), Jähne and Reimer (1990), and Hansen *et al* (1990). However, Banner

et al (1989) report wavenumber spectra obtained from stereophotogrammetric measurements in the short gravity–capillary wave region that differ from the wavenumber dependencies proposed by the theories above. Banner (1990b) suggests that the spectral equilibrium condition exists not in the energy containing part of the spectrum but at higher wavenumbers and the spectral form in that region is similar to the one suggested by Phillips (1958); and that the rear face of wave spectra expressed in the frequency is largely governed by the angular spreading of the wave components.

More experimental evidence is needed to resolve these discrepancies. Information obtained by spatial measurements is preferred because, in the short gravity–capillary range, the wave spectra obtained from temporal measurements are questionable due to possible Doppler frequency shifts (Kitaigorodskii *et al*, 1975). Attempts have been made (e.g. Sinitsyn *et al*, 1973; Reece, 1978; Evans and Shemdin, 1980; Ataktürk, 1984; Stolte, 1984, 1989; Richter and Rosenthal, 1986; Ataktürk and Katsaros, 1987) to correct for the Doppler frequency shifts, but the errors in the results are generally large due to lack of measurements of the surface currents and, of wide angular spreading of these small scale waves. Nonetheless, until practical spatial measurement techniques become available, this approach will be in use.

1.2 Overview of the Current Investigation

This dissertation is aimed at relating the surface roughness on a body of fresh water to environmental variables such as wind speed or stress, atmospheric stratification and water surface temperature. The investigation is based on the point measurements of wave heights, turbulent wind and temperature, and surface tension collected on Lake Washington.

The surface roughness is studied through the spectral analysis of wind–generated waves (0.03 to 5 m long) using a linear wave theory. Breaking

waves which are highly nonlinear are identified using a technique that we have developed previously (Weissman *et al*, 1984), and are excluded from the data. The energy spectra of short gravity–capillary waves, with wavelengths $0.03 \leq \lambda \leq 0.40\ m$, are corrected for Doppler frequency shifts. The correction scheme differs from that described by Ataktürk (1984) or Ataktürk and Katsaros (1987) in the estimation of the effective surface drift. The effects of surface films on the roughness elements are discussed. These were observed occasionally.

Surface fluxes of momentum, sensible heat and latent heat are obtained through the eddy correlation technique. Corresponding bulk transfer coefficients for 10 m height and neutral stratification are determined. Posssible links between measurements of surface roughness and bulk transfer coefficients are sought.

Finally, experimental results are used to evaluate the applicability of the available wave and surface flux models to our observations. Outcome of this work will also be supplemental to a continuing radar backscatter study and a planned project on spatial measurements of small scale roughness elements through stereophotogrammetry.

CHAPTER 2: REVIEW OF PREVIOUS RESEARCH

In this chapter, the existing literature relevant to this study is reviewed. The topics covered in the following sections are: statistical descriptions of a random wave field by Fourier analysis; parameterizations of the wave spectrum; surface currents and corrections for their signatures in a wave spectrum; suppression of wind waves by slicks; and, dependence of atmospheric surface layer dynamics on sea state.

2.1 Spectral Characterizations of Water Surface Roughness Elements

A random process has Gaussian properties and can be defined only statistically. Its fundamental measure is the joint probability density of characteristic variables. In deep water, surface waves are almost always random in the sense that the detailed configuration of the surface varies in an irregular manner in both space and time and the most common method of studying them is therefore by spectral analysis of the vertical surface displacements. In this section, the relation between the probability density and the energy density spectrum of wave heights is established. The correspondence between various forms of spectral representations are summarized. Also, the validity of spectral analysis for wind–generated waves is discussed.

2.1.1 Statistical Descriptions of Random Processes

One application of Fourier analysis is in probability theory of random variables. Following Hsu (1970), a random variable, ζ_r, taking real values between $-\infty$ and ∞ may be characterized by a probability distribution function, $p(\zeta)$, defined as

$$p(\zeta) = \Pr(\zeta_r < \zeta), \tag{2.1.1}$$

with the properties

$$p(-\infty) = 0, \;\; p(\infty) = 1. \tag{2.1.2}$$

where Pr is the probability that ζ_r has a value less than a given ζ. If $p(\zeta)$ is differentiable, then the probability density function is

$$P(\zeta) = \frac{dp(\zeta)}{d\zeta}, \tag{2.1.3}$$

with the normalization condition (Equations 2.1.2),

$$\int_{-\infty}^{\infty} P(\zeta) d\zeta = 1. \tag{2.1.4}$$

The n–th moment of ζ_r can be found from the expected value of ζ_r^n,

$$m_n = \int_{-\infty}^{\infty} \zeta^n P(\zeta) d\zeta. \tag{2.1.5}$$

The first and second moments are the mean, $\overline{\zeta}$, and the mean square, $\overline{\zeta^2}$, values of ζ_r. By definition, the characteristic function, $\phi(\kappa)$, where κ is an arbitrary real–valued parameter of a random variable ζ_r, is the expected value of $e^{i\kappa\zeta_r}$. $\phi(\kappa)$ can be expressed in a manner similar to the moments in Equation 2.1.5;

$$\phi(\kappa) = \int_{-\infty}^{\infty} e^{i\kappa\zeta} P(\zeta) d\zeta, \tag{2.1.6}$$

which is the Fourier transform of $P(\zeta)$ with a change in the sign of the exponential term. The inversion formula can be written as

$$P(\zeta) = (2\pi)^{-1} \int_{-\infty}^{\infty} \phi(\kappa) e^{-i\kappa\zeta} d\kappa. \tag{2.1.7}$$

By expanding the exponential term in Equation 2.1.6 in a Taylor series at the point $\kappa = 0$ and assuming that term–by–term integration is valid, it can

be shown that the derivatives of the characteristic function are related to the moments (Equation 2.1.5) by

$$\left.\frac{d^n\phi(\kappa)}{d\kappa^n}\right|_{\kappa=0} = i^n m_n. \tag{2.1.8}$$

The conclusion that can be drawn from these results is that the statistical properties of a random variable can be described either by its probability density function or by its moments, because they are interrelated via the characteristic function. The approach can be extended to two or more random variables and is extensively utilized in statistical analysis of surface waves (cf. Phillips, 1977).

2.1.2 The Wave Spectrum

The traditional statistical model of wind waves (Longuet–Higgins, 1962) assumes that the wave field consists of a linear superposition of independently propagating, sinusoidal waves that have Gaussian properties. The surface elevation, $\zeta(\mathbf{x},t)$, may be written in the form

$$\zeta(\mathbf{x},t) = \sum_{n=1}^{\infty} A_n \cos(\mathbf{K}_n \cdot \mathbf{x} - \Omega_n t), \tag{2.1.9}$$

where A_n is the amplitude, $\mathbf{K}$ and $\mathbf{x}$ are the horizontal wavenumber and position vectors, respectively, t is time, and Ω is radian frequency. Generally, $\zeta(\mathbf{x},t)$ is measured with respect to mean water level. Therefore, its first moment (i.e., average value) is zero. Its second moment yields the variance (i.e., the mean square value for zero mean) which is a measure of the wave energy. It is this parameter that is of crucial importance for studies of wave dynamics.

In the most general case, the covariance of the surface displacement

$$\begin{aligned} C(\mathbf{x},\mathbf{r};t_o,t) &= \overline{\zeta_1\zeta_2}, \\ &= \int_{-\infty}^{\infty}\int_{-\infty}^{\infty} \zeta_1\zeta_2 P(\zeta_1,\zeta_2)\, d\zeta_1\, d\zeta_2, \end{aligned} \tag{2.1.10}$$

depends on the space and time lags, i.e. $\mathbf{r}$ and t, respectively, where $P(\zeta_1, \zeta_2)$ is the probability density and $\zeta_1 = \zeta(\mathbf{x}, t_o), \zeta_2 = \zeta(\mathbf{x}+\mathbf{r}, t_o+t)$. Covariance at zero lag is the mean square surface displacement (Equation 2.1.5)

$$C(\mathbf{x}, \mathbf{0}; t_o, 0) = \int_{-\infty}^{\infty} \zeta_1^2 P(\zeta_1)\, d\zeta_1 = \overline{\zeta^2} = m_2. \tag{2.1.11}$$

In a statistically homogeneous and stationary wave field, we have

$$C(\mathbf{x}, \mathbf{r}; t_o, t) = C(\mathbf{r}, t). \tag{2.1.12}$$

Particular cases of Equation 2.1.10 are the covariance of the instantaneous surface displacement

$$C(\mathbf{r}) = C(\mathbf{r}, 0) = \overline{\zeta(\mathbf{x}, t_o)\zeta(\mathbf{x}+\mathbf{r}, t_o)}, \tag{2.1.13}$$

and the covariance of the surface displacement at one fixed point

$$C(t) = C(\mathbf{0}, t) = \overline{\zeta(\mathbf{x}, t_o)\zeta(\mathbf{x}, t_o+t)}. \tag{2.1.14}$$

If the waves are homogeneous, $C(\mathbf{r})$ is an even function of $\mathbf{r}$ and if they are stationary, $C(t)$ is an even function of t.

The Fourier transforms of the covariances given by Equations 2.1.10, 2.1.13 and 2.1.14 lead to various representations of the energy density spectrum of waves. Equation 2.1.11 provides the normalization condition such that the total energy is $\overline{\zeta^2}$. For example, the three–dimensional wavenumber–frequency spectrum, $E(\mathbf{K}, \Omega)$, is the Fourier transform of the covariance $C(\mathbf{r}, t)$

$$E(\mathbf{K}, \Omega) = (2\pi)^{-3} \int\int C(\mathbf{r}, t)\, e^{-i(\mathbf{K}\cdot\mathbf{r} - \Omega t)} d\mathbf{r}\, dt, \tag{2.1.15}$$

with the normalization condition

$$\int_{\mathbf{K}}\int_{\Omega} E(\mathbf{K}, \Omega)\, d\mathbf{K}\, d\Omega = \overline{\zeta^2}. \tag{2.1.16}$$

$E(\mathbf{K},\Omega)$ describes the density of contributions to $\overline{\zeta^2}$ per unit volume of $\mathbf{K}$–Ω space. Inverse Fourier transform of Equation 2.1.15 is,

$$C(\mathbf{r},t) = \int_{\mathbf{K}}\int_{\Omega} E(\mathbf{K},\Omega)\, e^{i(\mathbf{K}\cdot\mathbf{r}-\Omega t)} d\mathbf{K}\, d\Omega. \tag{2.1.16}$$

Reduced spectra can be obtained from $E(\mathbf{K},\Omega)$ by integration over $\mathbf{K}$ and over Ω. The two–dimensional wavenumber spectrum is given by

$$E(\mathbf{K}) = \int_{-\infty}^{\infty} E(\mathbf{K},\Omega)\, d\Omega. \tag{2.1.17}$$

$E(\mathbf{K})$ and $C(\mathbf{r})$ form a Fourier transform pair. This can be seen by putting $t=0$ in Equation 2.1.16, and using Equation 2.1.17;

$$C(\mathbf{r},0) = C(\mathbf{r}) = \int_{\mathbf{K}} E(\mathbf{K})\, e^{i\mathbf{K}\cdot\mathbf{r}} d\mathbf{K}, \tag{2.1.17}$$

whose inverse transform is

$$E(\mathbf{K}) = (2\pi)^{-2} \int_{\mathbf{r}} C(\mathbf{r})\, e^{-i\mathbf{K}\cdot\mathbf{r}} d\mathbf{r}. \tag{2.1.18}$$

The wavenumber spectrum is normalized such that

$$\int_{\mathbf{K}} E(\mathbf{K})\, d\mathbf{K} = \overline{\zeta^2}, \tag{2.1.19}$$

hence, it gives the density of contributions to $\overline{\zeta^2}$ per unit area of $\mathbf{K}$ space regardless of frequency.

The frequency spectrum is obtained by the integration,

$$E(\Omega) = \int_{\mathbf{K}} E(\mathbf{K},\Omega) d\mathbf{K}. \tag{2.1.20}$$

$E(\Omega)$ and $C(t)$ also form a Fourier transform pair which can be derived by putting $\mathbf{r}=\mathbf{0}$ in Equation 2.1.16. However, they are more commonly treated as a cosine transform pair. As mentioned above, $C(t)$ is an even function so

that its pair $E(\Omega)$ is real and symmetric about $\Omega = 0$. Therefore, the cosine transform is appropriate. Conventionally, the frequency is taken as positive, $\Omega \geq 0$. Hence,

$$C(\mathbf{0},t) = C(t) = \int_0^\infty E(\Omega)\cos\Omega t\, d\Omega, \tag{2.1.21}$$

and

$$E(\Omega) = \frac{2}{\pi}\int_0^\infty C(t)\cos\Omega t\, dt. \tag{2.1.22}$$

The normalization is done as before,

$$\int_0^\infty E(\Omega)\, d\Omega = \overline{\zeta^2}, \tag{2.1.23}$$

so that $E(\Omega)$ represents the density of contributions to $\overline{\zeta^2}$ per unit frequency interval regardless of the wavenumber vector.

Frequently, the waves are studied in terms of the directional frequency spectrum, $E(\Omega,\theta)$, which is defined as

$$E(\Omega,\theta) = 2\int_0^\infty E(K,\theta,\Omega)K\, dK,\ \ \Omega \geq 0, \tag{2.1.24}$$

and

$$\int_{-\pi}^{\pi}\int_0^\infty E(\Omega,\theta)\, d\Omega\, d\theta = \overline{\zeta^2}, \tag{2.1.25}$$

where $\mathbf{K} = (K\sin\theta, K\cos\theta)$ in polar coordinates. In particular,

$$E(\Omega) = \int_{-\pi}^{\pi} E(\Omega,\theta)\, d\theta. \tag{2.1.26}$$

Since $E(\Omega)$ is most easily observed, it is customary to represent the directional frequency spectrum by

$$E(\Omega,\theta) = E(\Omega)\, S(\Omega,\theta), \tag{2.1.27}$$

where S is the spreading function describing the angular distribution of the wave energy density (Mitsuyasu *et al*, 1975; Hasselmann *et al*, 1980; Donelan *et al*, 1985). From Equations 2.1.23 and 2.1.25, it follows that

$$\int_{-\pi}^{\pi} S(\theta)\, d\theta = 1. \tag{2.1.28}$$

Finally, a one–dimensional spectrum of wavenumber modulus, $E(K)$, can be obtained by averaging $E(\mathbf{K})$ or its polar form $E(K,\theta)$, over all directions;

$$E(K) = \int_{|\mathbf{K}|=K} E(\mathbf{K})\, d\mathbf{K} = \int_{-\pi}^{\pi} E(K,\theta) K\, d\theta, \tag{2.1.29}$$

which has the property,

$$\int_{0}^{\infty} E(K)\, dK = \overline{\zeta^2}. \tag{2.1.30}$$

The energy density spectra can be determined from field observations by a variety of techniques. Methods of measurement of the two– and three–dimensional spectra by an array of in situ sensors, first suggested by Barber (1963), are reviewed by Barnett and Kenyon (1975), Davis and Regier (1977), Long and Hasselmann (1979), and Long (1980). Variations of these methods have been employed to analyze the data from buoys (Longuet–Higgins *et al*, 1963; Mitsuyasu *et al*, 1975; Hasselmann *et al*, 1980), arrays of wave staffs (Donelan *et al*, 1985; Irani *et al*, 1986) and pressure transducers (Pawka *et al*, 1980). The results from these traditional techniques may be readily interpreted, however, achieving high quality requires the design of a multi element array optimized for maximum spatial resolution, i.e. maximum number of space lags r in Equation 2.1.10, and reduction of a large volume of data.

Remote techniques (Garrett, 1970; Tyler *et al*, 1974; McLeish *et al*, 1980; Pawka *et al*, 1980; Trizna *et al*, 1980; Gotwols and Irani, 1980; Irani *et al*, 1986) offer fine spatial resolution and large areal coverage, but they have their own disadvantages. For example, optical methods which respond to the wave

slope rather than the elevation have to deal with nonlinear surface illumination; and, radar techniques involve uncertainties in identifying the source and the mechanism of backscattering. A combination of in situ and remote techniques can provide complementary information.

The one–dimensional frequency spectrum is the most commonly measured quantity and is directly available from observations of wave heights (e.g., Hamilton *et al*, 1979; Donelan and Pierson, 1983). Among the spectral forms considered above, it contains the least amount of information. However, it is a practical and useful tool for studying unidirectional and long–crested waves that are usually observed in a fetch–limited environment.

For intercomparison purposes or for convenience in a particular application, it may be necessary to express the wave spectrum in a domain other than that of the measurements. A transformation is possible if there exists a deterministic relationship between $\mathbf{K}$ and Ω, a so called *dispersion relation*. (Note that when the measurements yield the three–dimensional wavenumber–frequency spectra, all characteristics of the surface are already available in both spatial and temporal domains. Hence, there is no need for a dispersion relation. In fact, it is measurements of this type that provide the desired relationship.) For infinitesimal gravity waves in deep water, the isotropic dispersion relation (cf. Phillips, 1977) is given by

$$\Omega^2 = gK, \tag{2.1.31}$$

where g is the acceleration due to gravity, and $K = |\mathbf{K}|$ is the modulus of the wavenumber vector. Then, the correspondence between the spectra of frequency and wavenumber modulus can be established using the normalization conditions given by Equations 2.1.23 and 2.1.30,

$$E(\Omega) = E(K)\frac{\partial K}{\partial \Omega}\,|_{K=\Omega^2/g},$$
$$= \frac{E(K)}{C_g}\,|_{K=\Omega^2/g}, \qquad (2.1.32)$$

where $C_g = \partial\Omega/\partial K$ is the magnitude of the group velocity. In a similar manner, expressions for other spectral forms given above can be found.

The discussion until now has involved infinitesimal sinusoids (Equation 2.1.9) that have Gaussian properties. Each component propagates at a phase speed, $C = \Omega/K$, characterized by its wavenumber and frequency (Equation 2.1.31) and there are no interactions between the components. Application of a linear wave theory based on these assumptions, to wind–generated wave fields must be handled with caution for several reasons. For instance, wind waves have finite amplitudes and show nonlinear deviations from sinusoidal shapes, i.e. narrow high crests and wide shallow troughs (Stokes, 1847). Such a wave form, the so called Stokes wave, requires the existence of a fundamental free wave and its bound harmonics with all components propagating at the phase speed of the free wave. Bound harmonics may become significant when waves are generated over a short fetch by strong wind action, such as in wind–wave tanks, and appear as enhanced energy at frequencies equal to integral multiples of the spectral peak frequency (cf. Lake and Yuen, 1978; Komen, 1980). Lack of such features in the wave spectra obtained from field measurements (Hasselmann *et al*, 1973; Donelan *et al*, 1985) indicates that the waves in the natural environment are predominantly free waves.

In a nonlinear wave field, the dispersion relation may differ from the linear dispersion, Equation 2.1.31, (Longuet–Higgins *et al*, 1963; Yefimov *et al*, 1972; Grose *et al*, 1972; Ramamonjiarisoa *et al*, 1978; Yefimov and Solov'yev, 1979; Mitsuyasu *et al*, 1979; Phillips, 1981b; Donelan *et al*, 1985), and the surface elevations may not be purely Gaussian (Kinsman, 1965; Longuet–Higgins, 1980;

Tayfun, 1980; Huang and Long, 1980; Hatori, 1984; Huang *et al*, 1986b). Also, numerous observed phenomena, such as evolution of the wave field with time and fetch, or wave instabilities and breaking, manifest the nonlinear interactions of different strengths among the wave components (e.g. Phillips, 1977; Phillips, 1981a; Su and Green, 1986).

Despite these complexities, much has been learned about the weakly nonlinear wind–generated waves using a linear wave theory with Stokes corrections. Stokes corrections which are small amplitude perturbations to the fundamental free waves, have been calculated to high orders (Longuet–Higgins, 1978a, 1985a; Hui and Tenti (1982; 1985). The resulting Stokes dispersion relation to the fourth order,

$$\Omega^2 = gK(1 + A^2K^2 + \frac{5}{4}A^4K^4), \tag{2.1.33}$$

has been verified experimentally by Donelan *et al* (1985), where AK is the wave slope. In the case of Stokes (1880) limiting steepness $AK = 0.44$, these corrections may amount as much as 20% increase in Ω (or decrease in K) and 10% increase in C. In a fully developed or relatively mature wave field, the difference between Equations 2.1.31 and 2.1.33 may be negligible for $\Omega \leq 2\Omega_p$ (Donelan *et al*, 1985), where the subscript p indicates a parameter associated with the spectral peak. A necessary condition for Stokes expansion is that the maximum vertical displacement of the free surface must be small compared with the shortest wavelength. Therefore, the approach cannot be extended to shorter waves indefinitely, but it is restricted to the gravity waves in a narrow band near the peak of the spectrum (Phillips, 1981a). The weakly nonlinear interactions of surface waves have characteristic time or length scales which are of order $(AK)^{-2} \approx 100$ times the period or the wavelength, respectively, of the dominant waves (Phillips, 1981a). Resulting variations in the wave spectra, although significant over long duration and fetch, are very slow. Therefore,

applications of a linear perturbation theory to weakly nonlinear waves in the vicinity of the spectral peak are acceptable.

The short gravity–capillary waves riding on the backs of the long gravity waves cannot be represented in terms of Stokes expansions (see the paragraph above). In addition, the short waves are strained, advected and distorted by the hydrodynamic interactions with the underlying long waves over a time scale comparable with or less than the dominant wave period. Therefore, the interactions between long and short waves cannot be included among the weak interactions. Wave–current interactions and wave breaking are some other examples of strongly nonlinear phenomena. The effects of strong interactions on the weakly nonlinear interactions, discussed by Longuet–Higgins (1978b) and Phillips (1981a), are not well known. However, due to their widely separated time scales in a local consideration of strong interactions, the influence of weak interactions can be ignored. Then, it is possible to assume a two–scale water surface roughness composed of long gravity waves (governed only by the weakly nonlinear interactions and insensitive to local disturbances over short periods of time) and short gravity–capillary waves (reflecting the rapid, local changes in the wave field). Separation of scales is rather arbitrary but, in general, the wavelengths of the short waves are of the order of the dominant wave height or less.

Distribution of the energy densities of small scale waves can be described in a similar manner by any one of the spectral forms above. However, defining a dispersion relation appropriate for these waves may not be straightforward. The restoring force for the short gravity–capillary waves includes both the gravity and the surface tension, γ. Therefore, the dispersion relation given by Equation 2.1.31 must be modified to account for the effects of the surface tension. For deep water, in the absence of long gravity waves and currents, the dispersion relation can be expressed as (see Phillips, 1977; Lighthill, 1978),

$$\omega^2 = (g + \rho_w^{-1}\gamma k^2)k, \tag{2.1.34}$$

where ρ_w is the density of the water, and the lower case letters are used to distinguish the parameters of the small scale waves from those of the long waves. For waves with wavelengths $\lambda = 1.71\ cm$ if γ has the clean water value of 73 $dyne/cm^2$, the two terms inside the parantheses in Equation 2.1.34 become equally important.

Small scale waves riding on the backs of the long waves propagate on a curved surface that is also in motion, therefore, they are subject to additional vertical accelerations. In such cases, g in Equation 2.1.34 may be replaced by the net vertical acceleration, g', experienced by the small scale waves (see Equation 2.3.5). Also, the intrinsic frequency and wavenumber of small scale waves are modulated along the phase of the long wave due to hydrodynamic interactions. These variations have been calculated by Longuet–Higgins and Stewart (1960), Longuet–Higgins (1978b) and Phillips (1981b) for various long–wave steepnesses, AK. The variations in ω are on the order of $(AK)^2$, thus negligible. In contrast, k varies as $(1 + AK\cos Kx)$ with a maximum on the crests and a minimum at the troughs of the long waves for ratios of long to short wavelength, Λ/λ, as small as 4.

The surface elevations are measured most commonly at a fixed point. In this case, if there is a surface current, $\mathbf{U}_s$, that causes advection of the short waves, then the measured frequencies, σ, differ from the intrinsic frequencies, ω, according to the Doppler shift equation, i.e.,

$$\begin{aligned} \sigma &= \omega + \mathbf{k}\cdot\mathbf{U}_s, \\ &= \omega + kU_s\cos\varphi, \end{aligned} \tag{2.1.35}$$

where φ is the angle between the directions of the wave propagation and the surface current that may result from underlying long waves, wind stress and tide. Nonuniform surface currents can have strong signatures in the energy density spectrum of measured frequency (Kitaigorodskii *et al*, 1975; Phillips, 1981b; Ataktürk, 1984; Ataktürk and Katsaros, 1987). If the surface current is known, then the energy density spectrum of intrinsic frequency can be determined from Equations 2.1.34 (with g' substituted for g), 2.1.35 and the relation;

$$\begin{aligned} E(\omega) &= E(\sigma)\frac{\partial \sigma}{\partial \omega}\mid_{\sigma=\sigma(\omega,\mathbf{k},\mathbf{U}_S)}, \\ &= E(\sigma)(1+\frac{\mathbf{U}_s}{\mathbf{C}_g}\cdot\frac{\mathbf{k}}{k})\mid_{\sigma=\sigma(\omega,\mathbf{k},\mathbf{U}_S)}. \end{aligned} \tag{2.1.36}$$

Generally, measurements of the near–surface currents are not available and corrections for the Doppler effects are based on estimates of the relevant surface currents (Sinitsyn *et al*, 1973; Reece, 1978; Evans and Shemdin, 1980; Ataktürk, 1984; Stolte, 1984, 1989; Richter and Rosenthal, 1986; Ataktürk and Katsaros, 1987). The uncertainties in the estimated magnitudes of the currents, and lack of knowledge of the directional aspects of the problem may lead to large errors in $E(\omega)$ (see Section 2.3). Furthermore, the high frequency end of the spectrum can be influenced by wave breaking even during moderate conditions due to enhancement of breaking of small scale waves in the presence of a wind–induced surface drift (Banner and Phillips, 1974). Nevertheless, the approach is simple and often useful, even if the accuracy of the results is limited at higher frequencies.

2.2 Equilibrium Range and Spectral Models of Wind Waves

Based on the idea that if the local surface acceleration at a wave crest reaches some fraction of the gravitational acceleration, then the wave would break, Phillips (1958) proposed an equilibrium range on the rear face of the

wave spectrum. He postulated that in this range the breaking process imposes an upper limit to the spectral density of the wave components independent of wind input. On purely dimensional grounds, he obtained the forms

$$E(k) = Bk^{-4}, \tag{2.2.1}$$

$$E(\omega) = \beta g^2 \omega^{-5}, \qquad \beta = 2B \tag{2.2.2}$$

for the frequency and the wavenumber spectra, respectively, of the gravity waves generated by wind, where β (the Phillips constant) and B are equilibrium range constants. These simple spectral models have been widely used to describe the waves with frequencies or wavenumbers greater than twice that of the spectral peak.

As more accurate and extensive measurements have become available, shortcomings of these saturation, rather than equilibrium, spectral forms (Equations 2.2.1 and 2.2.2) in describing the wind-wave spectra have become increasingly evident (Phillips, 1985). For example, Longuet–Higgins (1969a) related β to the wave age. Hasselmann *et al* (1973) applied the Phillips formulation (Equation 2.2.2) to the growing wave fields (JONSWAP spectrum) and the results clearly demonstrated that the coefficient β in the above formulation is not a universal constant but varies with the growth stage. Recently, reanalysis of the JONSWAP data by Battjes *et al* (1987) showed that in the equilibrium range a spectral slope of ω^{-4} gives a better fit to the measurements than ω^{-5} assumed by Hasselmann *et al* (1973). Also, direct measurements of small–scale surface waves in the field (Ataktürk, 1984; Ataktürk and Katsaros, 1987) or in large wave tanks (Jähne and Riemer, 1990), and remote sensing of the sea surface through Bragg backscattering indicate that the spectral densities of short gravity waves generated by wind are not limited by a hard upper limit (e.g., Beal *et al*, 1981).

Toba (1973) found empirically that his wind tunnel data could be represented better by an equilibrium spectrum of the form

$$E(\omega) = \alpha_* u_* g \omega^{-4}, \tag{2.2.3}$$

in the frequency range $1.5 < \omega/\omega_p < \omega_u$, where u_* is the friction velocity, ω_p is the frequency of the spectral peak and ω_u is a nondimensional upper frequency bound. Using a linear dispersion relation $C = g/\omega$, the Toba constant can be related to the Phillips constant as $\alpha_* = \beta C/u_*$. This empirical form (Equation 2.2.3) which is based on his so–called 3/2 power law for the significant wave height and the significant wave period, has been supported by a number of field investigations (Kondo *et al*, 1973; Kawai *et al*, 1977; Mitsuyasu *et al*, 1980; Kahma, 1981; Forristal, 1981; Battjes *et al*, 1987; Donelan *et al*, 1985; Hansen *et al*, 1990), although significant variability in α_* among different sets of data has been noted (Phillips, 1985; Battjes *et al*, 1987).

These experimental evidences led to reconsideration of the equilibrium range and new models were derived from a balance of all source terms (including wind input, wave–wave interactions, and dissipation) in a subrange of wavenumbers where the left hand side of the radiative transfer equation (Equation 1.1.3) becomes zero. Kitaigorodskii (1983) postulated the existence of a Kolmogoroff–type equilibrium in a random wave field in which the energy input from the wind is important only for $k \geq k_p$ and becomes asymptotically negligible for $k \gg k_p$, and the energy dissipation due to gravitational instability is restricted to much larger wavenumbers, say $k > k_g \gg k_p$. Then, this postulate implies the existence of a range of wavenumbers where all three source terms must vanish. On similarity grounds, he obtained the form of the wavenumber spectrum as

$$E(k) = A_u U g^{-1/2} k^{-7/2}, \tag{2.2.4}$$

for wavenumbers $k_p \ll k < k_g$. The corresponding frequency spectrum

$$E(\omega) = \alpha_u U g \omega^{-4}, \qquad \alpha_u = 2A_u \tag{2.2.5}$$

has a form similar to that in Equation 2.2.3 found by Toba (1973). The coefficients in Equations 2.2.3 and 2.2.5 can be related through $\alpha_u = C_D^{1/2}\alpha_*$, where $C_D = (u_*/U)^2$ is the drag coefficient. For $k > k_g$, Kitaigorodskii (1983) obtained the asymptotic saturation forms (Equation 2.2.1 and 2.2.2) suggested by Phillips (1958). Although the assumption made by Kitaigorodskii (1983) that the regions (in Fourier space) of wave generation and wave dissipation are separated may be questioned, his results were recovered by Phillips (1985) using a completely different approach. He assumed that in the equilibrium range, the processes of energy input from the wind, spectral flux divergence and loss by breaking are all of importance, and that the balance includes non–trivial contributions from all three.

Field measurements of the frequency–wavenumber spectra of gravity waves by Donelan *et al* (1985) provided the most detailed information on the growth of fetch–limited wind waves. The directional frequency spectrum deduced from that work is described by

$$E(\omega,\theta) = \frac{1}{2}\, E(\omega)\, b \operatorname{sech}^2 b(\theta - \overline{\theta}), \tag{2.2.6}$$

where $\overline{\theta}$ is the mean wave direction and the sech^2 term defines the angular spreading of wave components according to

$$b = \begin{cases} 2.61(\omega/\omega_p)^{+1.3}, & \text{for } 0.56 < \omega/\omega_p < 0.95; \\ 2.28(\omega/\omega_p)^{-1.3}, & \text{for } 0.95 < \omega/\omega_p < 1.6; \\ 1.24, & \text{otherwise.} \end{cases} \tag{2.2.7}$$

This angular spreading function which gives a narrower spreading near the spectral peak than $\cos^{2s}\theta$ form (where s is a parameter determined from the first two Fourier coefficients of the directional frequency spectrum) proposed by

Mitsuyasu *et al* (1975) and Hasselmann *et al* (1980), is a better fit to the observations (Donelan *et al*, 1985) and correctly predicts the propagation direction of waves in the asymmetrical fetch situations nearshore (Walsh *et al*, 1989).

According to Donelan *et al* (1985), the frequency spectrum, $E(\omega)$ in Equation 2.2.6, depends on the peak frequency, ω_p, and the ratio, U_{10}/C_p where C_p is the phase speed of the dominant waves and U_{10} is the component of the wind speed (at 10 m height) along the direction of C_p. The ratio, U_{10}/C_p, is described as follows. A wave field is fully developed when C_p becomes comparable to the speed of the air mass at the surface. At this stage, for which $U_{10}/C_p = 0.83$ (Donelan *et al*, 1985), the wind and wave fields are in equilibrium. $U_{10}/C_p < 0.83$ indicates a decaying wave field. Generally, the values of this ratio observed in the nature vary between 1 and 3, the larger one indicating an actively growing wave field. In laboratory studies when waves are generated under the strong action of the wind over a short fetch, U_{10}/C_p may assume values of the order of 10. Thus, this ratio is a measure of how strongly the wave growth is forced by the wind. Therefore, in the present study U_{10}/C_p is called the wind forcing. The empirical frequency spectrum suggested by Donelan *et al* (1985) is in the form

$$E(\omega) = \alpha_D g^2 \omega^{-5} (\omega/\omega_p) \exp\left[-\left(\frac{\omega_p}{\omega}\right)^4\right] \gamma^{\Gamma}, \qquad (2.2.8)$$

for $\omega/\omega_p < 3.5$. Equation 2.2.8 is essentially the JONSWAP spectrum (Hasselmann *et al*, 1973) modified by replacing ω^{-5} with $\omega^{-4}\omega_p^{-1}$. The exponential term forces the spectrum to vanish at frequencies below that of the spectral peak. γ is the peak enhancement parameter given by

$$\gamma = \begin{cases} 1.7, & \text{for } 0.83 < U_{10}/C_p < 1; \\ 1.7 + \log(U_{10}/C_p), & \text{for } 1 \leq U_{10}/C_p < 5, \end{cases} \qquad (2.2.9)$$

and Γ is as a function of the spectral width parameter, Υ;

$$\Gamma = \exp\left[-(\omega - \omega_p)^2/2\Upsilon^2\omega_p^2\right], \tag{2.2.10}$$

where

$$\Upsilon = 0.08\left[1 + 4/(U_{10}/C_p)^3\right], \qquad \text{for } 0.83 < U_{10}/C_p < 5. \tag{2.2.11}$$

The equilibrium range parameter, α_D, is described by

$$\alpha_D = 0.006(U_{10}/C_p)^{0.55}, \text{for } 0.83 < U_{10}/C_p < 5. \tag{2.2.12}$$

The numerical constant, 0.006 was determined from the average spectral energy density of the wave components in the equilibrium range, $1.5 < \omega/\omega_p < 3$ (see also Hansen *et al*, 1990). In the JONSWAP spectrum, the above parameters (Equations 2.2.9–2.2.12) have been defined in terms of the nondimensional fetch. However, the results of Donelan *et al* (1985) show that parameterization in terms of U_{10}/C_p is more appropriate especially for the description of the peak enhancement.

In terms of the nondimensional frequency, $\tilde{\omega} = \omega U_{10}/g$, the equilibrium range parameter can also be expressed as $\alpha_D = 0.006\tilde{\omega}_p^{0.55}$. Since, from Equations 2.2.3 and 2.2.8, $\alpha_* = (\omega_p u_*/g)^{-1}\alpha_D$, the data of Donelan *et al* (1985) indicate that $\alpha_* \propto \tilde{\omega}^{-0.45}$, i.e. the Toba constant (which should be a universal constant) increases with decreasing nondimensional peak frequency (Battjes *et al*, 1987). Using the empirical relationship $U_{10}/C_p = 11.6(gF/U_c^2)^{-0.23}$ (Donelan *et al*, 1985) where F is the fetch , it can be shown that the frequency spectrum (Equation 2.2.8) suggested by Donelan *et al* (1985) has approximately a linear dependence on the wind speed.

Recently, open ocean measurements of the wavenumber spectra of small–scale waves have been reported although with some conflicting results. For

example, Shemdin *et al* (1988) using strereophotography found that the spectral densities of 0.02–1.0 m long waves follow a $k^{-3.6}$ behavior and increase with wind speed in the range 1.5–5.0 ms^{-1}. On the other hand, stereophotogrammetric determination of the one–dimensional wavenumber spectra by Banner *et al* (1989) indicated a k^{-4} dependency for wavelengths 0.2–1.6 m and no significant change with wind speed in the range 7.0–13.3 ms^{-1}. Two–dimensional wave slope spectra measured by Jähne and Riemer (1990) in a large wind–wave tank using an imaging optical technique showed that the height wavenumber spectra go with $k^{-3.5}$ for wavelengths 0.03–0.24 m and increase linearly with u_* for winds 2.77–17.2 ms^{-1}. This is in agreement with the findings of Shemdin *et al* (1988). For shorter wavelengths, the spectral slope becomes steeper (k^{-4}) and dependence on wind becomes much stronger ($\approx u_*^{-2.5}$).

Banner (1990b) suggested that near the spectral peak, the equilibrium conditions prevail for wavenumber components in the dominant wave direction while lateral components are not in equilibrium (also, see Jähne and Riemer, 1990). Therefore, the energy–containing subrange just above the spectral peak, where ω^{-4} frequency spectra are reported, is not an equilibrium range. At very high wavenumbers both components are in equilibrium. Based on the observed wavenumber spectra for fetch–limited conditions he proposed a model for the form of the directional wavenumber spectrum slice in the dominant wave direction;

$$E(k,\theta_p) = 0.45\text{x}10^{-4}(U_{10}/C_p)^{1/2}k^{-4}. \qquad (2.2.13)$$

This form has a weak dependence on wind speed through the term $(U_{10}/C_p)^{1/2} \propto U^{0.23}$, see the formula above suggested by Donelan *et al* (1985). Then, using an empirical angular distribution function with a k/k_p dependence, he determined the directionally averaged wavenumber spectra as

$$E(k) \propto (U_{10}/C_p)^{1/2}(k_p)^{-0.65}k^{-3.35}, \tag{2.2.14}$$

for components just above the peak enhancement region out to about $k/k_p \approx 3.7$. Using a linear dispersion relation, the corresponding frequency spectrum is found to be

$$E(\omega) \propto (U_{10}/C_p)^{1/2}(\omega_p)^{-1.3}\omega^{-3.7}, \tag{2.2.15}$$

out to $\omega/\omega_p \approx 2$. At larger wavenumbers or frequencies, the spectral forms are similar to those in Equations 2.2.14 and 2.2.15, except that the spectral slopes go with k^{-4} and ω^{-5}, respectively. Since, $k_p \propto U^{-1.08}$, the model predicts that Equations 2.2.14 and 2.2.15 have a strong dependence on wind speed, proportional to $U^{0.93}$. Comparison with Equation 2.2.13 shows that this near–linear dependence on wind speed as predicted or observed by other scientists arises from the angular spreading of the wave components and the variation of the angular spreading with k/k_p. For wave components just above the spectral peak, the model proposed by Banner (1990b) is in good agreement with other studies. At smaller scales, the angular spreading of the wave components (hence, the forms described by Equations 2.2.14 and 2.2.15) is not certain, and the measured frequency spectra are subject to Doppler shifts resulting in spectral slopes that may range from -5 to -3.5, depending on the underlying dominant wave. Therefore, the model has not been confirmed at the high frequency tail of the spectra.

In short, there is strong evidence that the spectral slope in the energy containing part of the rear face of the wave spectrum follows an ω^{-4} law. However, the uniqueness of this spectral slope is not clear (see Liu, 1989), and the observed variations in the equilibrium range constant (Phillips, 1985; Battjes *et al*, 1987; Banner, 1990b) are not completely resolved. At somewhat higher frequencies, a transition to ω^{-5} is expected but due to the operational difficulties in

spatial measurements and Doppler frequency shifts in temporal measurements, there is a lack of experimental evidence.

2.3 Surface Currents and Doppler Frequency Shifts of Short Gravity–Capillary Waves

Spatial measurements can yield directly the wavenumber spectrum of short gravity–capillary waves which is the key quantity in characterization of waves and microwave remote sensing of the ocean surface. Such measurements are difficult to obtain, so attempts have been made to determine the wavenumber spectrum from frequency spectrum of wave height or slope observations conducted at a fixed point in the laboratory (Sinitsyn *et al*, 1973; Reece, 1978) or in the field (Evans and Shemdin, 1980; Ataktürk, 1984; Stolte, 1984, 1989; Richter and Rosenthal, 1986; Ataktürk and Katsaros, 1987). The approach requires relating the wavenumber and the frequency of wave components via a dispersion relation. In the presence of long waves and surface currents, the dispersion relation for short waves is greatly altered (Kitaigorodskii *et al*, 1975) and the problem is complicated.

In a Eulerian frame of reference, the observed frequency of a short wave depends on its translational speed as it passes by the probe. If a wave component is travelling at its phase speed,

$$c(\omega) = \omega/k, \tag{2.3.1}$$

then the observed frequency is its intrinsic frequency, ω, which is related to k via the dispersion relation (Equation 2.1.34). If the waves are riding on a surface which itself is in motion, then their observed translational speed is the sum of their phase speed, $c(\omega)$, and the component of the surface current, $\mathbf{U}_s$, in the direction of wave propagation specified by the unit vector $\mathbf{k}/k$;

$$c(\sigma) = c(\omega) + \mathbf{U}_s \cdot \frac{\mathbf{k}}{k}. \tag{2.3.2}$$

The wave field considered in this study is generated purely by the local winds over the limited fetch of a lake, where tide and swell are not present. Then, the surface velocity can be described as,

$$\mathbf{U}_s(t) = \mathbf{U}_\zeta + \mathbf{U}_{St} + \mathbf{U}_w, \tag{2.3.3}$$

where the three terms on the right hand side are the horizontal orbital velocity of the long gravity waves, wave–induced mass transport (Stokes drift), and wind–induced surface drift, respectively. From Equations 2.3.1–2.3.3, the relation between the frequency of encounter, σ, and the intrinsic frequency can be determined as

$$\sigma = \omega + (\mathbf{U}_\zeta + \mathbf{U}_{St} + \mathbf{U}_w) \cdot \mathbf{k}, \tag{2.3.4}$$

which is an explicit form of the Doppler frequency shift in Equation 2.1.35. The dispersion relation appropriate for this case may be described by Equation 2.1.34 with g replaced by the modified gravitational acceleration, g', normal to the long wave surface. Modification to gravity $\mathbf{g}$ arises from the additional acceleration, $d\mathbf{V}/dt$ of the fluid due to random motions, $\mathbf{V}$, of the surface (Garrett and Smith, 1976; Phillips, 1981b; Longuet–Higgins, 1985b). Assuming that the long waves are of small amplitude, to first order in long wave steepness, Equation 2.1.34 can be rewritten as

$$\begin{aligned} \omega^2 &= g'k + \rho_w^{-1} T k^3, \\ &\approx (g + \partial^2\zeta/\partial t^2)k + \rho_w^{-1} T k^3, \\ &\approx (g - \Omega^2\zeta)k + \rho_w^{-1} T k^3, \end{aligned} \tag{2.3.5}$$

where $-\Omega^2\zeta$ is the additional acceleration due the underlying long wave. At the crests of the long waves the elevation, $\zeta > 0$ thus, the effective gravity is reduced.

Correcting for Doppler effects requires knowledge of the local magnitude and direction (with respect to short wave propagation) of the net surface current at the point of observation. Generally, such information is not directly available, and must be obtained from estimates of the constituents, i.e. the terms on the right hand side of Equation 2.3.3. For example, in the studies cited at the beginning of this section, U_ζ has been calculated from the vertical surface displacements, and $(U_{St} + U_w)$ has been approximated by $0.03\,U_{10}$. Further, it has been assumed that the wind, the wind–generated waves and the currents induced by them, all move in the same direction. In the rest of Section 2.3, the basis and the validity of such approximations are discussed.

For dominant waves generated by the wind in a fetch–limited field, the assumption of unidirection is not unreasonable. Field measurements by buoys (Longuet–Higgins *et al*, 1963; Mitsuyasu *et al*, 1975; Hasselmann *et al*, 1980) and by an array of wave staffs (Donelan *et al*, 1985) show that in the vicinity of the spectral peak, angular spreading of the wave energy is narrow with a minimum at Ω=$0.95\Omega_p$ (Donelan *et al*, 1985). The dependency on wind forcing, U_{10}/C_p, of the angular spreading is negligible (Hasselmann *et al*, 1975; Donelan *et al*, 1985). As Ω/Ω_p increases, the mean direction of propagation of a wave component is more aligned with that of the wind, but its angular distribution widens. In particular, measurements of Donelan *et al* (1985) on Lake Ontario show that mean directions of the wind and the dominant waves are in excellent agreement when the wind blows directly offshore along the long axis of the lake. (This is supported by our visual observations also.) Then, if the Coriolis effect is not important, the surface currents induced by wind and dominant waves may be considered parallel to the mean direction of the wind.

However, the angle of concern in Doppler corrections (see Equation 2.3.4) is that between the currents and the short waves. As mentioned above, the directional variability of waves about the mean wind direction increases with frequency. Since point measurements do not provide any directional information, the Doppler shifts are generally corrected by assuming that all short waves propagate in the direction of the wind. The uncertainity resulting from this assumption can be large. Therefore, estimating the magnitude of the surface currents to a degree of accuracy beyond what follows next, is not justified.

2.3.1 Orbital Velocity of the Long Gravity Waves

Linear wave theory describing the irrotational motions in a deep, inviscid, and incompressible fluid can be found in general textbooks (for example, Kinsman, 1965; Phillips, 1977; Lighthill, 1978). Assume that a sinusoidal disturbance,

$$\zeta(\mathbf{r},t) = A\cos(\mathbf{K}\cdot\mathbf{r} - \Omega t), \tag{2.3.6}$$

propagates on a water surface which is initially at rest, where $\mathbf{K} \equiv (K_x, K_y)$ and $\mathbf{r} \equiv (x,y)$ are two–dimensional horizontal vectors. Water is an incompressible fluid, i.e. ρ_w is constant, so the equation of continuity takes the form,

$$\nabla\cdot\mathbf{U}_\zeta = 0, \tag{2.3.7}$$

where $\mathbf{U}_\zeta \equiv (U,V,W)$ is the velocity field associated with $\zeta(x,y,t)$, and $\nabla \equiv (\partial/\partial x + \partial/\partial y + \partial/\partial z)$. If the Reynolds number of the motion is large ($Re = \Omega/\nu K^2$, where ν is the viscosity), the effect of the wave–generated vorticity on the wave propagation is small (see Phillips, 1977). Hence, the motion can be considered as irrotational (or potential);

$$\nabla\times\mathbf{U}_\zeta = 0, \tag{2.3.8}$$

and a velocity potential, Φ, can be defined so that,

$$\mathbf{U}_\zeta = \nabla\Phi. \tag{2.3.9}$$

From Equations 2.3.8 and 2.3.9, it can be shown that Φ satisfies Laplace's equation,

$$\nabla^2\Phi = \frac{\partial^2\Phi}{\partial x^2} + \frac{\partial^2\Phi}{\partial y^2} + \frac{\partial^2\Phi}{\partial z^2}. \tag{2.3.11}$$

For water waves, there are two kinds of boundaries; rigid and free. At a rigid boundary, in particular at the bottom $z=-D$, there is no fluid velocity normal to the boundary;

$$\frac{\partial\Phi}{\partial n}\Big|_{z=-D} = 0, \tag{2.3.12}$$

where n is the normal direction.

At the free surface $z=\zeta(x,y,t)$, a kinematic boundary condition is imposed by the requirement that a fluid particle at the surface always remains at the surface;

$$\frac{d}{dt}\{z-\zeta(x,y,t)\}\Big|_{z=\zeta} = 0. \tag{2.3.13}$$

Expanding the total derivative and, using the definition $dz/dt=W$ and Equation 2.3.9, the kinematic boundary condition can be expressed in terms of Φ and ζ;

$$\frac{d\Phi}{dz}\Big|_{z=\zeta} = \frac{d\zeta}{dt} + (\nabla_h\Phi)_\zeta \cdot (\nabla_h\zeta), \tag{2.3.14}$$

where the subscript h indicates the horizontal components.

A dynamic boundary condition at the free surface follows from Bernouilli's equation, i.e. the integral of the momentum equation. In the absence of viscous, thermal and buoyancy forces and vorticity, the equation of motion in terms of

total pressure, p_t, inside the water at a distance z from the surface, can be written as

$$\frac{d\mathbf{U}_\zeta}{dt} = -\frac{1}{\rho_w}\nabla p_t - \mathbf{g}z, \tag{2.3.15}$$

where ρ_w is assumed constant and $\mathbf{g} \equiv (0,0,g)$. Expanding the total derivative and using Equation 2.3.9,

$$\nabla\left(p_t + \rho_w\frac{d\Phi}{dt} + \frac{\rho_w}{2}\mathbf{U}_\zeta^2 + \rho_w g z\right) = 0. \tag{2.3.16}$$

The terms inside the parenthesis are the total pressure (atmospheric pressure plus surface tension), pressure due to wave form, to local kinetic energy, and hydrostatic pressure, in order. Now Equation 2.3.16 can be integrated to obtain a form of the Bernouilli's equation (Phillips, 1977, p. 19);

$$p_t + \rho_w\frac{d\Phi}{dt} + \frac{\rho_w}{2}\mathbf{U}_\zeta^2 + \rho_w g z = f(t), \tag{2.3.17}$$

where $f(t)$ is an arbitrary function of time. Absorbing $f(t)$ in unknown Φ and taking the total derivative, the dynamic boundary condition at the free surface can be found as,

$$\frac{1}{\rho_w}\left[\frac{dp_t}{dt}\right]_{z=\zeta} + \left[\frac{\partial^2\Phi}{\partial t^2} + g\frac{\partial\Phi}{\partial z}\right]_{z=\zeta} + \left[\frac{\partial\mathbf{U}_\zeta^2}{\partial t}\right]_{z=\zeta} + \frac{1}{2}\left[\mathbf{U}_\zeta\cdot\nabla\mathbf{U}_\zeta^2\right]_{z=\zeta} = 0. \tag{2.3.18}$$

The boundary conditions given by Equations 2.3.14 and 2.3.18, are nonlinear and must be evaluated at the free surface which is unknown in advance. Once the velocity potential is determined, it can be shown that the ratio of a nonlinear term to a linear term is small (at most of the order of the wave slope, see Kinsman, 1965; Phillips, 1977). Hence, for infinitesimal waves ($AK \ll 1$) the nonlinear terms can be omitted and $z = \overline{\zeta} = 0$ can be taken as the free surface. For waves of finite amplitude in deep water $D/K \geq \pi/2$, the free

surface can be reduced to mean water level (Stokes, 1847) by Taylor series expansions about $z = 0$, i.e. by multiplying each term in Equations 2.3.14 and 2.3.18 with $(1 + \zeta\partial/\partial z + \frac{1}{2}\zeta^2\partial^2/\partial z^2 + \ldots)$. Also, by expanding Φ, ζ and $\mathbf{U}_\zeta$ in powers of a small ordering parameter ε (of the order of AK) such as $\Phi = \varepsilon\Phi_1 + \varepsilon^2\Phi_2 + \varepsilon^3\Phi_3 + \cdots$, and equating the terms proportional to ε, the governing equations and the boundary conditions to a first–order approximation become;

$$\left.\begin{aligned} \mathbf{U}_{\zeta 1} &= \nabla\Phi_1, \\ \nabla^2\Phi_1 &= 0, \\ \frac{\partial\zeta_1}{\partial t} &= \frac{\partial\Phi_1}{\partial z} \quad \text{at } z = 0, \\ \frac{\partial^2\Phi_1}{\partial t^2} + g\frac{\partial\Phi_1}{\partial z} &= 0 \quad \text{at } z = 0, \end{aligned}\right\} \tag{2.3.19}$$

where the derivative of the total pressure in the last equation was set to zero by assuming that atmospheric pressure at the surface can be taken as constant and for long gravity waves surface tension is not important. Using the set of linear equations above, the velocity potential for a given wave form can be determined (see Kinsman, 1965) and this completes the solution of the problem to the first order. For example, for the periodic wave in Equation 2.3.9 the velocity potential can be found as,

$$\Phi_1(x, y, z, t) = \frac{\Omega}{K} e^{Kz} A \sin(\mathbf{K} \cdot \mathbf{r} - \Omega t). \tag{2.3.20}$$

From $\mathbf{U}_\zeta = \nabla\Phi$ where Φ is given by Equation 2.3.20, now it can be verified that the nonlinear quadratic and advection terms in Equations 2.3.14 and 2.3.18 are of the order of a linear term multiplied by the wave slope. For waves near full development, $U_{10}/C_p \approx 1$, the slopes are rather gentle and $AK \approx 0.1$. Hence, the accuracy of the results from this linear approach is about 10%.

Higher order approximations where the nonlinear terms may be regarded as perturbations to the linear solution, can be obtained in a similar way. However,

for the purpose of this study, the problem is kept in its linearized version so that there exists a family of linearly independent solutions. Since any linear combination of these solutions is also a solution and, a general disturbance can be constructed by the superposition of Fourier components, the above results obtained for a uniform wave train can be applied to any wave of arbitrary shape.

In addition to being unidirectional, if the waves are long crested, i.e. the length of the crests normal to the direction of propagation is several times the wavelength, then in the above formulation the terms involving $\partial/\partial y$ or $\partial^2/\partial y^2$ can be omitted. Early in the generation stage, the water surface may have a choppy appearance but relatively mature waves, $U_{10}/C_p \leq 2$, can be considered as long crested. In this case, the vertical surface displacements can be represented by,

$$\zeta(t) = A\cos(Kx - \Omega t), \tag{2.3.21}$$

and the velocity potential becomes

$$\Phi(z,t) = \frac{\Omega}{K} e^{Kz} A\sin(Kr - \Omega t). \tag{2.3.22}$$

The corresponding horizontal and vertical components of the orbital velocity of the periodic wave are given by;

$$U_\zeta = \nabla_x \Phi = \frac{\partial \Phi}{\partial x} = \Omega e^{Kz} A\cos(Kx - \Omega t) = \Omega e^{Kz}\zeta, \tag{2.3.23}$$

and

$$W_\zeta = \nabla_z \Phi = \frac{\partial \Phi}{\partial z} = \Omega e^{Kz} A\sin(Kx - \Omega t), \tag{2.3.24}$$

respectively. Amplitudes of the velocity components are equal and decrease exponentially with depth, but W_ζ lags U_ζ and ζ in phase by $90°$.

Laboratory studies by McNamee *et al* (1983) of mechanically generated regular waves at intermediate depths show that Equations 2.3.23 and 2.3.24

can satisfactorily predict the relative amplitudes of the velocity components and attenuation of the velocity field with depth, but they overestimate the magnitude of individual components. Deviations between the predicted and the measured amplitudes of the orbital velocities were larger (up to 20%) near the surface and the bottom, possibly due to the experimental procedure (using a fixed velocity probe near the surface) and due to very small amplitudes, especially of the vertical component, near the bottom.

Field measurements by Cavaleri *et al* (1978) of the components of the orbital velocities are in agreement with the above results from the laboratory. Cavaleri *et al* (1978) found that the amplitudes of the orbital velocity components were about 10% less than expected on the basis of linear wave theory and, although the phase of the vertical component agreed with the linear theory, that of the horizontal component showed significant deviations. They suggested that the differences between measurements and theory were caused not by finite amplitude effects but rather by the influence of the turbulent velocity fluctuations near the surface.

2.3.2 Surface Drift Induced by Waves

From the last two equations, the particle trajectories in deep water from a linear wave theory can be found as circles with radius Ae^{Kz}. For infinitesimal waves, the vertical motions of the fluid particles can be omitted ($z \approx 0$), therefore the circles are closed. However, if the waves have finite amplitudes this assumption may not be necessarily true. Then, since the radius of the orbital motions decreases with depth, a particle must cover a larger distance while moving forward in the upper half of its circular path than moving backward at a greater depth in the lower half (for an illustration see, Starr, 1945). Hence, the circular particle orbits cannot be closed and, as first noted by Stokes (1847), finite–amplitude irrotational waves must be accompanied by a net transport of

water that diminishes with depth. This so called Stokes drift, U_{St}, can be calculated from the first–order, Eulerian solutions above to the irrotational problem in various ways (for example, see Kinsman, 1965; Phillips, 1977; Lighthill, 1978) and, its magnitude in deep water averaged over one wave period, $2\pi/\Omega$, is,

$$U_{St} = \Omega K A^2 e^{2Kz} = CK^2 A^2 e^{2Kz}. \tag{2.3.25}$$

This is a second order term in AK hence a small correction to the linear solution (Equation 2.3.23), and decreases rapidly with depth. Results obtained by Chang (1969) *ab initio* with Lagrangian equations of motion for random waves including the effects of viscosity near the boundaries, are similar to the Stokes irrotational solution above. However, Ünlüata and Mei (1970) showed that a second–order vorticity diffuses downward from the surface and can become significant in deep channels under prolonged wave action, in which case the surface currents may exceed that given by Equation 2.3.25. If the channel has a closed end (as in wave tanks), significant return flows may develop beneath the surface.

Results of the laboratory experiments (with mechanically generated waves and no wind) on the drift velocities of small particles by Russell and Osorio (1958) and by Chan (1969, with random waves) or, of monomolecular slicks by Lange and Hühnerfuss (1978) are in close agreeement with the above prediction. Similar measurements of the drift velocities of paraffin oil lenses by Alofs and Reisbig (1972) are much larger (by 35–150%) than those given by Equation 2.3.25, but this difference is thought to be due to the characteristics (such as, tangential stiffness and thickness) of the surface film they used (Lange and Hühnerfuss, 1978; Wu, 1983). As will be discussed in Section 2.3, in the presence of a surface film, the surface waves are suppressed and the energy lost by the waves can contribute to the surface currents by an amount that depends on both the wavelength and the slick characteristics.

In a random wave field, the Stokes drift may be calculated as the sum of contributions from individual Fourier components. Theoretical studies by Bye (1967) and Kenyon (1969) suggest that in a wind–generated wave field the major contribution to U_{St} comes from the dominant waves and at large fetch the surface drift induced by fully–developed waves may account for up to 25–30% of the total drift. Although this percentage is roughly twice the value generally observed at short fetches in wave tanks (Shemdin, 1972; Wu, 1975; Donelan, 1978), it may still be an underestimate (Shemdin, 1972). This is also supported by Wu (1983); based on many laboratory and field experiments, he proposed that the Stokes drift increases with fetch as a result of wave growth and may account for most of the total drift at a large fetch.

There is no quantitative information from the field on U_{St} alone. Because, generally, winds and waves there coexist and they both contribute to the surface drift. However, Lange and Hühnerfuss (1978) observed that the drift velocity of a large slick had a strong component in the direction of large gravity waves which were propagating normal to the local wind (12 m/s), the wind generated shorter waves and a tidal current (0.3 m/s) parallel to the wind direction. Qualitatively, their observations support the ideas that the Stokes drift is mainly due to dominant waves and that it becomes significant at large fetch.

2.3.3 Surface Drift Induced by Winds

On a body of water initially at rest, the wind–induced currents result from communication of a portion of the wind stress to the water surface through viscous drag or skin friction. Therefore, a relationship can be expected between U_w and the wind friction velocity, $u_* = (\tau/\rho_a)^{1/2}$. For example, laboratory measurements by Wu (1975) of the velocities of small floats indicate that $U_w = 0.55u_*$. This finding was obtained after subtracting a small (12%) wave–induced component (estimated according to Equation 2.3.25) from the measured total current. Earlier measurements by Keulegan (1951) and by Phillips

and Banner (1974) are consistent with this result. Plant and Wright (1980) arrived at a similar expression, $U_w = 0.60u_*$, from measurements of the phase speeds of wind–generated waves in the laboratory by using microwave Doppler spectrometry.

Jones and Kenney (1977) argue that the subsurface boundary layer could be scaled in a way similar to the turbulent boundary layer over a solid surface, i.e. with the friction velocity in the water, $u_{*w} = (\tau/\rho_w)^{1/2}$, and the depth. Laboratory and field measurements by Donelan (1978) of the turbulent and mean velocity field in the water are in support of this argument. By linearly extrapolating his observations to the surface, Donelan (1978) found that the wind–induced current could be described by $U_w = 15u_{*w}$. A similar result is also reported by Donelan *et al* (1985) from field observations, but laboratory measurements by Wu (1975) suggest a slightly higher value of $22u_{*w}$.

The shear stress across the air–sea interface is nearly continuous (Wu, 1984). With this approximation it can be found that $u_* \approx (\rho_w/\rho_a)^{1/2}u_{*w} \approx 30u_{*w}$. Hence, results on U_w scaled with u_{*w} are in accordance with those scaled with u_*. Since u_* may vary in a range of 2–5% of U_{10} depending on stratification, wind–induced surface currents can have values approximately 1–3% of U_{10}.

Observations of the vertical profile of U_w in laboratories (McLeish and Putland, 1975; Wu, 1975; Donelan, 1978; Wu, 1984) show the existence of a thin (1–2 mm) viscous sublayer where the wind–induced current falls off rapidly and linearly, and below this layer the gradient is much smaller and curved. Field measurements by Donelan (1978) indicate that when normalized by the friction velocity in water and the depth, the wind–induced drift profile at very short fetch is in good aggreement with the laboratory results, however, at large fetch the surface current beneath wind–generated waves has a weaker shear.

2.3.4 Superposition of Surface Drifts Induced by Wind and Waves

Several attempts have been made to determine the relative importance of winds and waves on water mass transport. For this purpose, surface currents have been measured in the presence of either waves (generated mechanically without wind), or wind only (using slicks to suppress the wind waves), or both wind and waves. Studies by Keulegan (1951) in laboratory and by van Dorn (1953) in an artificial pond showed that the ratio of surface drift to wind speed increased about 8% when waves were suppressed by adding soap or detergent to the surface. Reisbig *et al* (1973) found that the net transport in the case of coupled action was less than the sum of the currents when either winds or waves were present alone by an amount that depended on the wave steepness. Similar results were obtained by Lange and Hühnerfuss (1978) and Tsahalis (1979). In the latter work it was also shown that the effect was reversed when the wind opposed the wave propagation. These findings at first were considered surprising and led to the conclusion (Lange and Hühnerfuss, 1978) that the wind– and wave–induced components of the mass transport measured separately cannot be simply added to determine the resultant surface drift. However, the observations mentioned above can be explained if the partition of the wind momentum between waves and currents, and the dependence of this partioning on the sea state are taken into account (Wu, 1983).

The wind stress, τ, measured at a height where the influence of the surface waves is negligible, is transported downward by the atmospheric turbulence. Merzi and Graf (1988) experimentally found that this height depends on the dominant wavelength such that $z \geq 0.20\Lambda_p$. At the surface a portion, τ_w, of this momentum flux is extracted by the waves through form drag and skin friction, and the rest, τ_c, contributes to the surface currents through viscous drag (Stewart, 1961; Deardorff, 1967). The wave–supported stress obtained from laboratory studies over monochromatic waves by Hsu *et al* (1981) or over

wind waves by Hsu *et al* (1982) and from field measurements by Snyder *et al* (1981) is in good agreement and, $\tau_w \approx 0.6\tau$. On the other hand, Merzi and Graf (1988) found a much smalller value; $\tau_w \approx 0.2\tau$. This large difference may be due to the characteristics of the wave fields; estimates by Mitsuyasu (1985) show that the ratio τ_w/τ may vary from 2% to 100% as the wave steepness increases from 0.01 to 0.07. In general it is agreed that the waves may receive a large portion of the wind momentum, but they lose most of it to the underlying water through dissipative processes, i.e. wave breaking and viscous damping (Hsu *et al*, 1982; Mitsuyasu, 1985). If the waves are suppressed by surface films, all wave momentum may be lost and can contribute to the surface current. This is in accordance with the observations that the surface drift is larger in slick–covered areas than the neighbouring clean areas (Phillips, 1977).

Wu (1983) suggests a technique to calculate the components of the surface drift. For given fetch and wind speeed, the wave spectrum and the wind stress are calculated. Wave spectrum is used to determine the Stokes drift (Equation 2.3.25) and total momentum of the waves. Wind–induced drift is obtained from total atmospheric momentum flux minus the amount retained by the waves. His results show that at a given wind speed U_w decreases while U_{St} increases with increasing fetch and, for a given fetch both components increase with increasing wind speed. The total surface drift decreases with increasing fetch and approaches an asymptotic value of 3.1% of the wind speed at large fetch. This figure is in good agreement with the average total surface drift obtained from numerous laboratory and field experiments (Shemdin, 1972; Huang, 1979; Tsahalis, 1979; Wu, 1983).

2.3.5 Methods of Correction for Doppler Frequency Shifts

Corrections for Doppler frequency shifts can be made either in the frequency domain (Sinitsyn *et al*, 1973; Reece, 1978; Ataktürk, 1984; Stolte, 1984,

1989; Richter and Rosenthal, 1986; Ataktürk and Katsaros, 1987) or in the temporal domain (Evans and Shemdin, 1980). Outline of each technique with its advantages and shortcomings are given below. Details and intercomparisons of these two approaches can be found in Ataktürk (1984) or Ataktürk and Katsaros (1987).

For Doppler corrections in the frequency domain, the measured spectral energy density, $E(\sigma)$, is obtained from a block of length ΔT of the time series using the Fourier transform. The intrinsic frequency, ω, corresponding to a measured frequency, σ, is found by solving the Doppler shift equation (Equation 2.3.4) and the dispersion relation (Equation 2.3.5) simultaneously. The spectral estimate $E(\omega)$ in terms of intrinsic frequency is obtained using the transformation given by Equation 2.1.36. $E(\omega)$ can be converted to wavenumber spectrum, $E(k)$, as described by Equation 2.1.32 with the use of dispersion relation appropriate for short gravity–capillary waves (Equation 2.3.5). In applications this technique may have two drawbacks. The first one occurs when the surface current is not uniform but a function of time, that is $U_s = U_s(t)$. Since the correction is made in the frequency domain, time dependent variations in U_s within the data block ΔT are not allowed. Due to this constraint, ΔT must be chosen small enough so that $U_s(t)$ may be approximated by a constant value. Note that a shorter data length, in turn, implies a decrease in frequency resolution. This problem becomes less serious as the period of the dominant waves get longer. The second shortcoming arises when the short waves and the surface current are moving in opposite directions. In this case, for a given σ and $U_s < 0$, the solution to Equations 2.3.4 and 2.3.5 may be multi–valued (Phillips, 1981b; Ataktürk, 1984; Richter and Rosenthal, 1986; Ataktürk and Katsaros, 1987) and the technique fails.

Doppler corrections in the temporal domain were suggested by Evans and Shemdin (1980). In this approach, the measurements are translated from temporal domain to a space–equivalent domain. The translation is done according to

$$dX = c(\sigma)dt, \tag{2.3.26}$$

where dt is the time step between measured data points, dx is the spacing between points in the new domain, and $c(\sigma)$ is the apparent phase speed given by Equation 2.3.2. Fourier transform of this new series yields the wavenumber spectrum directly. However, note that although dt is usually constant, dX varies with time if the surface current is not uniform. Therefore, prior to Fourier transformation, the data points must be interpolated to a constant spacing. Aliasing does not pose a problem as long as the final spacing between the data points is less than one half of the shortest wavelength of interest (Evans and Shemdin, 1980). This approach has an advantage over the previous technique; since the transformation is done in the temporal domain, it allows the surface current to vary over the length of the data block analyzed. This means that not only can the surface currents be represented more accurately, but also a high spectral resolution can be achieved by increasing the length of the individual data blocks. However, there is a trade–off with the temporal domain technique; for a particular pass through the data, the phase speeds of the short waves in Equation 2.3.2 must be held constant. Since the water waves are dispersive and the water surface is composed of waves with different frequencies, this contraint can be significant (Richter and Rosenthal, 1986). However, since Evans and Shemdin (1980) are in general agreement with other work it appears that the error is not significant, at least if a narrow wavelength band is considered at a time (see, Ataktürk, 1984; Ataktürk and Katsaros, 1987). This technique also has limitations in the regions where the surface currents oppose the wave

propagation. In this case, the difference between $c(\omega)$ and U_s (hence, dX in Equation 2.3.26) may become quite small and may result in a poor wavenumber resolution.

2.3.6 Differential Advection of Small–Scale Surface Waves

It is common experience that the water surface is rougher at the wave crests than in the troughs. Therefore, it can be expected that the spectral energy density of a short wave component varies along the long wave phase such that it is maximum at the wave crests and minimum in the troughs (Longuet–Higgins, 1969b; Alpers and Hasselmann, 1978; Phillips, 1981b, 1981c). When small scale waves are subject to Doppler frequency shift due to underlying long waves, such variations in the measured spectrum become more pronounced (e.g., Reece, 1978; Ataktürk, 1984; Ataktürk and Katsaros, 1987). However, intrinsic frequency spectrum obtained from the measured spectrum after Doppler correction has been reported to indicate short wave energy being maximum in the region of long wave troughs (e.g., Richter and Rosenthal, 1986; Stolte, 1986, 1989). Such results are clearly in contradiction with the observations, and may arise if the Doppler velocities are overestimated.

As discussed in Section 2.3.1, orbital velocities predicted by a linear wave theory are in good agreement with the measurements. But, the assumption that all waves and the wind are unidirectional, that is assuming that the angle between U_s and k in Equation 2.3.2 is always zero, may lead to overcorrection. Another possibility that can cause overcorrection is that the short waves are advected by a Doppler velocity which is less than U_s evaluated at the surface. The first possibility was discussed earlier in this chapter. Results of some theoretical and experimental work concerning the second possibility are given below.

In all the previous studies (Sinitsyn *et al*, 1973; Reece, 1978; Evans and Shemdin, 1980; Ataktürk, 1984; Stolte, 1984, 1989; Richter and Rosenthal,

1986; Ataktürk and Katsaros, 1987) corrections for the Doppler frequency shifts have been made using the value of the surface current at $z = 0$, that is at the free surface. However, Stewart and Joy (1974) suggest that the waves are advected by the mean current at a depth corresponding to some fraction of a wavelength depending on the current profile (see Smith, 1990). This is also supported by the experimental results of Plant and Wright (1977, 1980) obtained in the laboratory. They found that the difference between measured and predicted phase speeds of short waves could be explained if the waves were advected by the mean current at a depth, $z = -0.044\lambda$. In arriving at this conclusion, they also assumed that the mean wind drift profile in their wind–wave tank could be represented by a logarithmic law;

$$U_w(z) = U_w \mid_{z=0} - \left(\frac{\rho_a}{\rho_w}\right)^{1/2} \frac{u_*}{\kappa} \ln\left(\frac{z_{wo} + z}{z_{wo}}\right), \qquad (2.3.27)$$

where $\kappa = 0.40$ (Zhang, 1988; Zhang *et al*, 1988) is von Kármán constant and z_{wo} is the roughness length in the water. Similar results were also reported by Donelan (1978) and Donelan *et al* (1985) but their observed profiles were gentler than those of Plant and Wright (1977, 1980) hence, their suggested depth was somewhat larger, $z = -1/k = -0.159\lambda$. Less strongly sheared surface currents are believed to be caused by the wave mass transport which although smaller than the wind drift at the surface, decays less rapidly (Donelan, 1978). For the small wave tank used by Plant and Wright (1977, 1980), the Stokes drift is less significant (e.g. Wu, 1983). Measurements by Shemdin (1972) in a circulating wind–wave tank also showed that the current profile closely follows the logaritmic law for constant stress turbulent boundary layers. Despite the quantitative disagreement between these experiments, the results are in accordance with the suggestions by Stewart and Joy (1974) that the short waves are advected not by the surface value of U_ζ but the value evaluated at some

depth that depends on the wavelength of the short wave and the shear current profile.

2.4 Suppression of Roughness Elements by Surface Films

Natural and man–caused sea surface films (slicks) may cover large areas particularly in coastal waters. Since these areas are identified by the unusual smoothness of the surface, for reasons given in Chapter 1, sea slicks may play an important role in air-sea interaction and microwave remote sensing of the ocean surface (Hühnerfuss and Garrett, 1981; Garrett, 1986; Wu, 1989). Although the calming effect of oil on water surface waves has been common knowledge for centuries, until recently little was known about the causes of this phenomenon (Scott, 1978, 1979). Now it is generally accepted that (e.g., Scott, 1986; Hühnerfuss *et al.*, 1987) monomolecular layers of surface–active materials may influence two characteristics of the water, namely, surface tension, γ, and surface dilational elasticity, ϵ. The second parameter describes surface tension gradients due to variations in surfactant concentration:

$$\epsilon \equiv \frac{d\gamma}{d(\ln A)} \ , \tag{2.4.1}$$

where A is the surface area per molecule. Pure water has a high surface tension (γ=73.05 mN/m at 18.3 $^{\circ}C$) and zero surface dilational elasticity corresponding to infinite compressibility. In the presence of slicks, *gamma* decreases while ϵ increases with increasing surfactant concentration.

A decrease in γ results in reduction of wave propagation speeds, because

$$c = [(g + \rho^{-1}\gamma k^2)/k]^{1/2} \ , \tag{2.4.2}$$

where c is the phase speed, g is the acceleration due to gravity, ρ is the density of water, and k is the wavenumber. The reduction in c is negligible for gravity waves (less than 3% if wavelength, $\lambda > 7\ cm$), but becomes increasingly significant for short gravity–capillary and capillary waves (p. 223 Lighthill, 1978).

On the other hand, surface tension gradients which result from the resistance of the surface film to expansion and compression type of motions such as those associated with waves, must be balanced by additional surface forces. These forces, that do not generally exist on a clean surface, modify the boundary conditions at the free surface and hence alter the flow pattern of the adjacent water layer. Consequently, strong velocity gradients are induced which cause enhanced viscous damping. This is called the Marangoni effect (Lucassen, 1981; Hühnerfuss *et al*, 1985a, 1985b; Lombardini *et al*, 1989). Therefore, ϵ is the key parameter for wave–calming by surface films. It should be noted that although the surface tension affects only very short waves, this is not necessarily true for surface dilational elasticity (Lucassen, 1981). Studies have also shown that dilational elasticity of a surface film stabilizes the shear flows at the interface thus, prevents wave generation by wind (Gottifredi and Jameson, 1968) and contributes to further smoothing of the water surface.

Depletion of wave energy at the high frequency end of the spectrum due to slicks (through additional viscous damping and reduced wind energy input) and redistribution of wave energy among all wave components by non–linear processes (Hasselmann, 1962, 1963a, 1963b) may lead to calming of dangerously large, low–frequency gravity waves provided that the area and duration of the slick are sufficiently large for the weak non–linear wave–wave interactions to take effect (Scott, 1978; Hühnerfuss *et al.*, 1987).

Laboratory studies covering a wide range of surface tension (from clean water value down to about 25 mN/m) show that degree of attenuation of short gravity and capillary waves depends on the characteristics of the slick, and

increases with wave frequency (Davies and Vose, 1965; Garrett, 1967; Hino *et al*, 1969; Lucassen–Reynders and Lucassen, 1969; Liu and Lin, 1979). Observations of "dips" in wave spectra, which imply stronger damping of certain waves, have been explained by a resonance–like interaction between transverse short gravity–capillary and longitudinal Marangoni waves of coincident wavelengths (Lucassen, 1981; Hühnerfuss *et al*, 1987; Lombardini *et al*, 1989). Lengths of longitudinal waves, which may not occur on a clean surface, are strongly governed by the surface dilational elasticity (Lucassen–Reynders and Lucassen, 1969). These results have been utilized for precise evaluation of γ and ϵ of film covered liquid surfaces in laboratories.

Generally, surface tensions on a natural body of water, which can be measured by Adam's (1937) technique, differ barely from the clean water value even in the presence of a clearly visible slick (Katsaros *et al*, 1989; also see Section 3.2.5). This is not surprising or contradictory, since at low wind speeds (4–5 m/s), a surface film with high γ and low ϵ can have greater calming effect than one with low γ and high ϵ (Scott, 1972, 1986). However, there is no technique available for direct determination of the surface dilational elasticity in the field. This hinders application of the above laboratory and theoretical findings to the oceans and necessitates further investigations in a natural environment.

Results of field experiments in salt water (Hühnerfusss *et al*, 1981, 1983; Yermakov *et al*, 1985; Ermakov *et al*, 1986; Wu, 1989; Lombardini *et al*, 1989) and in fresh water (Katsaros *et al*, 1989) with artificial or natural slicks, are generally in accordance with the present theories; frequency range and magnitude of wave attenuation may vary with slick composition but short gravity–capillary waves are subject to stronger damping than the long gravity waves. It should be noted that some of these results are based on the wave spectra which are not corrected for Doppler shifts experienced by the short gravity and capillary waves. Due to smearing effects by Doppler frequency shift (Ataktürk, 1984;

Ataktürk and Katsaros, 1987), frequencies and corresponding energy levels of short waves indicated by such spectra may differ from intrinsic values considerably, and must be used with caution.

2.5 Atmospheric Surface Layer

In the atmospheric boundary layer, the turbulent fluxes of momentum, sensible heat and latent heat, τ, H_S and H_L, respectively, monotonically decrease with height (e.g. Busch, 1973). The variation with height is gradual and the fluxes are still within about 10% of their surface values up to a height, say $z < 0.1h$ where h is the height of the boundary layer. The uncertainty in measurements of fluxes with present techniques is also about the same order of magnitude, i.e. 10%. Therefore, in this so called surface layer, the fluxes are considered constant. In this section, the conventional methods of studying the dynamics of the surface layer and formulations of some surface layer parameters are outlined.

2.5.1 Similarity Theory and Flux–Profile Relations

Under stationary and horizontally homogeneous conditions, the turbulence structure in the surface layer can be predicted by the Monin–Obukhov (1954) similarity theory. According to this theory, the height independent fluxes are scaled with the characteristic values of wind speed, temperature, specific humidity, and Obukhov (1946) length;

$$\left.\begin{aligned} u_* &= \left(\frac{\tau}{\rho}\right)^{1/2} = (-\overline{u'w'})^{1/2}, \\ T_* &= -\left(\frac{H_S}{\rho C_p}\right) u_*^{-1} = -\overline{w'T'}u_*^{-1}, \\ q_* &= -\left(\frac{H_L}{\rho L_e}\right) u_*^{-1} = -\overline{w'q'}u_*^{-1}, \\ L &= -\frac{T_v u_*^3}{g\kappa\overline{w'T_v'}}, \end{aligned}\right\} \qquad (2.5.1)$$

respectively, where $T_v = T(1 + 0.61q)$ is the virtual temperature in $^\circ K$, and $\kappa = 0.40$ (Zhang, 1988; Zhang *et al*, 1988) is the von Kármán constant (for rest of the notation, see Equation 1.1.1). L characterizes the height where the mechanical production and the buoyant energy production become equal, but it should be noted that this height is not exactly $z = -L$ (see Businger, 1973).

Similarity theory predicts that mean gradients in the surface layer are universal functions of the statification parameter, z/L;

$$\left.\begin{aligned} \frac{dU}{dz} &= \frac{u_*}{\kappa(z + z_0)}\phi_u(z/L), \\ \frac{dT}{dz} &= \frac{t_*}{\kappa(z + z_t)}\phi_t(z/L), \\ \frac{dq}{dz} &= \frac{q_*}{\kappa(z + z_q)}\phi_q(z/L), \end{aligned}\right\} \tag{2.5.2}$$

where z_0, z_t and z_q (all $\ll$ z) are the surface roughness lengths. Although, they have been introduced to prevent the unrealistic case of infinite shear at the surface, $z = 0$, they also have a physical meaning. For example, the momentum flux can be expressed (see Obukhov, 1946; Businger, 1973) in terms of the velocity gradient and, either the eddy transfer coefficient, K_m, or the mixing length, l, as

$$\tau = \rho K_m \left(\frac{dU}{dz}\right) = \rho l^2 \left(\frac{dU}{dz}\right)^2. \tag{2.5.3}$$

K_m represents the product of the eddy velocity and the eddy size, and l represents the turbulent length scale that is sometimes asssumed to be proportional to the distance from the solid boundary. As the roughness of the solid boundary increases, both the eddy size and the mixing length becomes larger resulting in higher levels of turbulence hence, the momentum flux is enhanced. For neutral stratification ($z/L = 0$ and $\phi = 1$, see Equation 2.5.5), comparisons of Equations 2.5.1–2.5.3 show that

$$K_m = u_* l = \kappa u_* (z + z_0). \tag{2.5.4}$$

Now, the physical meaning of z_0 becomes obvious. It represents the eddy size and the mixing length near the surface. Therefore, it is a measure of the roughness of the boundary. However, z_t and z_q must be related to some other processes as well, because their values are much smaller than z_0 (Liu *et al*, 1979; Large and Pond, 1982; Smith, 1988). Liu *et al* (1979) suggest dependence on the molecular diffusivities of the scalar in question. Molecular diffusivities for heat and salt are one order of magnitude to three orders of magnitude smaller than molecular viscosity. The roughness lengths are further discussed in the following subsections.

The functional relationships between ϕ and the dimensionless height z/L have emerged from a combination of theoretical work and experimental investigations conducted over land surfaces (Paulson, 1970; Businger *et al*, 1971; Monin and Yaglom, 1971; Dyer, 1974). There are no universally accepted forms. In particular, statification corrections to the humidity gradient are little known, and $\Phi_q = \Phi_t$ is assumed. A commonly used form (e.g. Liu *et al*, 1979; Large and Pond, 1982; Panofsky and Dutton, 1984) is given by the set of equations;

$$\left.\begin{aligned} \phi_u = \phi_t = \phi_q &= 1 + 7z/L; && z/L > 0, \\ \phi_u &= (1 - 16z/L)^{-1/4}; && z/L < 0, \\ \phi_t = \phi_q &= (1 - 16z/L)^{-1/2}; && z/L < 0. \end{aligned}\right\} \tag{2.5.5}$$

The profiles of velocity, temperature and humidity are obtained by integrating the above equations from the appropriate roughness length to an arbitrary height, z. The resulting flux–profile relationships are;

$$\left.\begin{aligned} U - U_s &= \frac{u_*}{\kappa}\left[\ln\frac{z}{z_0} - \psi_u(z/L)\right], \\ T - T_s &= \frac{t_*}{\kappa}\left[\ln\frac{z}{z_t} - \psi_t(z/L)\right], \\ q - q_s &= \frac{q_*}{\kappa}\left[\ln\frac{z}{z_q} - \psi_q(z/L)\right], \end{aligned}\right\} \tag{2.5.6}$$

with the statification correction functions given by;

$$\left.\begin{aligned} \psi_u = \psi_t = \psi_q &= -7z/L; && z/L > 0, \\ \psi_u &= 2\ln\left[\frac{1+X}{2}\right] + \ln\left[\frac{1+X^2}{2}\right] && \\ &\quad - 2\tan^{-1}(X) + \frac{\pi}{2}; && z/L < 0, \\ \psi_t = \psi_q &= 2\ln\left[\frac{1+X^2}{2}\right]; && z/L < 0. \end{aligned}\right\} \tag{2.5.7}$$

where $X = (1-16z/L)^{1/4}$. As mentioned earlier, the equations above are invalid when the requirements of the similarity theory, i.e. stationarity and horizontal homogeneity, are not satisfied. Also, they are not applicable very close to the surface where the turbulence is suppressed and the molecular transports through viscosity, conduction and diffusion become important.

Over land, the uncertainties in flux–profile relationships are mainly associated with stratification corrections and roughness lengths. Stratification effects are important at low to moderate wind speeds. At high wind speeds, $L \propto u_*^3$ becomes large and, since as $L \to \infty$, $(z/L) \to 0$ and $\psi(0) = 1$, this similarity theory predicts that the atmospheric surface layer can be assumed neutrally stratified. The surface roughness depends on the characteristics of the terrain.

In the marine environment, the uncertainties mentioned above become larger. One of the reasons is that the stratification correction functions have been derived from observations over land where humidity effects are negligible. Over water the effects of humidity on stratification must be considered

particularly in the case where either a cold air outbreak exists or the surface temperature is warm. Over warm water, particularly in the tropics, the changes in the atmospheric stratification may be due more to the latent heat flux than to the sensible heat flux. Another reason for larger uncertainties is that the surface roughness has a dynamic nature and it varies as the wave field evolves with wind speed, duration and fetch. The relationship between the characteristic surface roughness and the sea state is not well understood, and is a current subject of investigation (see Brown and Liu, 1982; Geernaert *et al*, 1986; Geernaert and Katsaros, 1986; Hsu, 1986; Huang *et al*, 1986a; Toba *et al*, 1990; Donelan, 1990).

In the presence of waves and currents, the surface is in motion. Hence, the flux–profile relationships may become even less certain due to severe practical constraints on detailed measurements at the surface, and to possible influences of wave and current actions on the distributions of the bulk quantities. For example, at the air–sea interface, U_s is no longer zero, but it is the along–wind component of surface currents, measurements of which may not be available. T_s is the skin temperature of the water, but it is generally approximated by the bulk temperature measured at some depth. The difference between these two temperatures may be significant (e.g. Hasse, 1971; Katsaros, 1977; Liu *et al*, 1979). q_s is determined from the bulk water temperature assuming that the air at the interface has the same temperature and is saturated with a relative humidity of 100% over fresh water or 98% over salt water (e.g. Large and Pond, 1982). Also, influence of the water surface waves on the wind profiles may not be negligible (e.g. Hasse *et al*, 1978). Over breaking waves, the wind stress may be enhanced by as much as 100% (e.g. Banner, 1990a), and evaporating sea spray may affect both sensible and latent heat fluxes (see Bortkovskii, 1987; DeCosmo *et al*, 1988; Smith, 1989; DeCosmo, 1991; Donelan, 1990; Fairall *et al*, 1990). In the presence of slicks, the water surface waves are suppressed

(see Section 2.4). Depending on the size and duration, the slicks may affect the air–sea interaction processes. Therefore, in the marine surface layer, the flux–profile relationships must be used with caution.

2.5.2 Bulk Aerodynamic Coefficients

Direct measurements of the surface fluxes are difficult to obtain. Therefore, it is desirable to estimate them from more easily measured mean quantities. The bulk aerodynamic formulation serves this purpose. In this formulation, the fluxes are related to the differences in mean wind speed, temperature and specific humidity between the surface and some height, z, using a set of nondimensional bulk transfer coefficients (see Equations 1.1.2 and 2.5.1);

$$\left.\begin{aligned} \frac{\tau}{\rho} &= C_D(U(z)-U_s)^2 = u_*^2 \\ \frac{H_S}{\rho C_p} &= C_H(U(z)-U_s)(T_s-T(z)) = -u_*T_* \\ \frac{H_L}{\rho L_e} &= C_E(U(z)-U_s)(q_s-q(z)) = -u_*q_* \end{aligned}\right\} \tag{2.5.8}$$

where C_D is the drag coefficient, C_H is the Stanton number, and C_E is the Dalton number. Despite the great deal of efforts (see Geernaert, 1990), parameterizations of the bulk transfer coefficients are not complete (e.g. Blanc, 1985, 1987; Donelan, 1990).

Using Equations 2.5.6 and 2.5.8, the bulk transfer coefficients can be expressed as;

$$\left.\begin{aligned} C_D &= \kappa^2\left[\ln\frac{z}{z_o}-\psi_u(z/L)\right]^{-2}, \\ C_H &= \kappa^2\left[\ln\frac{z}{z_o}-\psi_u(z/L)\right]^{-1}\left[\ln\frac{z}{z_t}-\psi_t(z/L)\right]^{-1}, \\ C_E &= \kappa^2\left[\ln\frac{z}{z_o}-\psi_u(z/L)\right]^{-1}\left[\ln\frac{z}{z_q}-\psi_q(z/L)\right]^{-1}. \end{aligned}\right\} \tag{2.5.9}$$

It is seen that C_D, C_H and C_E are height dependent (unlike the fluxes in the surface layer), and they are functions of the roughness lengths and the atmospheric stratification. Therefore, before the bulk transfer coefficients obtained from different experiments can be compared, they must be adjusted to the same reference state. Generally, the reference height is taken as $z = 10\ m$ above the surface, and the atmospheric stratification effects are adjusted to neutral conditions, $\psi = 0$. However, the concept of a reference surface roughness is not yet clear.

The bulk transfer coefficients corresponding to the reference state of neutral stratification and 10 m height are calculated according to;

$$\left.\begin{aligned} C_{DN} &= \kappa^2 \left[\ln \frac{10}{z_0}\right]^{-2}, \\ C_{HN} &= \kappa^2 \left[\ln \frac{10}{z_0} \ln \frac{10}{z_t}\right]^{-1} = \kappa C_{DN}^{1/2} / \ln \frac{10}{z_t}, \\ C_{EN} &= \kappa^2 \left[\ln \frac{10}{z_0} \ln \frac{10}{z_q}\right]^{-1} = \kappa C_{DN}^{1/2} / \ln \frac{10}{z_q}. \end{aligned}\right\} \qquad (2.5.10)$$

The remaining variations in these adjusted exchange coefficients must be due to the differences in wind speed and surface roughness. A summary of the results reported by a large number of investigators is given by Geernaert (1990). The highlights of these comparisons can be outlined as follows. C_{DN} shows a clear, mostly linear trend that increases with wind speed. At low wind speeds, $U_{10} \approx 4\ m/s$, all measurements converge to $C_{DN} \approx 1 \times 10^{-3}$ with some scatter. However, toward higher wind speeds, the linear trends diverge systematically such that C_{DN} at a given wind speed is larger for shallow fetch–limited sites than for deep open oceans. Since the waves associated with the former environment generally have a larger steepness, the observed behavior of the drag coefficient is believed to indicate the influence of the wave field hence, of the characteristic surface roughness (e.g. Smith, 1988). On the other hand, C_{HN}

and C_{EN} show no significant dependence on either wind speed or surface roughness (except for the data set of Anderson and Smith [1981] obtained from the surf zone, see Smith, 1989; Bortkovskii, 1987). There may be a slight hint of increase with higher wind speeds however, but due to the scarcity of the available data and large scatter, no conclusion can be drawn (Large and Pond, 1982). Liu *et al* (1979) proposed a model which predicts a decrease in heat transfer coefficients with wind speed due to the shadowing of the wave troughs at high wind speeds. However, their predicted neutral coefficients are well within the scatter of the other measurements. Therefore, C_{HN} and C_{EN} or equivalently, $\kappa/\ln(10/z_t)$ and $\kappa/\ln(10/z_q)$, can be assumed constant for wind speeds up to about 14 m/s. Preliminary results from HEXOS (Humidity EXchange Over the Sea, Katsaros *et al*, 1987) are in support of this conclusion (Decosmo *et al*, 1988; DeCosmo, 1991).

These arguments indicate that there is an immediate need for parameterization of the water surface roughness for varying stages of the evolution of a wave field. Such parameterization is necessary to obtain more accurate estimates of not only the momentum flux, but also heat and water vapor fluxes (see Equation 2.5.10) for all conditions. In addition, more experimental evidence is required to refine the estimated fluxes both at low wind speeds (that prevail over much of the world's oceans) when stratification effects become significant and surface slicks may alter the surface roughnesses; and, during storm conditions when breaking waves and sea spray can dramatically enhance the transfer processes.

2.5.3 Characteristic Surface Roughness of Wind Waves

Studies of turbulent flows over a rigid surface (e.g. Tennekes and Lumley, 1972) have shown that near the surface the turbulence is suppressed and the flow is entirely determined by the viscous shear. This condition is called aerodynamically smooth flow and it occurs when $zu_*/\nu < 5$, where $\nu = 1.4 \times 10^{-5}\ m^2/s$

is the kinematic viscosity of air. In this so called viscous sublayer, the velocity profile is linear. Away from the boundary, when $zu_*/\nu > 30$, i.e. at large roughness Reynolds number, the viscous effects become negligible, and the total stress is accounted for by the turbulent transfer. In this region the velocity profile is logarithmic. The height, at which the asymptotes of the linear and logarithmic velocity profiles intersect (Schlichting, 1968),

$$\delta_\nu = 11.6\nu/u_* \tag{2.5.11}$$

is taken as the viscous sublayer thickness. Then, for aerodynamically smooth flow, the virtual origin of the logarithmic profile or the roughness length can be found as (Donelan, 1990),

$$z_0 = 0.11\nu/u_*; \qquad u_* < 2(\nu g)^{1/3}. \tag{2.5.12}$$

The upper bound of the friction velocity in the above equation is approximately $u_* = 0.1\ m/s$, i.e. $U_{10} \approx 3\ m/s$. The corresponding thickness of the viscous sublayer (Equation 2.5.11) is on order of 1 mm, and decreases with increasing u_*.

Laboratory measurements by Kahma and Donelan (1988) showed that the inception wind speed for wave growth is about $u_* \approx 0.02\ m/s$ ($U_{10} \approx 0.4\ m/s$), and the resulting waves which are not visible yet, have a characteristic height $(4\overline{\zeta^2}^{1/2})$ of about 10 μm. Therefore, at such low wind speeds the waves are buried within the viscous sublayer, and the surface roughness length for aerodynamically smooth flow given by Equation 2.5.12 may be appropriate. Similar results have been reported by Kondo *et al* (1973).

As u_* increases, the viscous sublayer gets thinner (see Equation 2.5.11) hence, z_0 first decreases; meanwhile the waves evolve with duration and fetch. Consequently, the waves start to penetrate through the viscous sublayer and interact with the outer turbulent flow (e.g. Kondo *et al*, 1973). Following this

transition of the surface from a relatively smooth to a rough state, the roughness length increases. On dimensional grounds, Charnock (1955) suggested that the surface roughness length over wind generated waves can be described by the wind stress $u_*^2 = \tau/\rho$ according to

$$z_o = a u_*^2/g, \tag{2.5.13}$$

with the Charnock (1958) constant being $a = 0.012$. Comparisons (Smith, 1988) between the neutral drag coefficients estimated from Equation 2.5.10 with z_o given by Equations 2.5.12 and 2.5.13, and those obtained from measurements over deep, open oceans (Smith, 1980; Large and Pond, 1981) have shown that the Charnock formula with $a = 0.011$ can successfully describe the observed dependence of C_{DN} on wind speed except at very high wind speeds where it underestimates the measured stress. However, applications of the same approach to other data sets obtained from marine sites with limited depth or fetch have required the Charnock constant to be an adjustable parameter (Garratt, 1977; Wu, 1980; Geernaert and Katsaros, 1986; Geernaert *et al*, 1986).

In a fully developed wave field, the dominant waves traveling at speeds comparable to the wind velocity receive little direct energy and momentum from the wind (Dobson and Elliott, 1978; Snyder *et al*, 1981; Hsiao and Shemdin, 1983; Hasselmann *et al*, 1986). In accordance with this, Phillips (1977) argued that the wind input is mainly received by the small scale waves with phase speeds $c < 5u_*$ and, the root mean square height of these waves is proportional to u_*^2/g. His physical argument, in which the contribution of the dominant waves to z_o is neglected, leads to the Charnock formula originally suggested on the basis of dimensional analysis. However, the characteristics of the small scale waves depend not only on wind stress but also on surface tension (see Section 2.4), water temperature (Kahma and Donelan, 1988), drift currents (Banner and Phillips, 1974), and modulations by the underlying long waves (e.g.

Keller and Wright, 1975; Wright, 1978; Wright *et al*, 1980; Ataktürk, 1984). In addition, under the conditions of strong wind forcing and limited fetch or depth, the dominant waves may support a significant portion of the total wind stress. Therefore, Equations 2.5.12 and 2.5.13 may describe the asymptotic roughness lengths for some special cases only and they cannot predict the variation of the measured wind stress with sea state, fetch, and depth, as outlined by Geernaert (1990) and Donelan (1990).

Many attempts have been made to parameterize z_0 including the effects of the underlying long waves. Among the existing schemes, the most commonly accepted one (see Huang *et al*, 1986a; Donelan, 1990; Geernaert, 1990) is that by Kitaigorodskii (1968, 1973). It is based on the suggestion by Kitaigorodskii and Volkov (1965) that in the presence of surface waves the wind profile in a frame moving with the wave phase speed, c, can be written as

$$\begin{aligned} U &= c - \frac{u_*}{\kappa} \ln \frac{z}{a_*}, \\ &= \frac{u_*}{\kappa} \ln \frac{z}{h_s}, \end{aligned} \tag{2.5.14}$$

where $h_s = a_* \exp(-\kappa c/u_*)$ is the roughness height. Comparison between Equations 2.5.6 and 2.5.14 shows that $z_0 \propto h_s$, but the nature of the relationship must be determined experimentally (e.g. Geernaert *et al*, 1986; Huang *et al*, 1986a). Invoking a similarity argument Kitaigorodskii (1968) found that

$$h_s^2 = 2 \int_0^\infty E(k) \exp(-2\kappa c(k)/u_*)\, dk, \tag{2.5.15}$$

i.e. h_s is the root mean square wave height weighted by a function of the wave age, c/u_*. Application of this approach requires that the wave energy density spectrum is known over all wavenumber space. However, such measurements may not be available particularly at high wavenumbers, and generally an empirical or theoretical spectral form is adopted. If the latter approach is

used, Equation 2.5.15 and other parameterizations which utilize the wave spectra (e.g. Byrne, 1982; Donelan, 1982) reduce to some generalized form of the Charnock relation (see Kitaigorodskii, 1973; Geernaert *et al*, 1986; Huang *et al*, 1986a). Therefore, in search of a more practical scheme, various extensions of the Charnock relation have been considered.

A general expression for Equation 2.5.13 was first suggested by Stewart (1974);

$$gz_0/u_*^2 = f(C_p/u_*), \tag{2.5.16}$$

where C_p is the phase speed of the dominant waves. Particular forms of $f(C_p/u_*)$ reported from different investigations have been reviewed by Toba *et al* (1990; see also Toba and Ebuchi, 1990). Since the waves are assumed in equilibrium with the local wind, the parameters defining the wave field and its dependence on wind speed or wind stress are related, and these particular forms can be expressed in many ways. Choosing the form proposed by Masuda and Kusaba (1987);

$$gz_0/u_*^2 \propto (\omega_p u_*/g)^m, \tag{2.5.17}$$

Toba *et al* (1990) showed that the value of the exponent varies from one investigation to the other; $m = 1$ from Masuda and Kusaba (1987), Kusaba and Masuda (1988), Janssen (1989), Maat *et al* (1990) and Donelan (1990); $m = 1/2$ from Hsu (1974); $m = 0$ from Charnock (1955) and Wu (1988); $m = -1$ from Toba (1979), Toba and Koga (1986) and Toba *et al* (1990). Toba *et al* (1990) and Toba and Ebuchi (1990) attempted to explain the results of these comparisons by the existence of multiple regimes in wave–dependent wind stress, but their conclusion was that the wave dependence of z_0 cannot be resolved by a simple expression as in Equation 2.5.17.

A general parameterization of z_0 over a rough sea surface may become feasible if the relative importance of the stress transfer mechanisms (skin friction and form drag), and the distribution of the received wind energy between wave components are known over the full spectrum of wind waves (long gravity, short gravity–capillary, and capillary waves) for various evolutionary stages of the wave field (growing, fully developed and decaying waves). Even then, the problem will not be fully solved until the effects resulting from the presence of swell or wave breaking are incorporated. Currently, these topics are not completely understood.

CHAPTER 3: EXPERIMENTAL PROGRAM

3.1 Experimental Site

The field data utilized in this study were collected during the summers of 1986 through 1989 at Sand Point, Lake Washington, Seattle. The research facility is operated by the University of Washington, Department of Atmospheric Sciences. It consists of a mast located 15 m offshore, a hut situated on a beached barge and a floating dock between the mast and the land. On the beach, the dock is mounted on a rotating base so that the offshore end can swing between the barge and the mast. In order to prevent interference with the measurements, during data acquisition the dock is secured along the shore away from the mast. A data link between the instruments on the mast and the recorders and the monitors in the hut is supplied by underwater cables. Until the early summer of 1988, the station was powered by a diesel generator. Since then line power has been available.

Ideal experimental conditions at this site are achieved during northerly winds when the fetch over the lake reaches a maximum of about 7 km (Figure 3.1.1). The location offers a unique opportunity to study surface waves generated by the local wind on a natural body of water under a variety of environmental conditions without the complexities that may arise from the presence of swell or tidal currents. The water depth, D, by the mast is approximately 4 m and increases rapidly further offshore. We estimate the degree of reflection of the gravity waves from the inclined beach to be 5% or less (Miche, 1951). When $kD > \pi/2$, where k is the wavenumber, the waves are said to be in deep water (Phillips, 1977, p. 37). This corresponds to $\lambda = 2\pi/k < 16\ m$, where λ is the wavelength. Since this condition was met in all cases (typically $\lambda \approx 5\ m$ for

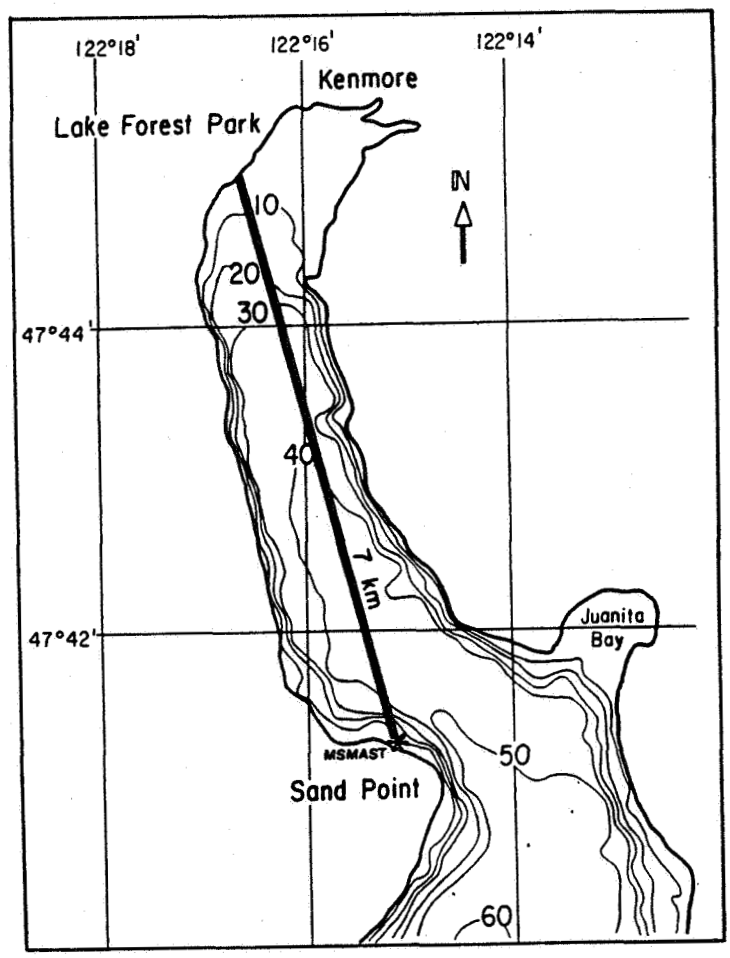

Figure 3.1.1: Location of the experimental site (MSMAST) on the shores of Lake Washington. The mast is 15 m offshore and at a depth of 4 m. The contours show the water depth in meters.

the dominant gravity waves), the location can be considered as representative of deep water.

3.2 Instrumentation

The parameters of interest for the present study were amplitudes of water surface waves, wind speed and stress, air temperature, water temperature, water surface tension and atmospheric stratification. Continuous visual records of the water surface were also obtained to identify breaking waves, supression of surface roughness due to surfactants and contamination of wave measurements due to boat waves or sea weeds. Acquisition of such complete sets of data was achieved employing several instruments which are described next.

3.2.1 Wave Gauge

The water surface elevations were measured using a resistance wire gauge (Ataktürk, 1984; Ataktürk and Katsaros, 1987). The diameter of the stainless steel wire was 0.13 mm. The resistance of the portion of the wire exposed to the air is a linear function of the water surface elevation, to a very good approximation. However, comparisons with a laser displacement gauge in a wave tank showed that at high frequencies the dynamic response of the wire gauge to vertical surface displacements was limited (Liu *et al*, 1982). The correction for the reduced dynamic response was made according to

$$E(f) = \begin{cases} 1.0E'(f)\left(\frac{f+6}{8}\right)^{1.0}, & \text{for } 2 \leq \text{f} \leq 10 \text{ Hz}, \\ 3.4E'(f)\left(\frac{f}{20}\right)^{0.77}, & \text{for } 10 < \text{f} \leq 40 \text{ Hz} \end{cases} \tag{3.2.1}$$

where $E'(f)$ and $E(f)$ are the measured and the corrected spectral energy densities, respectively (see Figure 3.2.1). The correction in the lower frequency range $2 \leq f \leq 10\ Hz$ was determined from Figure 6 of Liu *et al* (1982) in a form similar to that given by them for the higher frequencies (second equation above).

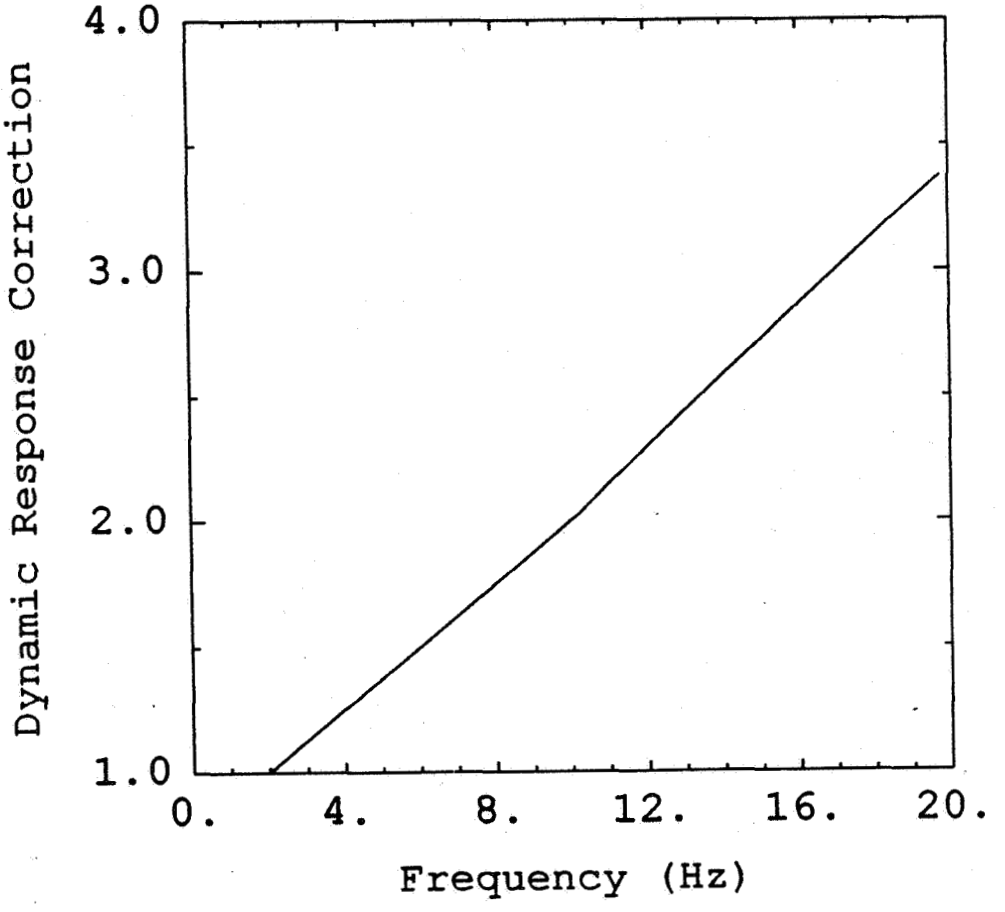

Figure 3.2.1: Correction curve for the dynamic response of the wire wave gauge (see Equation 3.2.1).

After these corrections for the effects of the meniscus and possibly distortion of the wave field in the presence of the probe, Liu *et al* (1982) observed good to excellent agreement between the spectra of the wire data and the LDG data in the frequency range $10 < f \leq 40\ Hz$.

The output voltage of the wire gauge was contaminated by electronic noise (60 Hz and much higher frequencies) present in the environment. Therefore, a 60 Hz notch–filter and a 50 Hz low–pass filter were used to suppress this noise. The frequencies specified with the filters indicate the half–amplitude points. These filters modify the signals at frequencies much higher than the maximum frequency (12 Hz) used in this study, therefore no corrections were made for their effects. This maximum frequency resulted from the dynamic range limitations of the analog FM recorder. Above 12 Hz, the signal to noise ratio becomes small. (In order to avoid this limitation, the high frequency portion of the wave signal was separated by an analog high–pass filter and amplified prior to recording on a different FM channel. However, the nonlinear phase shifts and overshooting associated with the Chebyshev filter used were found undesirable, and could not be corrected. Therefore, this signal was not used.) In the process of analog to digital conversion, output of which was denoted by ζ, the wave signal was low–pass filtered at 10 Hz. Corrections for the frequency response of this analog filter were made in the frequency domain according to

$$E(f) = \frac{E'(f)}{R_a^2(f)} \tag{3.2.2}$$

where R_a is the frequency response displayed in Figure 3.2.2.

High frequency fluctuations in ζ are due to the small–scale waves that are subject to Doppler shifts (see Section 2.3). For the technique of Doppler shift correction used in this study (Section 4.2), it is convenient to treat the high frequency part of the wave height time series as a separate signal, ζ_h.

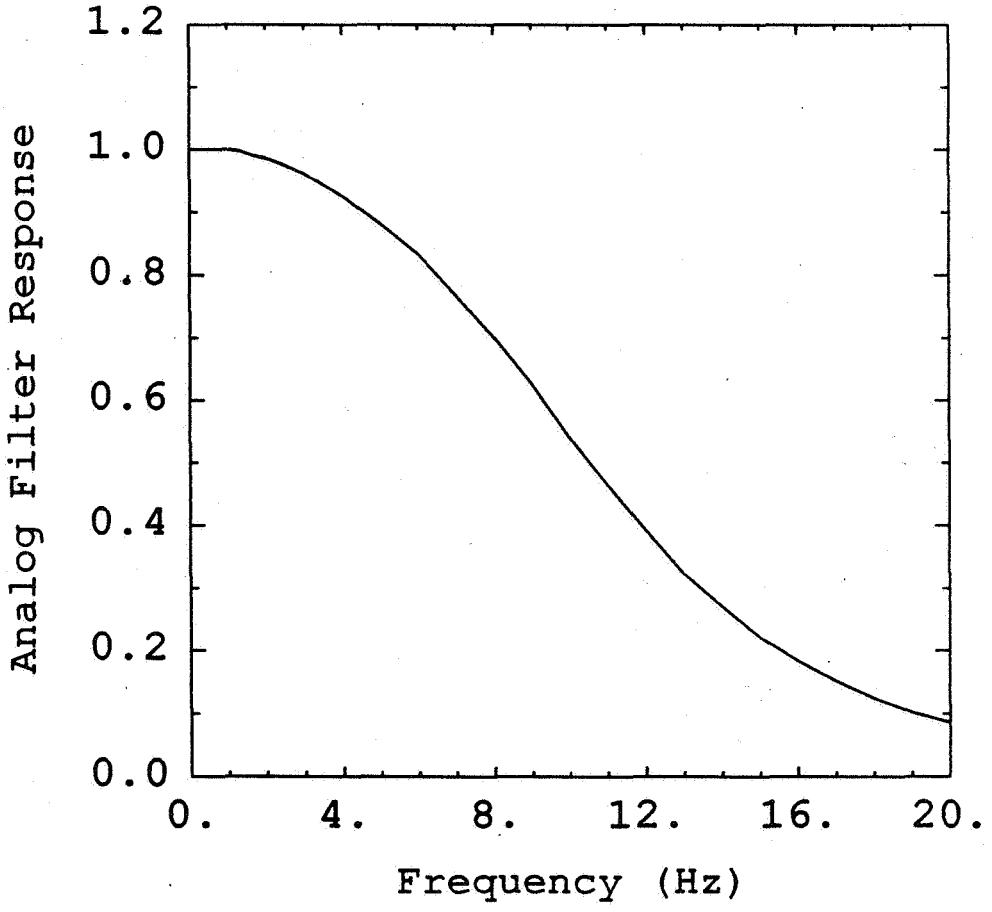

Figure 3.2.2: Frequency response curve for the 10 Hz low–pass analog filter (see Equation 3.2.2).

For this purpose, a 3–17 Hz band–pass, linear phase, finite impulse response (FIR) digital filter was designed by using a computer program (see Rabiner and Gold, 1975) based on the REMEZ exchange algorithm. The 128–point filter was applied to the data to remove the low frequency portion of the time series. Corrections for the frequency response of this digital filter were made in the frequency domain according to

$$E(f) = \frac{E'(f)}{R_d^2(f)}, \tag{3.2.3}$$

where R_d is the frequency response displayed in Figure 3.2.3.

The calibration of the wave gauge output voltage as a function of water surface height was made in the field during calm conditions. The process involved adjusting the length of the wire exposed to the air such that the output voltage of the low–pass channel averaged over a period of 1 min, was approximately -5 V. Then the wire was lowered into the water by small increments (about 2 cm) and for each step the wire length and the corresponding average voltage was recorded. The process was repeated until the output voltage reached +5 V. The conversion factor for the wave height was obtained from the slope of a linear fit to the calibration data as 8.83 cm/V for 1986–1988 data and as 10.0 cm/V for 1989 data. Our experience has shown that a gain factor of this magnitude is well suited for this site. In FM mode the analog recorder attenuates the signals to achieve the optimum signal to noise ratio. The attenuation factors that are relevant only to 1986 and 1987 data sets were 2.076 and 1.446, respectively. The calibration equations for the wave signal can be summarized as

$$\zeta = \zeta_h = \begin{cases} V_\zeta(V)18.32(cm/V), & \text{for 1986 data,} \\ V_\zeta(V)12.76(cm/V), & \text{for 1987data,} \\ V_\zeta(V)\ 8.83(cm/V), & \text{for 1988 data,} \\ V_\zeta(V)10.00(cm/V), & \text{for 1989 data,} \end{cases} \tag{3.2.4}$$

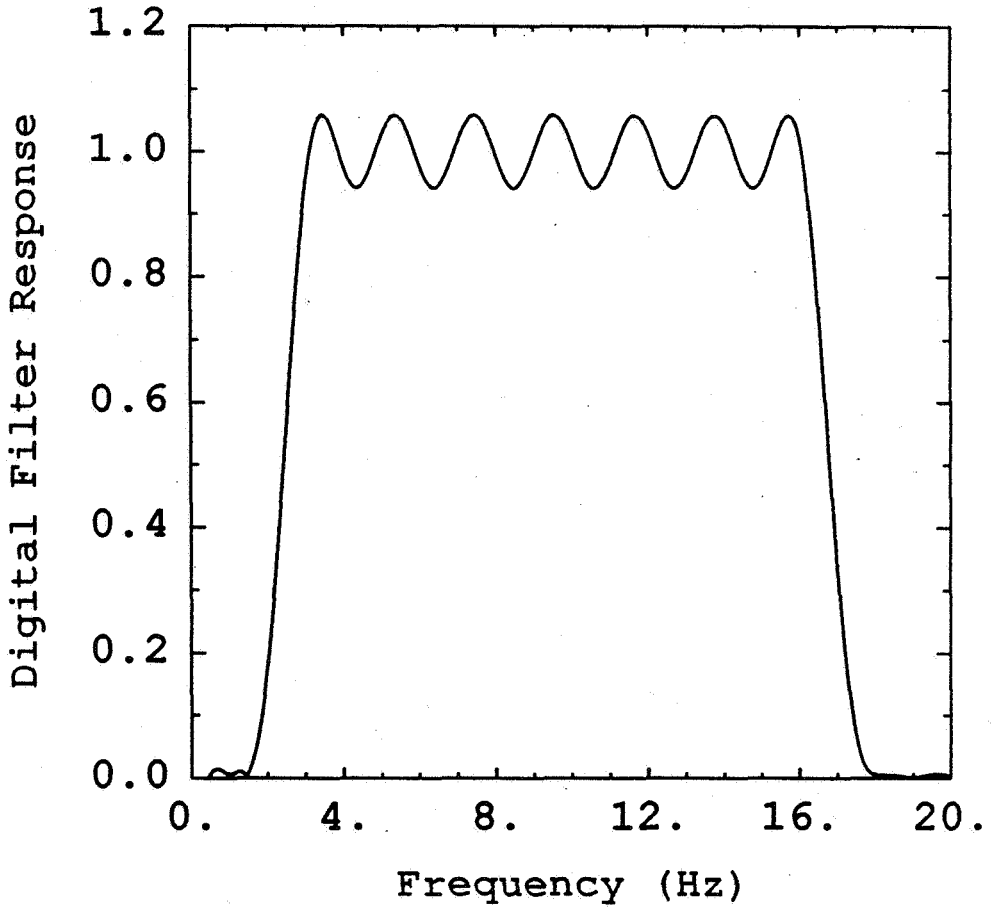

Figure 3.2.3: Frequency response curve for the 3–17 Hz band–pass digital filter (see Equation 3.2.3).

where V_ζ is the output voltage of the wave gauge recorded as the low–pass channel.

3.2.2 Propeller–Vane Anemometers

Wind data were collected at several heights. Low level observations (0.5 to 4.0 m above the mean water level) of the wind speed and direction were made by the Gill single propeller–vane anemometers (Holmes *et al*, 1964; Gill, 1975). A different type of device, the K–Gill twin propeller–vane anemometer (Ataktürk and Katsaros, 1989) was placed at heights ranging from 4.5 to 8.5 m. The K–Gill yields the wind speeds along the axes of its two propellers, one looking up and one looking down at angles of $\pm 45°$. A level sensor attached to the instrument measures the inclination angle of the propellers. In addition to these, the angular response characteristics of the propellers predetermined through wind tunnel studies, are required to obtain the vertical and the downstream horizontal components of the wind vector from which the wind stress (see Section 4.1) can be calculated. The method of resolving the wind components employed in this study is described by Ataktürk and Katsaros (1989).

There are various kinds of propellers and vanes that can be used with Gill anemometers. The type of the propeller used on the K–Gill system is critical for flux calculations. The diameter and the composition of the four–bladed helicoid–shaped propellers used were; 0.18 m polypropylene in 1986, 0.19 m polystyrene in 1987, and 0.22 m polystyrene in 1988–1989. The dimensions of the wind vane were 0.25 m by 0.25 m. For specifications, see Ataktürk and Katsaros (1989). The 0.22 m polystyrene propeller is similar to the $0.23m$ polystyrene propeller except for a slightly shorter distance constant of 1.0 m.) Calibration studies in a wind tunnel showed that the anemometer output voltage, V_a, and the wind speed, U', measured along a propeller axis were related via,

$$U' = V_a(V)3.74(ms^{-1}/V). \tag{3.2.5}$$

Since all the propellers had identical pitch of 0.30 m, Equation 3.2.5 is applicable to all data sets regardless of the kind of the propeller used.

When the wind blows at an angle δ with respect to the propeller axis, the measured wind speed must be compensated for the non–cosine angular response of the propeller. The angular response is defined as the ratio of the measured wind speed to the true wind speed (see Figure 3 in Ataktürk and Katsaros, 1989). For small δ, the angular response was nearly unity. Therefore, no correction was applied to the wind speed measured by the horizontally mounted Gill anemometer. However, in the case of the K–Gill anemometer, where δ was about 45° on the average for both propellers, this correction could not be omitted and was included in the K–Gill algorithm (see Ataktürk and Katsaros, 1989).

The level sensor of the K–Gill anemometer was calibrated using the setup in the wind tunnel. For a range of $\pm$ 3°, the calibration data could be well approximated by the linear fit,

$$\Delta\psi = V_l(V)3.85(°/V) - 0.33(°) \tag{3.2.6}$$

where $\Delta\psi$ is the tilt angle and V_l is the output voltage of the level sensor.

For momentum flux measurements by the eddy correlation method, the response of the instrument to high frequency fluctuations is critical. Generally, the frequency response of propeller anemometers is less than ideal for this purpose (e.g. Hicks, 1972; McBean, 1972; Garratt, 1975; Ataktürk and Katsaros, 1989). However, techniques have been developed to restore the phases and amplitudes of the output signals so that information at frequencies above the cutoff frequency of a slow–response sensor can be obtained. Conventional approach for frequency response correction is to consider the sensor as a simple

analog RC circuit with a time constant $\mathcal{T}$ (Gill, 1967; Hicks, 1972). The first order dynamic response of such a system is expressed by

$$\mathcal{T}\frac{dY}{dt} + Y(t) = X(t), \tag{3.2.7}$$

where X and Y are the input and the output of the system (or in this case, the true and the measured wind speed), respectively. The transfer function of this system for a known input signal can be easily determined. By applying the inverse transfer function to the spectrum of the output signal, the correction is completed. However, the time constant, $\mathcal{T}_p$ of a propeller depends on the wind speed as well as on the angle between the wind and the propeller stem, Ψ, of the wind, (see Figure 5 in Ataktürk and Katsaros [1989]). Therefore, in the present work, the corrections were made in the time domain according to

$$X(t) = Y(t) + \mathcal{T}_p(t)\frac{Y(t) - Y(t-\Delta t)}{\Delta t}, \qquad \text{for } t > 0, \tag{3.2.8}$$

assuming $X(0) = Y(0)$, and

$$\mathcal{T}_p = \frac{\mathcal{D}_p \cos^{-1/2}\Psi}{X(t)}, \tag{3.2.9}$$

so that instantaneous, rather than average, values of U and Ψ can be used. Here, $\Delta\, t$ is the time step between the data points and, $\mathcal{D}_p$ is the distance constant of the propeller for $\Psi = 0$. The cosine term in Equation 3.2.9 describes the variation of $\mathcal{D}_p$ with wind attack angle when Ψ is large (Hicks, 1972; Garratt, 1975; Ataktürk and Katsaros, 1989) as in the case of the K–Gill anemometer. For small Ψ, a linear dependence may be more appropriate (Hicks, 1972). The above set of equations which is nonlinear in X, can be easily incorporated into the K–Gill algorithm (Ataktürk and Katsaros, 1989) and solved by iteration. The technique works well as long as the signal to noise ratio is high and

$\Delta\ t \ll T_p$. Intercomparisons of the momentum fluxes measured during HEXMAX (DeCosmo *et al*, 1988; DeCosmo, 1991) by the K–Gill anemometer and a sonic anemometer showed that K–Gill results were lower by 10% to 20%. After corrections, in the frequency domain following Hicks (1972), to the K–Gill data the differences were reduced to 5% or less. The atmospheric stratification during HEXMAX was mostly neutral or slightly unstable. Since the eddies with dimensions smaller than the spacing between the propellers are not resolved, the performance of the K–Gill anemometer is expected to be poorer during stable conditions when a significant portion of the momentum flux come from small eddies.

3.2.3 Thermocouples

The dry–bulb, T_d, and the wet–bulb, T_w, temperatures were measured using thermocouples. The instrument is described by Shaw and Tillman (1980) in detail. The chromel–constantan sensors were 50 μm in diameter. The wet–bulb sensor was wrapped with cotton thread that was kept moist with a controlled flow of water from a reservoir. A pair of sensors was usually used at a height of 2 m. A second pair was mounted just below the lower propeller of the K–Gill anemometer, but far enough to prevent flow distortion. A thermocouple psychrometer and the K–Gill anemometer together provided the data to calculate the sensible and latent heat fluxes across the air–sea interface.

The thermocouple sensors were calibrated in water baths. During the experiments, their calibrations were periodically tested with an Assman type psychrometer. The linear calibration equations for the dry and wet sensors of the unit marked as $HEXP1$, were determined as

$$\left.\begin{aligned} T_d &= V_d(V)10.17(^\circ C/V) + 14.74(^\circ C), \qquad \text{for } 1987-1989 \text{ data,} \\ T_w &= V_w(V)10.08(^\circ C/V) + 10.01(^\circ C), \qquad \text{for } 1987-1989 \text{ data.} \end{aligned}\right\} \quad (3.2.10)$$

where V_d and V_w are the sensor output voltages. The calibrations for the unit marked as $HEXP2$, were

$$T_d = \begin{cases} V_d(V)\ 2.78(°C/V) + 13.97(°C), & \text{for 1986 data,} \\ V_d(V)10.05(°C/V) + 13.77(°C), & \text{for 1987-1989 data,} \end{cases} \tag{3.2.11}$$

and

$$T_w = \begin{cases} V_w(V)\ 2.78(°C/V) + 9.97(°C), & \text{for 1986 data,} \\ V_w(V)10.07(°C/V) + 9.74(°C). & \text{for 1987-1989 data,} \end{cases} \tag{3.2.12}$$

The large differences in gain factors between the two sets in Equation 3.2.11 or in Equation 3.2.12, are due to a modification in the amplifier electronics of the unit.

As mentioned in the previous section, for computation of the surface fluxes from atmospheric turbulence measurements, sensors with a short response time are required. Generally, a bare, fine wire thermocouple, such as the one used in this study to measure the sensible heat flux, meets this requirement. However, when the same thermocouple is used to measure the wet–bulb temperature, its response time may be reduced by a factor of 10 due to the water–soaked wick around it. The specific humidity, q in g/Kg, from which the latent heat flux is calculated, depends on the difference between the dry– and wet–bulb temperatures,

$$q = 622 * e/(P - e), \tag{3.2.13}$$

$$e = a_1 \exp\left[\frac{T_w\,(a_2 - T_w/a_3)}{(a_4 + T_w)}\right] - b_1(1 + b_2 T_w)P(T_d - T_w), \tag{3.2.14}$$

where e and P are the water vapor and atmospheric pressures (in mb), respectively, and a_1=6.1078, a_2=18.61, a_3=240.7, a_4=256.1, b_1=0.00066, and b_2=0.00115. These equations show that any difference between the dry– and

wet–bulb temperatures that may result from unmatched response times of the sensors, can cause large errors in the specific humidity and may significantly change the shape of the humidity spectrum (e.g. Shaw and Tilmann, 1980).

Matching the frequency responses of two sensors by speeding up the wet–bulb signal has been discussed by Sano and Mitsuta (1968), Shaw and Tillman (1980) and Tsukamoto (1986). The techniques they offered are based on the same principle that the dynamic responses of the fine wire thermometers can be described by a first order differential equation characterized by a single time constant (as in Equation 3.2.7).

The time constant can be determined theoretically (Sano and Mitsuta, 1968), but it may not be easy for a wet sensor due to the difficulty in estimating the weight and the effective diameter of the water column that surrounds the thermocouple (Tsukamoto,1986). The sensor response can also be determined experimentally from comparisons of the variance spectra with a fast response instrument. For thermocouples similar to ours (except for a diameter of 25 μm) and a wind speed of $7 m/s$, Shaw and Tillman (1980) determined the cutoff frequencies, f_c (half–power point in the variance spectrum), of the wet and dry sensors to be about 0.4 Hz and 4 Hz, respectively. Similar values were also obtained by DeCosmo (1991) through the intercomparisons of the psychrometer used in this study with a Lyman–α hygrometer. Therefore, the time constants, $\mathcal{T} = 1/2\pi f_c$, corresponding to the cutoff frequencies given above were determined as $\mathcal{T}_{d,7} = 0.04\ s$ and $\mathcal{T}_{w,7} = 0.4\ s$ where the subscript 7 indicates the wind speed in m/s.

Tsukamoto (1986) suggests a time constant of 0.1 s or less for both sensors to measure humidity fluctuations up to 1 Hz. Although our dry thermocouple had an adequate time constant, the traces of both sensors were corrected according to Equation 3.2.8 to match up the sensor responses. The variation of

the time constants with the wind speed was described by (see, Table 1 in Shaw and Tillman, 1980; Figures 4 and 5 in Tsukamoto, 1986)

$$\mathcal{T} = \mathcal{T}_7 \left(\frac{7}{X(t)} \right)^{-1/2} . \tag{3.2.15}$$

The effects on $\mathcal{T}_w$ of the surrounding temperature were neglected (see, Figure 5 in Tsukamoto, 1986).

3.2.4 Thermistors

The water temperature was measured using an array of thermistors with average depths of the sensors ranging from 0.30 to 0.80 m below the mean water level. The information from the sensor closest to the surface was used to determine the water surface tension and the temperature difference between air and water. The sensors were calibrated in the field using water baths. A linear calibration equation for the sensor used in this study was described by

$$T_{30} = \begin{cases} V_{30}(V)2.30(^\circ C/V) + 17.88(^\circ C), & \text{for 1986-1987 data,} \\ V_{30}(V)2.17(^\circ C/V) + 27.66(^\circ C), & \text{for 1989 data,} \end{cases} \tag{3.2.16}$$

where V_{30} is the output voltage of the thermistor at a mean depth of $0.30m$.

3.2.5 Surface Tension Measurements

During the experiments in 1987, the surface tension of the lake water was measured using a series of solutions of increasing spreading pressure (Adam, 1937). The solutions were composed of non–spreading pure mineral oil modified by increasing concentrations of n–dodecyl alcohol (Katsaros *et al*, 1989). Drops of solution were applied to the surface in order of increasing spreading pressure until spreading against pre–existing surfactants were observed. The surface tension, γ in mN/m, may be estimated from the spreading pressure, P in

mN/m, of the solution that spread first according to the relationship (Sverdrup *et al*, 1942, p. 70)

$$\gamma = 75.63 - 0.144T + 0.0221S - P, \tag{3.2.17}$$

where T is the sea water temperature in ^{o}C and S is the salinity in parts per thousand. Since the lake water is fresh water, the salinity term may be ignored. During this study, mostly #1 ($P = 0.42\ mN/m$) and occasionally #2 ($P = 0.83\ mN/m$) solutions were observed to spread first, i.e the tension of the water surface was very close to that of the clean fresh water. These solutions were given a post–experiment test against an independent set of solutions in 1988, and their specifications were found to be correct (Gucinski and Katsaros, personal communication).

3.2.6 Recording System

During the period of 1986–1988, the signals from the sensors were recorded on a HP 3968A instrumentation recorder. The wave signals were recorded in FM mode. The other signals were sent through a frequency shift keying (FSK) device that scans up to 16 channels of analog data at a total rate of 408 Hz and puts them in a sequential format which can be recorded directly on a single channel. The tape recorder also had a voice channel for observer's comments.

Development of a digital data logging system was completed in June 1989. The system consists of a filter box, a HP 6942A Multiprogrammer and a HP 9826 Computer/Instrument Controller. Up to 64 channels of analog voltage can be input to the filter box which contains interchangable low–pass filters with cutoff frequencies ranging from 5 to 50 Hz. The Multiprogrammer can be instructed to scan through these channels either sequentially or randomly. In sequential mode, all selected channels are digitized at the same rate. In random

mode, each channel may be assigned a specific sampling rate that is appropriate for that signal. If the sampling rates vary widely, as in our case, the latter approach can save large amounts of data storage space. The selected signal which must be within $\pm 10.24\ V$, is digitized with a resolution of 5 mV (i.e. 12 *bit* converter). The Multiprogrammer is capable of taking 18,000 readings per second and can store up to 65,536 digital readings in its internal memory before it interrupts the controller for transfer of data. In this way, while data acquisition continues in the background, the controller can process, graphically display, and store the most recent block of data. Once data acquisition is completed the raw data are stored on a 1/4 *inch* cartridge tape with a capacity of 65 *Mbytes*.

3.2.7 Video Camera and Recorder

Visual records of the fine features on the water surface were made by a Panasonic WV–3110 color video camera and a Panasonic NV–8200 video cassette recorder. The comments by the observer were recorded on the audio channels of both the instrumentation and the video recorders. In this way, the two recorders could be synchronized during playback. The video records were used to identify sections of the data affected by breaking events, boat waves, sea weeds and surface slicks.

3.2.8 Computer facilities

The data were processed in the computer facilities of the Department of Atmospheric Sciences, University of Washington. The analog signals were originally digitized on a Raytheon 704 computer using a 12 *bit* analog to digital converter. The digitized data were written on 1/2 *inch*, 7 *track* magnetic tapes and were transferred to a Prime 9955 computer where the software development had been done. Preliminary analyses of the 1986–1987 data sets indicated a malfunctioning of the analog to digital converter. Therefore, the digitization

process of these sets had to be repeated and was done on the new digital data acqusition system. Analyses of all data sets were completed on a Masscomp 5520 computer.

3.3 Description of the Data Sets Analyzed

The field data for this study were collected between 1986 and 1989 at Lake Washington, Seattle. The environmental conditions during these 51 data sets each approximately 2 hr long, are summarized in Table 3.1. All observations were made during northerly winds. The wind speeds, averaged over the whole run and adjusted to the 10 m height, were in the range $2 \leq U_{10} \leq 7\ m/s$. The water temperatures near the surface (0.30 m below the mean water level on the average) were mostly between 21 and 24 $^{\circ}C$, except during May 1987 when it was about 15 $^{\circ}C$. The differences betweeen the air temperature (at 10 m height) and the water surface temperature varied between $\pm$ 5 $^{\circ}C$, approximately, indicating that the experimental conditions included all possible cases of atmospheric stratification, i.e. unstable, neutral and stable. The atmospheric stratification parameter, z/L, calculated for each data set was mostly within the range $-0.7 \leq z/L \leq 0.5$, except during very light winds, $U_{10} \approx 2\ m/s$, when values of $|z/L| \geq 2$ were found.

In general, the growth stage of the observed wave fields varied from relatively mature to fully developed as measured by the wind forcing parameter $1 \leq U_{10}/C_p \leq 2.5$, where C_p is the phase speed of the dominant waves. Some cases with $U_{10}/C_p \leq 1$, i.e. decaying wave fields were observed during decreasing wind conditions. On May 18 1987, under the action of relatively strong winds the wave field reached its fully developed stage with a significant wave height of 0.32 m, a spectral peak frequency of 0.45 Hz, and a wavelength of about 8 m. At our experimental site, these values may be considered as the extremes during northerly winds. Generally, the significant wave heights do not

Table 3.1: Description of the data sets analyzed.

	DATE	TIME	$U \pm SD$	T_{a-s}	T_s	Q_{a-s}	Q_s	DOMINANT f_p	λ_p	ak	WAVE $H_{1/3}$
		Local	*m/s*	*°C*	*°C*	*g/kg*	*g/kg*	*Hz*	m		*m*
1	8/25/86	15:32	4.3±0.5	1.2	23.3	8.0	18.0	0.67	3.46	0.09	0.13
2	8/25/86	17:36	4.7±0.9	1.2	23.1	7.5	17.9	0.70	3.22	0.09	0.12
3	8/26/86	11:20	4.2±0.5	1.8	23.1	8.0	17.8	0.75	2.93	0.08	0.09
4	8/26/86	15:00	5.1±0.5	2.7	23.8	8.1	18.6	0.64	3.83	0.10	0.13
5	8/27/86	12:03	3.3±1.0	2.6	23.3	8.1	18.0	0.70	3.21	0.07	0.10
6	8/27/86	14:21	2.1±0.4	4.0	23.8	9.1	18.7	0.67	3.66	0.06	0.08
7	9/11/86	18:35	5.8±1.2	-4.2	20.5	10.1	15.2	0.55	5.18	0.12	0.18
8	9/12/86	14:41	4.3±0.6	-1.8	21.0	11.3	15.7	0.66	3.75	0.10	0.13
9	9/12/86	16:43	1.8±0.5	-1.2	21.0	11.4	15.7	0.52	3.95	0.06	0.10
10	5/ 5/87	16:25	5.2±0.6	3.6	15.2	3.2	10.8	0.56	4.92	0.06	0.09
11	5/ 6/87	13:00	5.1±0.5	3.9	15.0	3.2	10.7	0.63	3.93	0.05	0.06
12	5/ 6/87	15:11	4.9±0.4	4.9	15.1	3.3	10.7	0.62	4.14	0.05	0.07
13	5/ 7/87	13:10	4.5±0.6	5.0	16.1	3.2	11.4	0.65	3.95	0.09	0.12
14	5/15/87	12:30	5.8±1.2	-3.6	16.3	7.4	11.6	0.55	5.24	0.12	0.19
15	5/15/87	14:45	5.2±1.3	-2.9	16.4	8.0	11.7	0.59	4.52	0.11	0.17
16	5/18/87	14:13	6.1±1.8	-4.3	14.9	4.4	10.6	0.48	6.94	0.14	0.25
17	5/20/87	13:53	5.1±0.6	-0.2	16.5	3.0	11.7	0.58	4.74	0.11	0.17
18	8/19/88	15:39	5.9±0.6	-3.4	21.6	7.5	16.2	0.60	4.42	0.13	0.19
19	8/19/88	16:40	6.5±1.0	-3.4	21.7	7.7	16.3	0.57	4.85	0.14	0.21
20	8/19/88	17:47	6.9±1.2	-4.3	21.7	8.4	16.3	0.53	5.64	0.14	0.24
21	8/20/88	16:38	3.6±0.9	-3.8	21.3	8.8	15.9	0.65	3.80	0.08	0.12
22	8/20/88	17:50	5.7±0.7	-3.8	21.5	8.8	16.1	0.60	4.37	0.15	0.22
23	8/21/88	11:35	4.5±0.6	-4.1	21.3	8.0	15.9	0.67	3.81	0.10	0.15
24	8/21/88	13:27	5.4±0.5	-2.7	21.5	8.2	16.1	0.60	4.59	0.13	0.19
25	8/21/88	14:35	5.3±0.6	-2.3	21.7	8.3	16.3	0.61	4.16	0.12	0.19

(continued)

Table 3.1: (continued)

	DATE	TIME	$U \pm SD$	T_{a-s}	T_s	Q_{a-s}	Q_s	DOMINANT f_p	λ_p	ak	WAVE $H_{1/3}$
		Local	*m/s*	*°C*	*°C*	*g/kg*	*g/kg*	*Hz*	m		*m*
26	8/22/88	11:05	5.5±0.6	-2.3	21.9	7.8	16.6	0.58	4.65	0.13	0.20
27	8/22/88	14:57	6.1±0.7	0.2	22.2	7.4	16.9	0.56	4.96	0.12	0.19
28	8/22/88	16:21	6.3±0.5	0.7	22.2	7.2	16.9	0.55	5.18	0.14	0.22
29	8/23/88	11:44	7.1±0.5	0.1	22.3	6.9	17.0	0.54	5.43	0.13	0.22
30	8/23/88	13:03	6.1±0.6	1.5	22.3	6.5	17.0	0.57	4.90	0.12	0.19
31	7/ 5/89	15:51	5.7±0.6	-0.3	20.4	8.3	15.1	0.59	4.50	0.12	0.18
32	7/ 5/89	18:36	6.3±0.6	-0.7	20.1	7.9	14.8	0.54	5.27	0.12	0.20
33	7/ 6/89	14:31	5.9±0.8	0.3	20.8	8.3	15.5	0.59	4.56	0.11	0.18
34	7/11/89	12:45	2.9±0.8	-1.1	21.8	8.0	16.5	0.67	3.88	0.06	0.08
35	7/11/89	15:07	3.2±0.9	0.6	22.1	8.8	16.8	0.62	4.11	0.07	0.10
36	7/12/89	11:20	4.5±0.6	0.6	21.8	7.4	16.4	0.69	3.33	0.09	0.12
37	7/12/89	14:51	3.7±0.6	1.3	22.5	8.0	17.2	0.62	4.13	0.08	0.12
38	7/18/89	16:50	6.6±0.9	0.7	20.8	5.3	15.5	0.56	4.95	0.13	0.21
39	7/18/89	19:02	6.1±0.7	-0.7	20.9	5.9	15.5	0.55	5.22	0.12	0.21
40	7/19/89	17:05	7.0±0.8	-1.1	22.1	8.2	16.7	0.57	4.96	0.13	0.21
41	7/19/89	19:39	4.6±0.9	-2.1	21.7	8.3	16.4	0.57	4.87	0.12	0.18
42	7/21/89	14:56	2.4±0.7	-2.3	21.5	8.9	16.2	0.74	3.27	0.06	0.08
43	7/21/89	18:14	6.0±0.7	-1.7	21.7	9.1	16.3	0.55	5.15	0.12	0.20
44	7/24/89	13:35	4.0±1.3	-0.1	21.6	8.9	16.2	0.62	4.03	0.10	0.13
45	7/25/89	12:27	4.4±0.7	-0.1	22.4	8.5	17.0	0.66	3.62	0.09	0.13
46	7/25/89	15:47	4.9±0.4	2.0	22.7	9.2	17.4	0.59	4.51	0.10	0.14
47	8/ 3/89	19:13	4.1±0.9	-1.5	21.0	6.4	15.7	0.65	3.76	0.10	0.15
48	8/ 4/89	20:18	4.6±0.8	-1.8	21.8	7.1	16.5	0.60	4.30	0.11	0.16
49	8/ 7/89	17:00	5.8±1.1	2.1	22.4	9.3	17.1	0.58	4.63	0.11	0.18
50	8/10/89	18:47	6.0±0.7	-2.0	20.7	7.6	15.4	0.56	4.97	0.12	0.20
51	8/11/89	18:12	5.7±0.8	-0.9	22.0	9.3	16.7	0.57	4.98	0.12	0.19

exceed 0.20 m, and the peak frequency is about 0.55 Hz corresponding to a wavelength of about 5 m.

Analyses of the long waves and the surface fluxes of momentum, sensible heat and latent heat were carried through for all the data sets listed in Table 3.1. Studies of small scale waves including their suppression by surface slicks were conducted through the data sets of 1986 and 1987 which covered most of the range of the environmental parameters observed overall.

CHAPTER 4: METHODS OF DATA ANALYSIS

In this chapter, the methods that were used in the analyses of the field data are described. Data processing included calculating the fluxes of momentum, sensible heat and latent heat in the surface layer; adjusting the measured wind speed, temperature and specific humidity to a reference state, i.e. 10 m height and neutral atmospheric stratification; and determining the wavenumber and intrinsic frequency spectra of water surface waves. For various tasks, Fourier transformations of the time series were necessary and the procedure followed is described in the next section.

4.1 Fourier transformations

Some terminology that will be frequently used in the following sections are defined below. More details about the Fourier analyses are given by Brigham (1974). Fourier representation of a time series; $X(0), X(\Delta t), X(2\Delta t), \ldots X((N-1)\Delta t)$, consisting of $N(= 2^i \; ; i = \text{integer})$ points sampled at every Δt (in seconds), is given by

$$X(l\Delta t) = \sum_{m=0}^{N/2} a_{Xm} \cos \frac{2\pi lm\Delta t}{N\Delta t} + b_{Xm} \sin \frac{2\pi lm\Delta t}{N\Delta t}, \qquad (4.1.1)$$

where the Fourier coefficients, a and b, are unique for each record. The frequencies, $f = m/N\Delta t$, in Equation 4.1.1 range from 0 to $1/2\Delta t$ Hz, i.e. the Nyquist frequency. These coefficients can be obtained by applying a fast Fourier transform (FFT) algorithm to the time series.

The quantity

$$A_{Xm}^2 = \frac{1}{2}(a_{Xm}^2 + b_{Xm}^2), \qquad (4.1.2)$$

is the contribution to the total variance, $\overline{X^2}$, by the m–th harmonic. The energy density spectrum, $E(f)$, of X is obtained by following Parseval's theorem,

$$\overline{X^2} = \int_0^{1/2\Delta t} E_X(f)df \approx \frac{1}{N}\sum_{l=0}^{N-1}[X(l\Delta t) - \overline{X}]^2 \approx \sum_{m=0}^{N/2} A_{Xm}^2, \qquad (4.1.3)$$

where $\overline{X}$ is the mean of the time series.

For the case of two variables, X and Y, each having a time series that can be represented as in Equation 4.1.1, the quantity

$$C_{XYm}^2 = \frac{1}{2}(a_{Xm}a_{Ym} + b_{Xm}b_{Ym}), \qquad (4.1.4)$$

is the contribution to the total covariance, $\overline{XY}$, by the m–th harmonics of the Fourier transforms of X and Y. The cospectrum, $\Phi_{XY}(f)$, of X and Y is obtained from the relation

$$\overline{XY} = \int_0^{1/2\Delta t} \Phi_{XY}(f)df = \frac{1}{N}\sum_{l=0}^{N-1}[X(l\Delta t) - \overline{X}][Y(l\Delta t) - \overline{Y}] = \sum_{m=0}^{N/2} C_{XYm}^2, \qquad (4.1.5)$$

where $\overline{X}$ and $\overline{Y}$ are the means of the two time series. The correlation coefficient, R_{XY} which expresses the strength of the association between X and Y can be found as

$$R_{XY} = \overline{XY}/(\overline{X^2Y^2})^{1/2}. \qquad (4.1.6)$$

In the present study, the Fourier coefficients were determined by an FFT algorithm, called $FFAFFS$ (see Cooley and Dolan, 1979). The algorithm includes two subroutines: FFA does the forward fast Fourier transformation and finds the coefficients in Equation 4.1.1; FFS performs the inverse transformation, i.e. given the Fourier coefficients it constructs the corresponding time series.

Prior to a forward Fourier transformation, the mean and any linear trend of a time series were removed and a Hanning window was applied (see Brigham, 1974). The total variances before and after the application of the window were calculated and the windowed data points were scaled to conserve the total variance. When smoothing was desired, the $N/2$ spectral estimates were band averaged to produce N_S smoothed estimates. The nonoverlapping frequency bands were chosen such that mid–frequencies of the bands were equally spaced on a logarithmic axis. Generally, $N_S = 40$ was used. For long wave spectra, $N_S = 100$ was taken to obtain finer resolution in the vicinity of the spectral peak.

4.2 Surface fluxes and environmental parameters

The surface fluxes were determined directly by the eddy–correlation method (see Busch, 1973), where the vertical transport of an entity by the atmospheric turbulence is obtained from the covariance between that entity and the vertical component of the wind. The covariance may be calculated either in the temporal domain or in the frequency domain. In this study the latter approach was used because it provides information about the contributions to the total flux from eddies with different frequencies. Since the general appearance of the ensemble average of nondimensional turbulence spectra (e.g. Busch, 1973) from surface layer shows similarities that depend only on the atmospheric stratification, the measurements can be tested against these spectral forms to determine the instrument response or to investigate the intermittent nature of the turbulent fluxes.

The fluxes of momentum, sensible heat and latent heat were calculated from

$$\tau = -\rho \int_{f_1}^{f_2} \Phi_{uw}(f)df, \tag{4.2.1}$$

$$H_S = \rho C_p \int_{f_1}^{f_2} \Phi_{wT}(f)df, \tag{4.2.2}$$

$$H_L = \rho L_e \int_{f_1}^{f_2} \Phi_{wq}(f)df, \tag{4.2.3}$$

respectively. The limits, f_1 and f_2, of integration should be chosen such that all frequencies contributing to the fluxes are included. Depending on the atmospheric stratification, contributions to surface fluxes may come from eddies with nondimensional frequencies of the order of $10^{-3} \leq n \leq 10$ (e.g. Miyake *et al*, 1970; Busch, 1973; Wyngaard, 1973), where $n = zf/\overline{U}$ and $\overline{U}$ is the mean wind speed measured at a height z. For the data sets presented in Table 3.1, $z/\overline{U}$ was of the order of unity, giving $n \approx f$. In a recent review, Donelan (1990) suggested that for the marine boundary layer fluxes, the most appropriate sampling interval is about 20 *min*, but each 20 *min* estimate so poorly represents the mean flux that as many consecutive 20 *min* samples as the constraint of stationarity will allow should be averaged. Effects of secondary roll flows in the planetary boundary layer on the results obtained from short period observations are discussed by Brown (1980). Large and Pond (1981) suggested an averaging period of about 1 *hr* (i.e. pooling the results from 3 consecutive samples each 20 *min* long). In accordance with these suggestions, in the present study the sampling interval was taken as approximately 17 *min* (corresponding to $f_1 \approx 10^{-3}$ *Hz*) and depending on the steadiness of the conditions up to 4 consecutive samples were averaged.

The ideal upper limit, $n \approx f_2 = 10$ *Hz*, of integration in Equations 4.2.1–4.2.3 is above the frequency range of our flux measuring system consisting of the K–Gill anemometer and a thermocouple psychrometer. The limitation of the system results from the slow frequency responses of the propellers and the

thermocouples, in particular that of the wet–bulb sensor, as well as from the physical separation between the sensors (see Chapter 3; Ataktürk and Katsaros, 1989). The resulting errors in measured fluxes were partially compensated by speeding up the signals from the K-Gill propellers and the thermocouples (see Sections 3.2.2 and 3.2.3). However, due to the limited spatial resolution of the system, above 1 Hz the signal to noise ratio was low and contributions to the fluxes above this frequency could not be measured. Therefore, although the Nyquist frequency was 4 Hz the upper frequency limit was chosen as $f_2 = 1\ Hz$. Error analyses presented by Ataktürk and Katsaros (1989) show that this limitation may become more serious during stable atmospheric stratification when contributions at frequencies $> 1\ Hz$ may constitute a significant portion of the total fluxes.

For each data set the means; U_z, T_z and q_z at the measurement height, z, were determined. The variances of these parameters were found as described by Equation 4.1.3. Ignoring the surface currents induced by winds and waves, U_s was set to zero. T_s was approximated by the bulk water temperature. q_s was calculated from Equations 3.2.13 and 3.2.14 assuming that $T_d = T_w = T_s$ and the relative humidity is 100% at the surface. With the surface fluxes calculated from Equations 4.2.1–4.2.3, the characteristic scales; u_*, T_* and q_*, of the wind speed, temperature and specific humidity, respectively, and Obukhov length, L, were determined according to Equation 2.5.1. The characteristic roughness lengths; z_0, z_t and z_q were calculated as in Equation 2.5.6 with the stratification effects given by Equation 2.5.7. Using these last two equations and the mean values of U_z, T_z and q_z at the measurement height, the averages; U_{10}, T_{10} and q_{10} corresponding to a height of 10 m and neutral stratification were found. The bulk transfer coefficients; C_{DN}, C_{HN} and C_{EN} for neutral statification and 10 m height, were obtained from Equation 2.5.8 using the mean values adjusted to the reference state.

4.3 Long gravity waves

Following Phillips (1981b) and Donelan *et al* (1985) the long wave field was studied through the surface height fluctuations, $\zeta(t)$, with frequencies $f = \omega/2\pi < 4\omega_p/2\pi$, ω_p indicating the frequency of the spectral peak. For the data sets analyzed, the peak frequency was approximately 0.5 Hz (Table 3.1) therefore, characteristics of the long waves were calculated from Fourier components with $f < 2$ Hz. The Nyquist frequency was 4 Hz, i.e. the time series was sampled at every 1/8 s.

The energy density spectra of the long gravity waves were calculated from samples 1024 s ($\approx$ 17 min) long. Uncertainties in the measured variance of surface elevations were estimated following Donelan and Pierson (1983) who showed that the distribution of $A^2_{\zeta m}$ (Equation 4.1.2) can be described by a chi square distribution with two degrees of freedom. Given one $A^2_{\zeta m}$, the value of the spectrum is not known to within a factor of 58 at the 90% confidence level; when 16 values are averaged the degrees of freedom is 2×16 and the factor is reduced to 2.3 at the same confidence level (Donelan and Pierson, 1983). Therefore, the spectral estimates must be smoothed by some kind of averaging. In the present study, smoothing was done both over frequency (Section 4.1.1) and over samples from consecutive spectra.

The wavelength, Λ_p, and the phase speed, C_p corresponding to the spectral peak frequency were found using the linear dispersion relation in Equation 2.1.31. Since the wind forcing during the experiments was in the range $1 \leq U_{10}/C_p \leq 2.5$, the finite amplitude effects on the phase speeds described by Equation 2.1.33 were neglected (see Donelan *et al*, 1985). The significant wave height was estimated as $H_{1/3} = 4\overline{\zeta^2}^{1/2}$. According to Donelan and Pierson (1983), under steady conditions and for a record length of 17 min, the uncertainties in ω_p and $H_{1/3}$ due to the sampling variability are typically about $\pm 5\%$ and $\pm 12\%$, respectively at the 90% confidence level.

Time series of the horizontal component of orbital velocity, U_ζ, and that of vertical acceleration, $\ddot{\zeta} = \partial^2\zeta/\partial\zeta^2$, due to the long gravity waves were constructed as described by Ataktürk (1984) and Ataktürk and Katsaros (1987). This information was used for correcting the Doppler frequency shifts experienced by the small scale waves. Briefly, for a monochromatic wave train, $\zeta(t)$, with radian frequency ω_o; $U_\zeta(t) = \omega_o\zeta(t)$ and $\ddot{\zeta}(t) = -\omega_o^2\zeta(t)$. For a random wave field, $U_\zeta(t)$ (or $\ddot{\zeta}(t)$) was determined by: finding the Fourier coefficients, $a_{\zeta m}$ and $b_{\zeta m}$ for $\zeta(t)$ (Equation 4.1.1); multiplying the coefficients of each Fourier harmonic by its frequency $\omega_m = 2\pi m/N\Delta t$ (or $-\omega_m^2$); and, taking the inverse Fourier transform of this new Fourier series. The error in these estimates resulting from using a linear wave theory is of the order of the long wave slope which was typically about 0.1 during this study. Our previous experience (Ataktürk, 1984; Ataktürk and Katsaros, 1987) has shown that for the narrow–band spectra observed, U_ζ and $\ddot{\zeta}$ can be determined by including the contributions from harmonics with frequencies up to about $3\omega_p$. The higher harmonics were excluded by setting their coefficients to zero. The resulting time series of U_ζ and $\ddot{\zeta}$ had the same sampling rate as that of ζ.

4.4 Short gravity–capillary waves

High frequency part, ζ_h, of the wave signal was processed using the techniques that we have developed earlier. The procedure used in the present investigation closely follows that described by Ataktürk (1984) and Ataktürk and Katsaros (1987), except for the estimation of the surface drift effective in advection of the small scale waves. In this section the general approach and its new aspects are discussed.

The time series of the short gravity–capillary waves was obtained from the original wave height data sampled at a high rate (128 Hz) by applying a digital band pass (3–17 Hz) filter (see Section 3.2.1). These frequencies are subject

to Doppler shifts due to the motions of the underlying surface which must be corrected for. Doppler corrections were made using the most common approach, i.e. the frequency domain technique (Sinitsyn *et al*, 1973; Reece, 1978; Ataktürk, 1984; Stolte, 1984, 1989; Richter and Rosenthal, 1986; Ataktürk and Katsaros, 1987). Comparisons of this technique with the alternative approach of Evans and Shemdin (1980) are given by Ataktürk (1984) and Ataktürk and Katsaros (1987). General description of the Doppler correction schemes are also given in Section 2.3.5.

At our experimental site the surface currents, U_s, responsible for the advection of small scale waves were the horizontal component of the long–wave orbital velocity, U_ζ, the wind drift, U_w, and the wave mass transport (Stokes drift), U_{St} (Section 2.3). Traditionally, U_ζ has been estimated from the long wave height using a linear wave theory (as discussed above) and the total surface drift has been approximated by $U_w + U_{St} = 0.03U_{10}$. The review presented in Section 2.3 shows that these estimates are in good agreement with laboratory and field observations and they have been used for Doppler shift corrections. However, a point that has not been taken into account in correcting the Doppler shifts is the differential advection of the short waves by the wind drift (Section 2.3.6; Stewart and Joy, 1974; Plant and Wright, 1977, 1980; Donelan, 1978; Donelan *et al*, 1985; Smith, 1986, 1990). For the range of wavelengths considered here, 0.38 to 0.03 m, these effects may vary approximately from 90 to 50%. Therefore, in this study the wind drift and the Stokes drift were estimated separately and differential advections of the short waves were included. Having no direct quantitative measurements, the waves and the wave– and wind–induced currents were assumed to be in the mean direction of the wind. This assumption in particular considering the variability in the directions of the small scale waves, may be frequently violated. Therefore, seeking an overall accuracy better than 10–15% cannot be justified. Hence, in the present study of surface

waves the nonlinear terms proportional to the long wave steepness, $AK \approx 0.10$ typically, and their effects of less than 10% were ignored.

The mean surface value of U_w was estimated from $0.6u_*$ (Kawai, 1979; Plant and Wright, 1980; Wu, 1983; Donelan *et al*, 1985) and following Plant and Wright (1977, 1980) a short wave component with wavelength λ was assumed to be advected by the value of the wind drift evaluated from Equation 2.3.27 at a depth $z = 0.044\lambda$. A logarithmic velocity profile as in Equation 2.3.27 (Shemdin, 1972; Plant and Wright, 1977,1980) is only an approximate representation of the strong shear current in a very thin layer just beneath the surface, the existence of which has been well established (McLeish and Putland, 1975; Wu, 1975, 1984; Okuda *et al*, 1977; Donelan, 1978; Okuda, 1982; Donelan *et al*, 1985). The flow in the subsurface boundary layer, in a manner similar to the turbulence in the atmospheric surface layer, can be scaled by the surface value of the drift current and the thickness of the viscous sublayer (Jones and Kenney, 1977). Depending on the application the flow characteristics can be represented by any one of the profiles such as linear–logarithmic, purely logarithmic, exponential and error function–like profiles, generally with little effect on the results (e.g. van Gastel *et al*, 1985; Smith, 1986). In this investigation, 8 short gravity–capillary wavelengths were considered: 3, 5, 8, 12, 17, 23, 30 and 38 *cm*. Since most of the shear current is confined to a layer at most 2 *mm* in thickness (e.g. Phillips, 1977; also see the references above), the relative current depths for $\lambda \geq 4.5$ *cm* will be larger than the thickness of the strong shear layer. Therefore, for the purpose of this study, the particular form of the drift profile inside the viscous layer was not critical.

Discussions above were in terms of ensemble averages. Characteristic scales of the wind drift may significantly change along the phase of the underlying long waves due to straining by the divergence of the orbital velocity field and due to the modulation of the surface roughness and tangential wind stress at the wavy

surface. Turbulent and mean velocity measurements under waves subjected to wind stress (Shemdin, 1972; Jones and Kenney, 1977; Donelan, 1978) have shown that long wave orbital velocities play little or no direct role in the flux of momentum and do not affect the shear current profile.

The effects of straining on various parameters are described by Phillips (1977). Depending on the steepness, AK, of the underlying long wave and the ratio U_w/C_p, the drift current may be significantly augmented with a maximum at the long wave crest. For $AK = 0.1$ and $U_w/C_p = 0.05$ which are typical of our conditions, the variations in the surface value of U_w along the long wave profile is about 10%. Variations in short wavenumber due to straining is also of the same order of magnitude and those in short wave intrinsic frequency are much smaller, $\propto (AK)^2$ (Phillips, 1977). Therefore, these effects of straining by the long wave orbital velocities were neglected.

Implications of a variable wind stress and surface roughness on the wind drift have been theoretically investigated by Smith (1986, 1990). His results indicated that augmentation of the wind drift at the surface caused by these processes can be much stronger than the effects of straining. However, his findings on the depth and time scales of the response of the wind drift layer to this augmentation were not certain and were sensitive to various ill defined parameters that must be verified experimentally. Considering that the depth scales relevant to the wavelengths studied were mostly much greater than the thickness of the wind drift layers observed, as a first approximation the wind drift layer was assumed to be uniform along the phase of the long waves.

The effects of straining by the orbital velocities of long waves and the variable wind stress and surface roughness were assumed to be important primarily for amplitude modulations of short waves (Smith, 1990) and for enhancement of incipient breaking of small scale waves by the augmented wind drift (Banner and Phillips, 1974). It should be noted that when wave breaking occurs, the

above arguments about the wind drift (see Banner and Phillips, 1974; Okuda *et al*, 1977) as well as the linear wave theory are no longer valid. Therefore, breaking waves were noted from video records of the water surface at the location of the wave gauge. The breaking events were also identified in the data using a scheme we have developed earlier (Weissman *et al*, 1984) and excluded from the results. Breaking waves will be investigated in a later study.

Stokes drift, U_{St}, is generally a small quantity. However, its effect is cumulative and decays slowly with depth; therefore, it should not be neglected (Donelan 1978; Donelan *et al*, 1985). U_{St} was estimated from the long wave spectra according to Equation 2.3.25 (Bye, 1967; Kenyon, 1969). Calculations were done over the full length of a data set with a sampling interval of 5 $min.$ As noted in Section 2.3.2, contributions to Stokes drift mainly come from the Fourier components in the vicinity of the spectral peak, and the error introduced by neglecting contributions from the short gravity–capillary waves is insignificant (e.g. Wu, 1983). Typically, U_{St} was about 2–4 cm/s or 25% of the total drift at the surface at most.

For Doppler shift corrections, a time series of the short wave spectral energy density, $E(\sigma)$, was created. This procedure was identical to that described by Ataktürk (1984), Weissman *et al* (1984) and Ataktürk and Katsaros (1987). Fourier transformation of $\zeta_h(t)$ was done using 64 data points at a time. The corresponding sampling interval was 0.5 s. Therefore, the fundamental and Nyquist frequencies were 2 Hz and 64 Hz, respectively. The consecutive 64–point FFTs were overlapped by 75%, giving one spectrum every 0.125 s. Note that the time series of wind speed and long wave parameters (heights, orbital velocities and vertical accelerations) were constructed with the same resolution. Typically, the dominant waves at our experimental site had a period of about 2 s (Table 3.1). Hence, we obtained 16 estimates of the short wave spectra per long wave period.

Doppler corrections were made using portions of the data where wind speed and direction were steady and the changes in the wave field were gradual. For each time step of the process, the instantaneous values of $U_\zeta(t)$ and $\ddot{\zeta}(t)$ corresponding to mid–time of the FFT blocks were used. U_{St} and U_w were treated as constants and approximated by their average values appropriate for that portion of the data set. For each time step of 0.125 s, the surface current, U_s, effective in short wave advection was calculated from Equation 2.3.3 according to the descriptions given above. When $U_s \leq -15\ cm/s$, due to the existence of multi–valued solutions to the pair of Doppler Equations 2.3.4 and 2.3.5 (e.g. Ataktürk, 1984; Ataktürk and Katsaros, 1987), processing was continued with the next time step. The intrinsic frequencies, ω_i, corresponding to the preassigned wavelengths ($\lambda_i = 2\pi/k_i$ =3, 5, 8, 12, 17, 23, 30 and 38 cm) were determined from modified dispersion relations (Equations 2.3.5). Using Equation 2.3.4, for each pair of k_i, ω_i an equivalent Doppler shifted frequency, σ_i, was found. For the range $2 \leq \sigma_i/2\pi \leq 10\ Hz$, $E(\sigma_i)$ was obtained by linear interpolation from two adjacent measured spectral energy densities, $E(\sigma)$. The intrinsic frequency spectra, $E(\omega_i)$, can be determined from $E(\sigma_i)$ as described by Equation 2.1.36. In the present analyses, a similar conversion was used to obtain the wavenumber spectra, $E(k_i)$.

The process of determining the corresponding apparent and intrinsic frequencies described above was the inverse of the general approach followed by us and others previously. In the more customary approach, the apparent frequencies separated by a fixed interval are used to determine the intrinsic frequencies. Since the Doppler current is not uniform and the relation between apparent and intrinsic frequencies is not linear, the intrinsic frequency corresponding to a fixed apparent frequency varies for each time step. Therefore, for each step every calculated intrinsic frequency must be saved for further analysis. Later

these intrinsic values are sorted into some frequency bins. In the present approach, we start with preassigned wavelengths, i.e. fixed intrinsic frequencies and wavenumbers, and progress in the opposite direction to determine the apparent frequencies corresponding to these preassigned values. Both approaches produce the same results. However, the advantage of the present approach is that the results can be stored in a compact form and later analyses can be carried out with significantly reduced efforts. The experimental results obtained with these techniques are presented in Chapter 5.

CHAPTER 5: RESULTS AND DISCUSSIONS

The results obtained from this study are presented and evaluated in the following order. The atmospheric turbulence measurements are examined through the statistics of turbulence variances and characteristic roughness lengths to determine the quality of the collected data (Section 5.1). Statistics of the long–wave parameters and the form of the wave spectra near the spectral peak are used to test the applicability of available wave prediction models to our conditions (Section 5.2). Another independent estimate of the surface roughness length, $z_{o\zeta}$, is obtained from wave observations and is compared to the results of Section 5.1 and other studies (Section 5.3). The bulk transfer coefficients are determined using atmospheric turbulence and wave measurements, and are compared to the results from other studies (Section 5.4). Intrinsic frequency spectra of short gravity–capillary waves and attenuation of wind waves by surface films are investigated in Sections 5.5.

5.1 Atmospheric Turbulence and Surface Fluxes

The experimental data sets summarized in Table 3.1 consisted of observations carried out over approximately 100 hours. During the periods of data acquisition the wind direction was always from NNW along the long axis of the lake. This provided a fixed, limited fetch throughout the experiments. Therefore, these data sets may be considered as collected from a *natural laboratory* under different conditions of wind speed, atmospheric stratification and sea state. Except during gusty periods on May 18 1987, the wind speeds encountered were less than 8 m/s. On the other hand, the atmospheric stratification varied within the range, $-0.8 \leq z/L \leq 0.3$. At the low wind speeds encountered, the effects of nonneutral stratification on atmospheric turbulent transport, hence on flux–profile relationships may not be negligible. Therefore, the

mean values of measured wind speed, temperature and specific humidity were adjusted to 10 m height by including the stratification effects as described in Equations 2.5.6 and 2.5.7. These adjusted values are used for discussions in the rest of this dissertation.

After preliminary analysis of the atmospheric measurements using all the data sets, 79 measurement periods each 30 min to 1 h long, were selected for further investigation. The selection was mostly based on the steadiness of the winds during a period with $U_{10} \geq 3.5\ m/s$. Five of the selected periods were from conditions following a sudden 2 to 4 m/s change in the mean wind speed. Also a few cases of rising or calming winds were included to achieve wider ranges of wind speeds and air–water temperature differences. But even then the changes in the mean wind speed were gradual and the differences between the minimum and the maximum values were less than 2 m/s. In Figure 5.1.1, distribution of the stratification parameter, z/L, with wind speed, U_{10}, for the selected periods is displayed. Of these selected cases, 45 were during unstable, 10 during stable and 24 during near neutral stratification, defined as $-0.1 \leq z/L \leq 0.05$. As illustrated in Figure 5.1.2, in the selected periods the ratio of the standard deviation, σ_U, to the average wind speed varied between $0.06 \leq \sigma_U/U_{10} \leq 0.18$ and was less than 0.13 for 74 cases. The overall average is $\sigma_U/U_{10} = 0.10 \pm 0.025$. Higher ratios of σ_U/U_{10} were mostly associated with unstable stratification and lower wind speeds, conditions under which free convection is likely to take place. With increasing wind speed, both the variability and the mean value of σ_U/U_{10} decrease slightly. This trend is also supported by the value $\sigma_U/U_{10} \approx 0.06$ reported by other investigators (Smith, 1980; Large and Pond, 1981; Geernaert *et al*, 1987) as the average over wind speeds in the range $5 \leq U_{10} \leq 25\ m/s$.

At high winds the stratification effects become negligible, but for the range of wind speeds considered here the atmospheric stratification may have strong

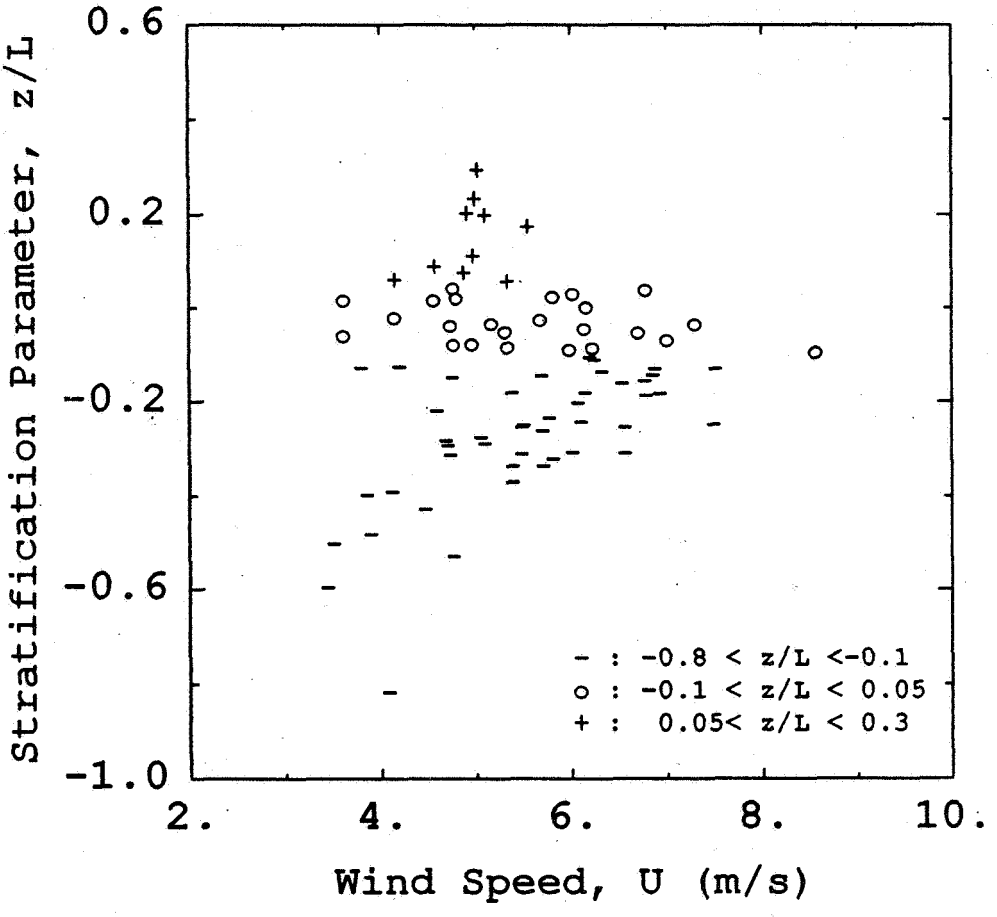

Figure 5.1.1: Distribution of the stratification parameter, z/L, with the wind speed, U_{10}, for the data sets selected after preliminary analysis. z/L was estimated using the bulk formulation of Large and Pond (1982). The symbols illustrate the distribution of the data points with respect to different regimes of atmospheric stratification.

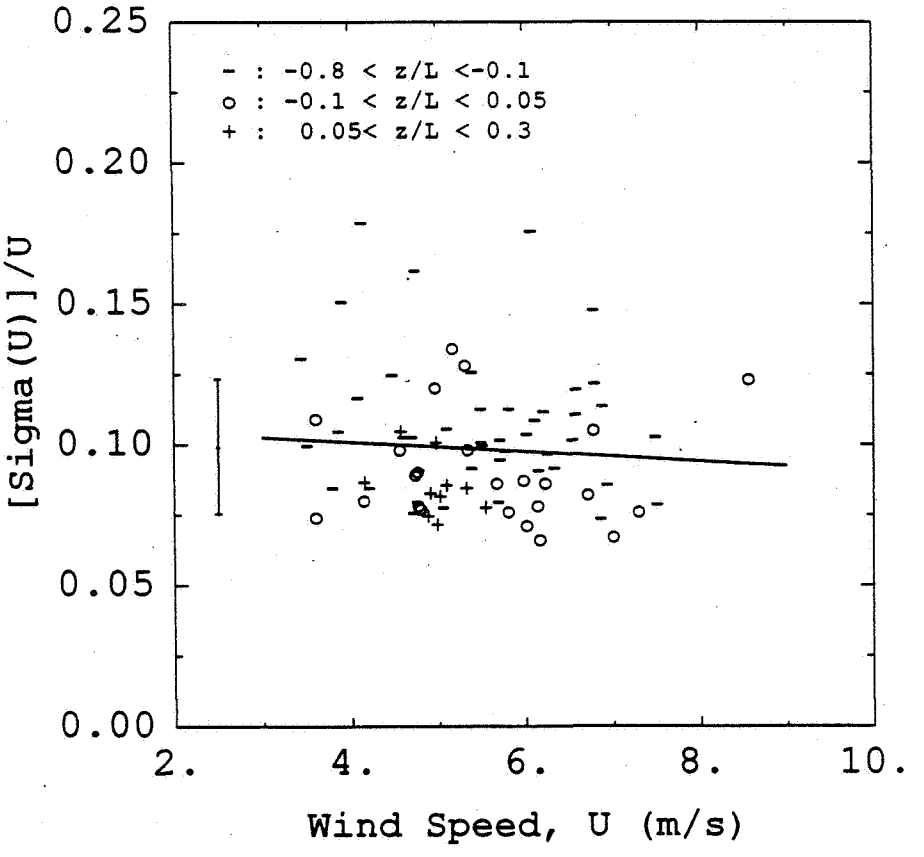

Figure 5.1.2: Ratio of the standard deviation of the wind speed to its average value versus U_{10} for the selected runs. Of the 79 sets, 45 runs were during unstable, 10 during stable and 24 during near neutral stratification defined as $-0.1 \leq z/L \leq 0.05$. The vertical line is centered at the overall mean value and extends one standard deviation on each side. The horizontal line is a linear fit to all points and shows that airflow is more variable at lighter winds. The figure also shows that σ_U/U_{10} is greater for unstable cases.

effects on the character of the turbulence as well as on the flux measurements. In the range $-0.8 \leq z/L \leq 0.3$ of our experimental conditions, assuming neutral stratification ($z/L = 0$) leads to the following errors at the extremes: 175% and -80% in z_o, 435% and -80% in z_t or z_q, 25% and -15% in C_{DN}, 30% and -10% in C_{HN} or C_{EN}. Therefore, the stratification parameter, z/L, determined from measured fluxes (Equation 2.5.1) was tested against two other estimates. One estimate was obtained according to Large and Pond (1982) and is based on their large amount of data collected over the ocean. Another estimate was calculated using the surface flux model by Liu *et al* (1979) and Equation 2.5.1. Liu *et al* (1979) had verified their model with observations made also on Lake Washington.

Since z/L values from measured fluxes had considerable scatter, all estimates were intercompared using that of Large and Pond (1982) as reference (Figure 5.1.3). z/L values from Liu *et al* (1979) were in good agreement for $|z/L| \leq 0.2$ but larger outside this range particularly in the unstable regime (by a factor of 2 at $z/L = -0.8$). Consistently higher values predicted by the model of Liu *et al* (1979) may have resulted from their bulk transfer coefficients for heat fluxes rising to a maximum value at these wind speeds hence, overestimating the sensible and latent heat fluxes.

The stratification parameter determined from flux measurements were comparable to the estimates by Large and Pond (1982) when $U_{10} > 6\ m/s$ and $z/L \leq 0.2$. At lower wind speeds significant deviations were observed particularly in the strongly stable regime. A systematic difference remains between our measurements and estimates based on the formulation by Large and Pond (1982). This bias may be real and related to a small difference in our estimated turbulent exchange coefficients for heat and water vapor. If the difference is real we suspect that it is related to our short fetch conditions. After these intercomparisons it was concluded that under these conditions of wind speeds

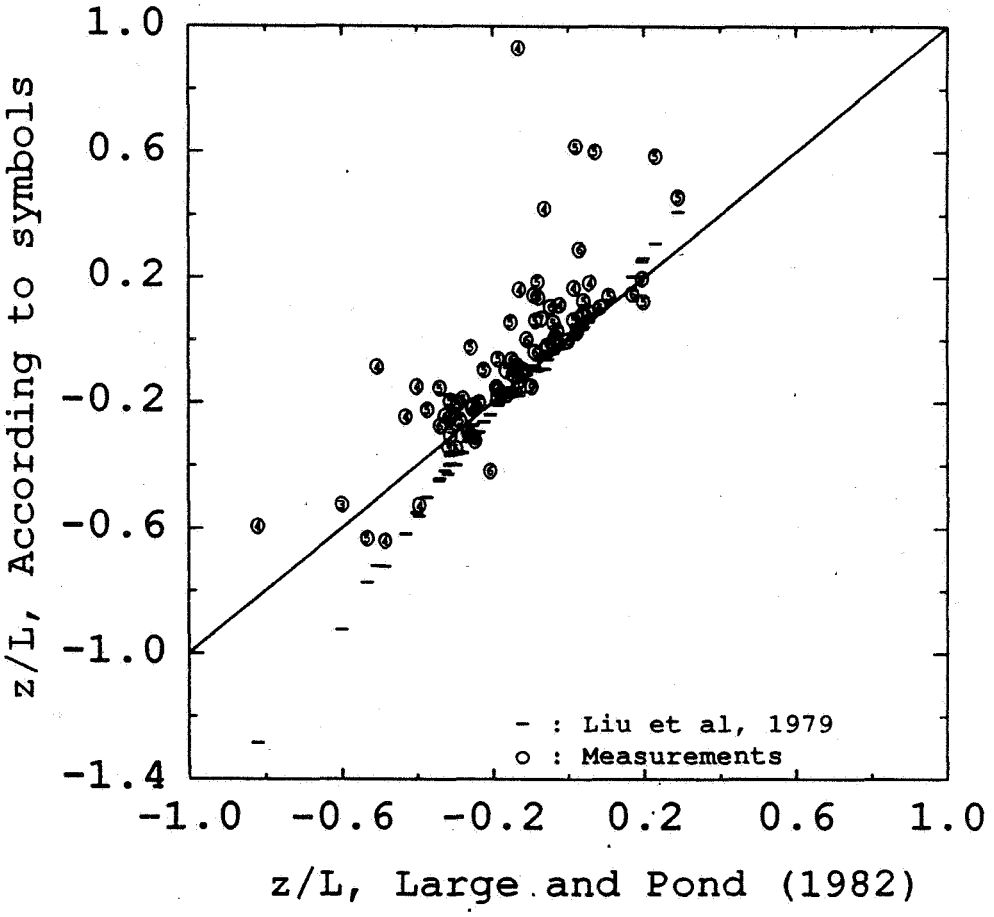

Figure 5.1.3: Comparisons of the measured and estimated stratification parameters for the selected runs. On the horizontal axis are the values from Large and Pond's (1982) model; (-) from Liu *et al* (1979); (o) from measurements with the numbers inside the circles indicating the approximate mean wind speed in m/s for that data run.

and stratification, stratification estimates obtained from a verified bulk formulation would reduce the uncertainty in the other experimental results. Since we cannot claim great certainty for the few measurements we have in this regime, z/L estimates for each data set were determined according to Large and Pond (1982) and used in the rest of the discussions. (Figures 5.1.1 and 5.1.2 were also constructed using these values.)

Considering the uncertainties in the stratification parameter determined from measured fluxes, the selected runs were further examined through the turbulence variance statistics. Although variations in σ_U/U_{10} (Figure 5.1.2) were relatively small, the ratio σ_U/u_* showed large scatter. As illustraded in Figure 5.1.4, the scatter did not reflect any systematic variation with z/L. Since low frequency atmospheric motions caused by mesoscale features can make significant contributions to horizontal velocity variances and they do not obey the similarity theory, this result is not unexpected. In the presence of these mesoscale features such as large convective eddies during unstable stratification and gravity waves during stable conditions the correlations between the horizontal and vertical wind fluctuations decrease, hence momentum is transfered less efficiently (Businger, 1973). Despite the scatter, this is also evident in Figure 5.1.4 where the correlation coefficients, R_{uw} (see Equation 4.1.6), are the highest between near neutral and slightly unstable regime. Also, in the same stratification range σ_U/u_* ratios attain their lowest values which implies either that σ_U is small, i.e. more uniform airflow (as seen in Figure 5.1.2), or that u_* is large, i.e. strong momentum flux, or both.

For neutral stratification, values of σ_U/u_* obtained in other studies range from 1.5 to 4, but the average values are generally between 2 and 2.5. For example: 2.25 ± 0.32 was found by Geernaert *et al* (1987) over oceans, 2.3 by Monin and Yaglom (1971) and McBean (1971), 1.8 by Kaimal *et al* (1972), and 2.39 by Panofsky and Dutton (1984) over land. At varying levels of correlations,

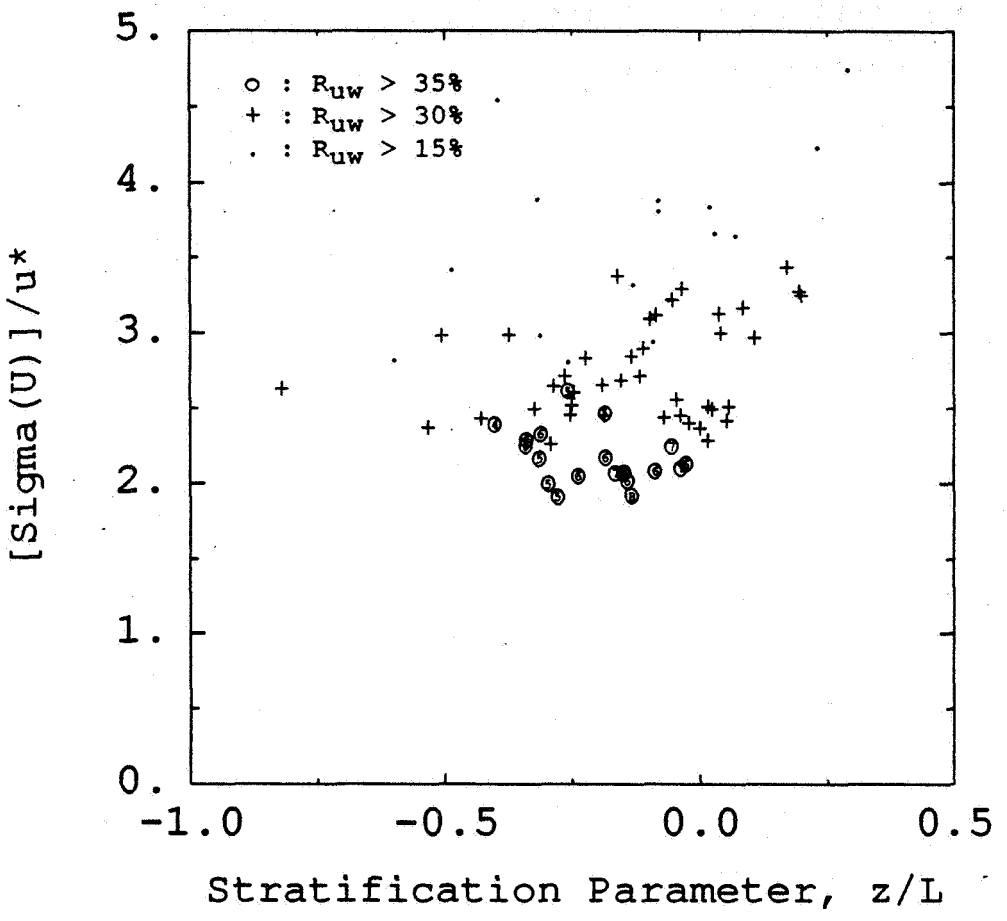

Figure 5.1.4: The ratio of the standard deviation of wind speed to the friction velocity versus the stratification parameter at varying levels of correlations, R_{uw} defined by Equation 4.1.6. (o) $R_{uw} \geq 35\%$ with the numbers inside the circles indicating the approximate mean wind speed in m/s; (+) $R_{uw} \geq 30\%$; and, (.) $R_{uw} \geq 15\%$.

the data points in Figure 5.1.4 can be described by $\sigma_U/u_* = 2.15 \pm 0.16$ for $R_{uw} \geq 35\%$, $\sigma_U/u_* = 2.37 \pm 0.32$ for $R_{uw} \geq 30\%$, and $\sigma_U/u_* = 2.77 \pm 0.63$ for $R_{uw} \geq 15\%$, i.e. depending on the selection criteria the mean changes by 30% and the standard deviation varies by a factor of 4. Considering its high sensitivity to low frequency motions and possibly to the technique used for removing the trend from the time series, σ_U/u_* is not expected to provide quantitatively exact information about the atmospheric turbulence.

On the other hand, the ratio of the standard deviation of vertical velocity to the friction velocity was confined to a narrow range, $1 \leq \sigma_w/u_* \leq 1.7$. Its variations with the stratification parameter is displayed in Figure 5.1.5, where the observed magnitudes decrease in the unstable regime with decreasing $-z/L$; reach a minimum near neutral stratification; and increase rapidly in the stable regime. The behavior in the unstable region is similar to the prediction according to the free convection similarity, $\sigma_w/u_* \approx 2|z/L|^{1/3}$ valid for $z/L \leq -0.1$ (Businger, 1973; see the curve in Figure 5.1.5). In the free convection regime the correlations between u and w decrease with increasing unstable stratification. This does not mean that momentum flux diminishes, just that the transfer process is different. There is no clear trend or formulation to explain the increase in the stable regime where the vertical motions are expected to be supressed. However, Businger (1973) suggests that in addition to decreasing correlations between u and w, it may be due to contributions to σ_w from gravity waves. This view is also supported by the distributions of the correlation coefficients in Figure 5.1.5 where data points with $R_{uw} \geq 35\%$ lie in the range $-0.4 < z/L < 0$.

The average value for σ_w/u_* including all data points was 1.28 ± 0.16 and, unlike for horizontal wind speed, its variation at various correlation levels was within 10%. This magnitude is in good agreement with other observations: 1.27 ± 0.15 by Geernaert *et al* (1987), 1.21 by Smith and Banke (1975), 1.24 by

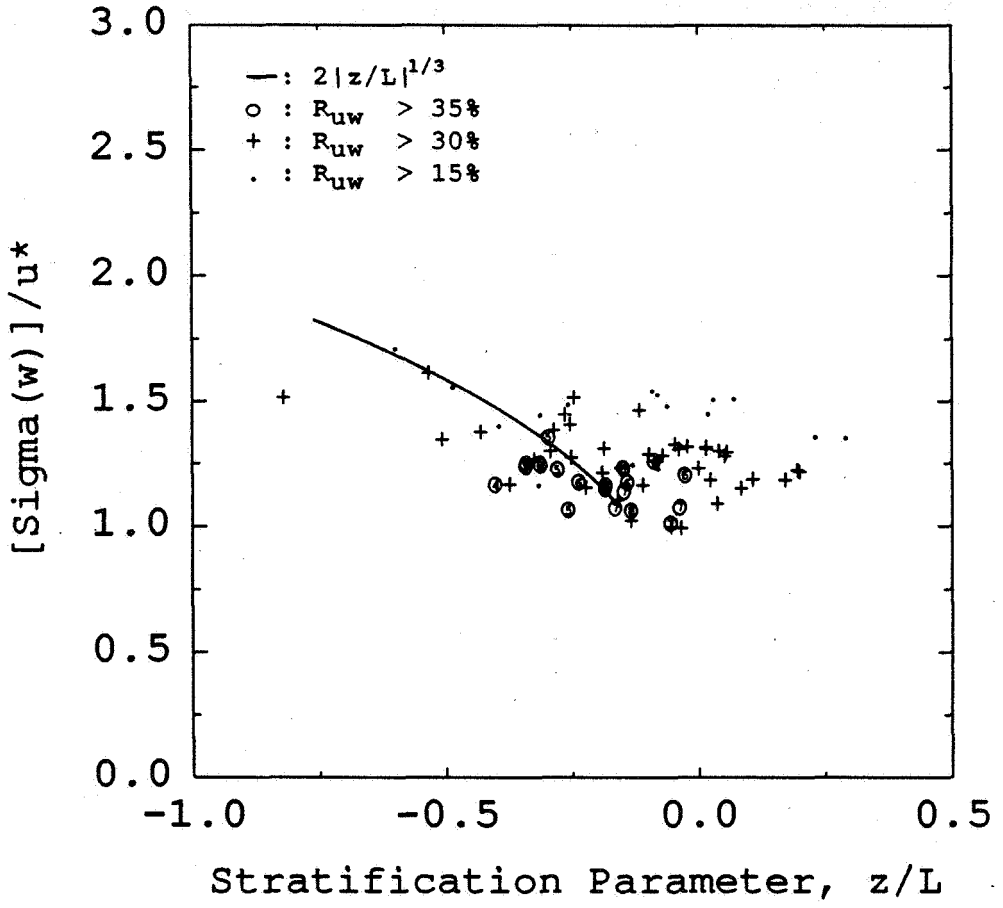

Figure 5.1.5: The ratio of the standard deviation of vertical wind velocity to the friction velocity versus the stratification parameter at varying levels of correlations, (o) $R_{uw} \geq 35\%$ with the numbers inside the circles indicating the approximate mean wind speed in m/s; (+) $R_{uw} \geq 30\%$; and, (.) $R_{uw} \geq 15\%$. The curve indicates the prediction according to free convection similarity (Businger, 1973).

Large and Pond (1981) over oceans; and, 1.25 by Panofsky and Dutton (1984) over land. Since the measurements were made at elevations of 5 to 8 m from mean water level, the effects of the water surface waves (with significant heights less than 40 cm) on these variance statistics were assumed negligible.

Within the range of our observations, the turbulence statistics for temperature and specific humidity fluctuations normalized by their characteristic scales were similar both in magnitude and in their variations with stratification (Figures 5.1.6 and 5.1.7). In the unstable regime, they increase with decreasing $-z/L$ as $0.95|z/L|^{-1/3}$ predicted by the free convection theory of Wyngaard *et al* (1971). This trend which is opposite of that for σ_w/u_* indicates that as atmospheric stratification becomes more unstable, heat is transfered more efficiently than momentum. This is also evident from high values of R_{wt} at large negative values of z/L. In near neutral conditions, a sudden jump in the magnitudes in Figure 5.1.6 may partially be due to the difficulties in measuring very small temperature differences accurately. However, as pointed out by Busch (1973), neutral stratification is a transitional state during which stationarity may be lacking. Under such conditions, the measurements may have large errors because the ergodicity assumption, that time average over a long period is equivalent to space average, may not be fully satisfied for typical sampling periods. In Figures 5.1.6 and 5.1.7 the scatter was too large to draw any conclusion.

The average values of σ_T/T_* and σ_q/q_* reported by other investigators for $|z/L| < 0.1$ vary considerably; for example, 1.6 to 2.5 from McBean (1971) and Wyngaard *et al* (1971), 0.7 to 4 from Weseley *et al* (1970), 5.7 from Geernaert *et al* (1987). In Figures 5.1.6 and 5 1.7, the data points with high correlation coefficients lay between 1.5 and 2.5 just outside the range where large values occur.

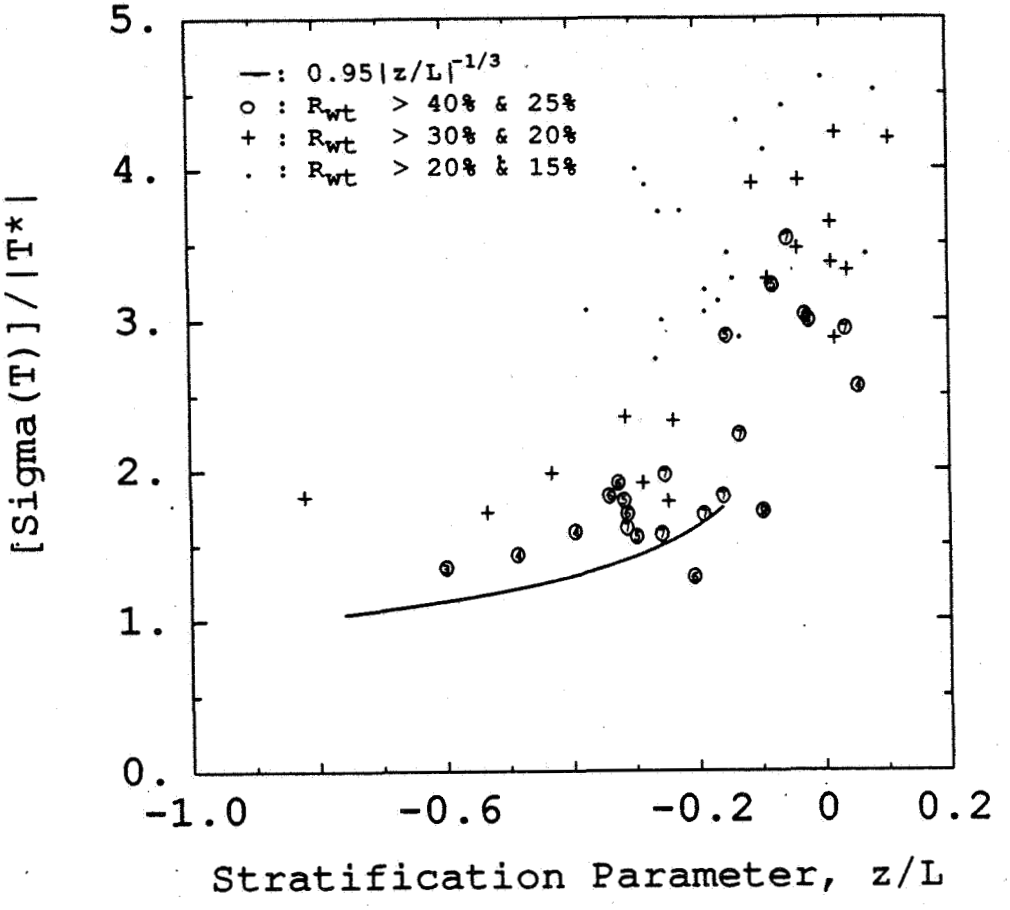

Figure 5.1.6: The ratio of the standard deviation of air temperature to its characteristic scale versus the stratification parameter at varying levels of correlations, R_{wt}. For this illustration the data were separated into two groups; (i) $\sigma_T/T_* < 2.5$ and (ii) $\sigma_T/T_* > 2.5$. The first group had larger R_{wt} than the second group. The symbols correspond to; (o) $R_{wt} \geq 40\%$ (i) & 25% (ii) with the numbers inside the circles indicating the approximate mean wind speed in m/s; (+) $R_{wt} \geq 30\%$ (i) & 20% (ii); and, (.) $R_{wt} \geq 20\%$ (i) & 15% (ii). The curve indicates the prediction according to free convection similarity (Wyngaard *et al*, 1971).

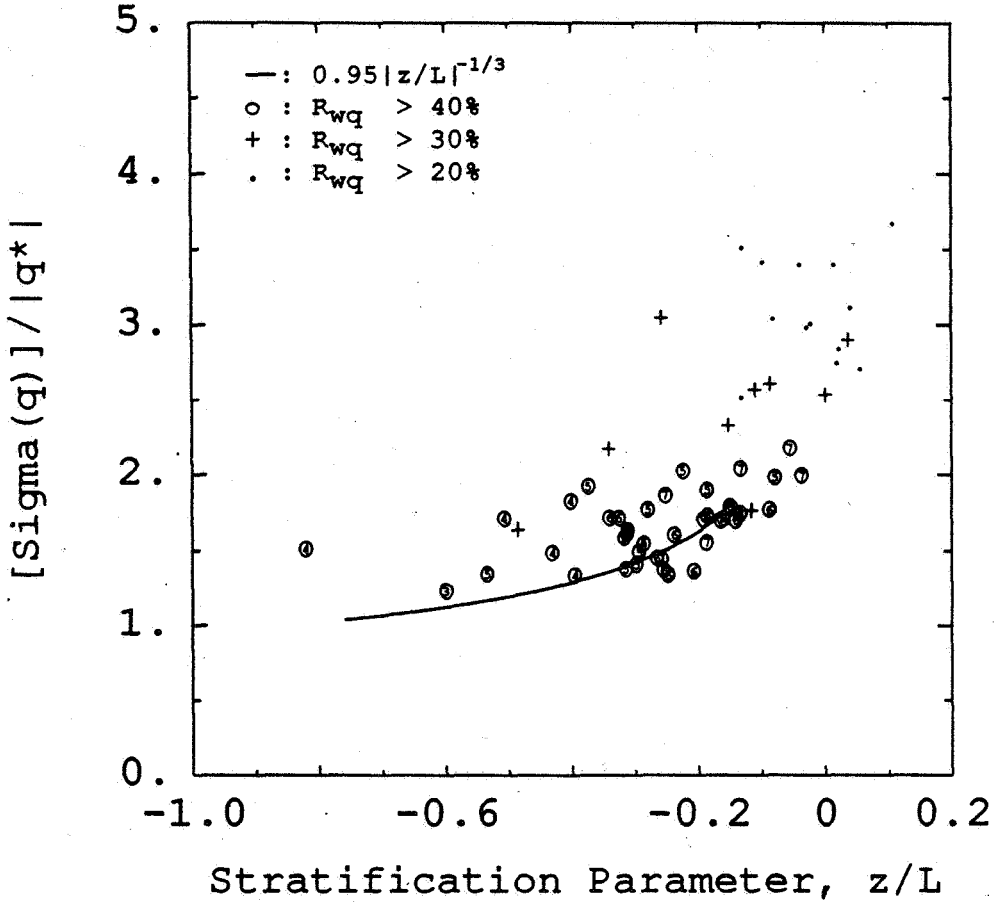

Figure 5.1.7: The ratio of the standard deviation of specific humidity to its characteristic scale versus the stratification parameter at varying levels of correlations, (o) $R_{wq} \geq 40\%$ with the numbers inside the circles indicating the approximate mean wind speed in m/s; (+) $R_{wq} \geq 30\%$; and, (.) $R_{wq} \geq 20\%$ The curve indicates the prediction according the free convection similarity (Wyngaard *et al*, 1971).

In summary, the statistics presented above can indicate when the measured fluxes may be questionable and lead to erroneous conclusions, but due to their large inherent variability they cannot provide an estimate of the magnitude of surface fluxes with accuracies better than 50%. In the case of momentum flux, the turbulent measurements may have been contaminated by the mesoscale features during strongly nonneutral stratification, and may be in error due to lack of stationarity in near neutral conditions. But, so far, there is no obvious reason to exclude any data points. The measured heat fluxes, particularly the sensible heat flux near neutral and in stable conditions, must be handled with great caution or excluded from any further analysis. However, drawing a line of exclusion without introducing bias in the results requires more evidence.

Further insight into the quality and validity of the turbulence measurements was gathered from analysis of the characteristic surface roughness lengths. The surface roughness length, z_o, calculated from Equation 2.5.6, is shown in Figure 5.1.8. Of the three curves drawn for reference, the lower dotted line is the prediction for aerodynamically smooth flow (Equation 2.5.12), i.e. when momentum is transfered by viscosity. This is the primary mechanism when $u_* \leq 0.1\ m/s$ or $U_{10} \leq 3\ m/s$. At higher wind speeds as surface waves evolve, other mechanisms such as skin friction and form drag quickly dominate the transfer processes and z_o is determined by the roughness elements of the surface (Section 2.5). For $U_{10} \geq 3\ m/s$, the flow becomes rough and viscosity effects are negligible. This is described by the other two lines. The solid line corresponds to Charnock's relation (Equation 2.5.13) with a coefficient $a = 0.0144$ (Garratt, 1977) and is representative of lower z_o values or bulk momentum transfer coefficients observed in open oceans (e.g. Smith, 1980; Large and Pond, 1981). The surface roughness lengths over limited fetch and in coastal waters are generally higher as indicated by the upper dotted line given by Kondo (1975). This prediction is also used by the surface flux model of Liu

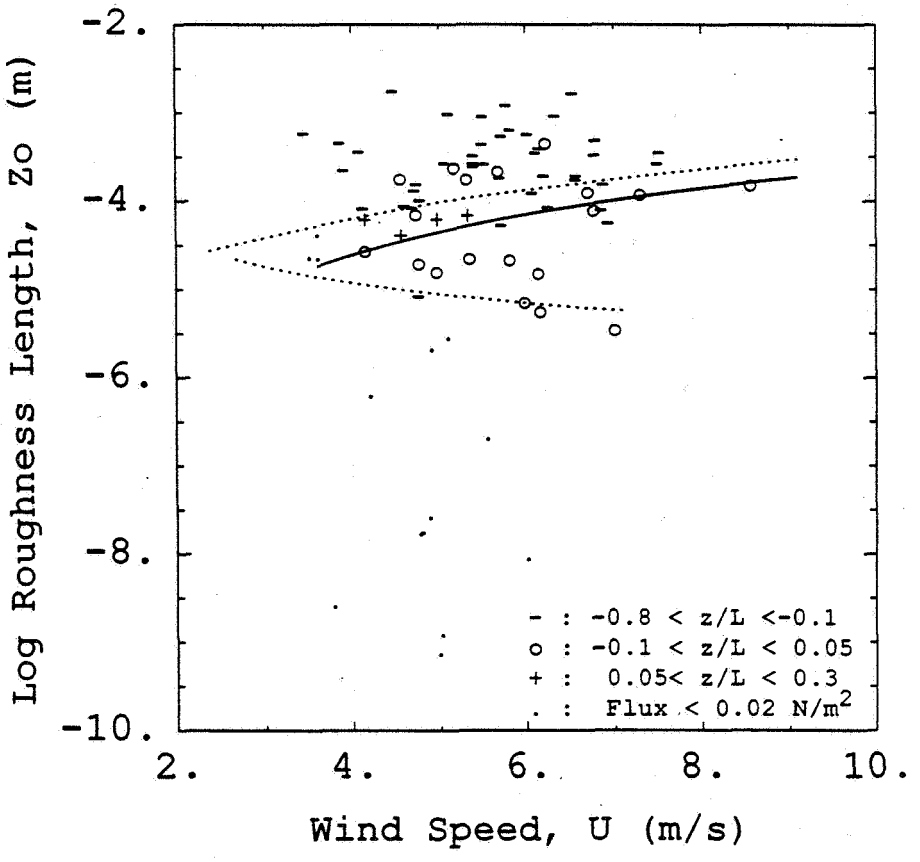

Figure 5.1.8: Surface roughness length, z_o, versus the wind speed, U_{10}, for different stratification regimes. The curves describe z_o for: (lower dotted) aerodynamically smooth flow (Equation 2.5.12); (solid) open oceans according to Charnock relation Equation 2.5.13 with a coefficient of 0.0144 (Garratt, 1970); (upper dotted) coastal, fetch limited waters according to Kondo (1975).

et al (1979) which will be tested for its applicability to the present observations. Dependency of z_0 on sea state will be discussed in Section 5.3.

The interest of this work is in the regime $u_* \geq 0.12$ where wind waves are effectively responsible for the surface roughness. Therefore, all data points with $\tau < 0.02\ N/m^2$ (corresponding to $u_* \approx 0.12$) that lie below the smooth flow curve may be ignored. These data points, that deviate from other similar cases by 50% or more, cannot be explained by the uncertainty in flux measurements which is typically 10% and 20% at most. However, during the periods corresponding to the two highest and the three lowest points below the smooth flow curve at $U_{10} = 5\ m/s$, suppression of wind waves was observed both in video records and in wave gauge measurements. These cases will be discussed in Section 5.5. The rest of the low values must be attributed to sampling error. On the other hand, the highest values of $z_0 \propto 10^{-3}$ imply a neutral drag coefficient, $C_{DN} \approx 2 \times 10^{-3}$. Such high values of C_{DN} are usually observed at wind speeds $U_{10} \geq 12\ m/s$ (see the review by Geernaert, 1990). From the time series of wind speed, some of these cases were identified as occurring in conditions of dying winds, i.e. there was little, if any, momentum flux from wind to waves. This unrealistic picture results from applying Monin–Obukhov similarity theory to transitional conditions when stationarity and horizontal homogeneity are lacking (see Section 5.4). The remaining points are generally above the level predicted for open oceans and scatter around the fit for limited fetch and coastal waters. Since z_0 strongly depends on the sea state, subject of the next section, its quantitative evaluation will be saved for Section 5.3 where another estimate obtained from wave observations is presented.

Near the interface, heat and mass are transported by the same process, namely molecular diffusion. Therefore, variations of z_t and z_q with surface roughness are expected to be similar (e.g. Liu *et al*, 1979). This was also evident from our measurements and to illustrate this similarity, z_t and z_q were presented

together in Figure 5.1.9. Also included are the mean values reported by Large and Pond (1982): $z_t = 4.9 \times 10^{-5}\ m$ (the upper solid line) and $z_q = 9.5 \times 10^{-5}\ m$ (the dashed line) for unstable conditions; and, $z_t = 2.2 \times 10^{-9}\ m$ (the lower solid line) for stable stratification. These values have been obtained from a large set of data collected over open ocean. Based on the observations by Anderson and Smith (1981) in the surf zone, Large and Pond (1982) suggested that the mean value of z_q is similar in unstable and stable regimes. As pointed out by Friehe and Schmitt (1976), due to the difference in the diffusivities for heat and water vapor in air, z_q is slightly larger than z_t resulting in $C_E > C_H$. In the unstable regime, z_q from this study does not show any trend; and the data points scatter along the line suggested by Large and Pond (1982). In the near neutral zone, z_q shows a sudden drop in magnitude. Due to the limited extent of the data points in the stable regime, the trend is not clear. However the measured values are obviously much lower thanthose in the unstable region. The general behavior of z_t is similar to that of z_q, except for its overshoot in near neutral conditions before it assumes small values in the stable regime.

The nature as well as the similarity of z_t and z_q became more obvious when the same data as in Figure 5.1.9 were viewed as a function of air–water temperature differences rather than of z/L. This is shown in Figure 5.1.10. The solid and dashed lines are the same as in the previous figure. (Note that here the indicated range of validity may not be exact.) The asymptotic behavior of z_t, both upward and downward, near zero temperature difference is due to measurement errors. With the isolation of these asymptotic points, the scatter in z_t in the region of negative temperature differences (the unstable regime) is greatly reduced. Comparisons of the remaining points provide further support for the discussions given in the previous paragraph that z_t and z_q have similar characteristics in the unstable regime. Noting that both z_t and z_q are approaching the lower solid line, the average value for z_t suggested by Large and

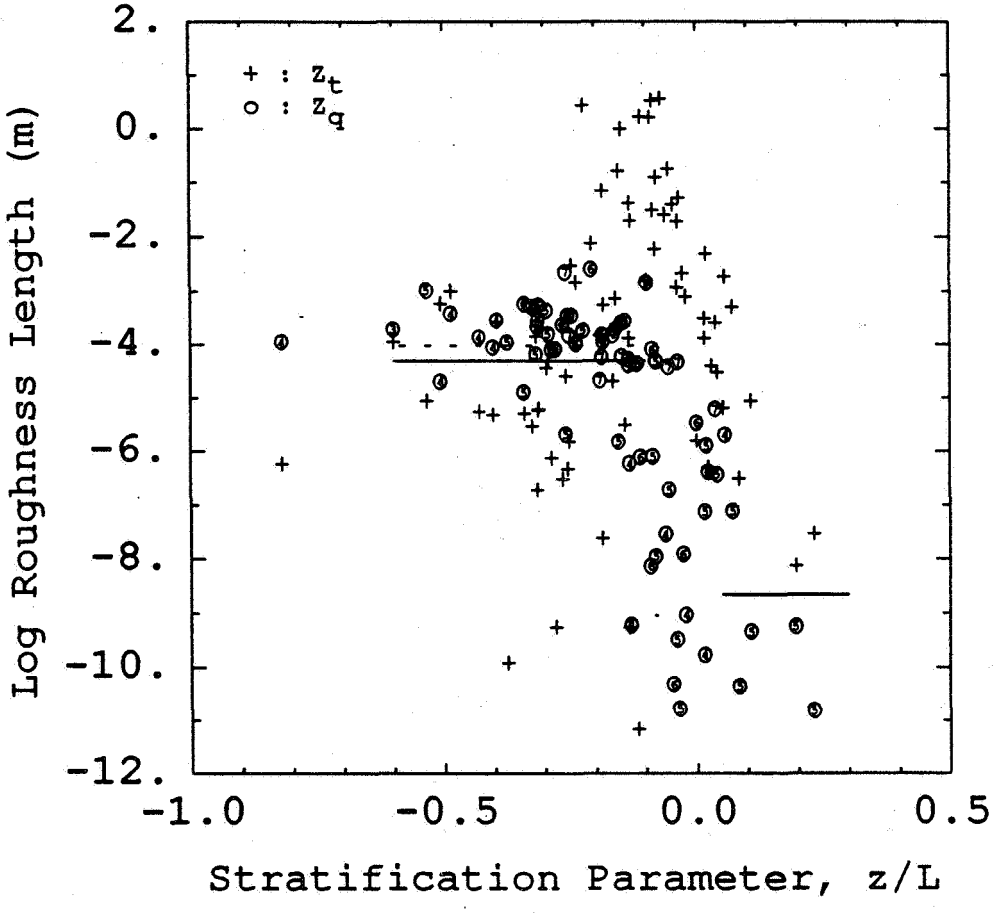

Figure 5.1.9: Surface roughness lengths, (+) z_t and (o) z_q, versus the stratification parameter, z/L. The numbers inside the circles indicate the approximate mean wind speed in m/s. z_q appears to be constant for $z/L < -0.1$. In the case of z_t this is not obvious, but there is no trend showing otherwise. Generally, z_q has larger values than z_t. In the stable regime, despite the scatter, a drop in magnitudes of both z_q and z_t are observed. The solid and dashed lines indicate the mean values for z_t and z_q, respectively, as constants valid in the range shown (from Large and Pond, 1982).

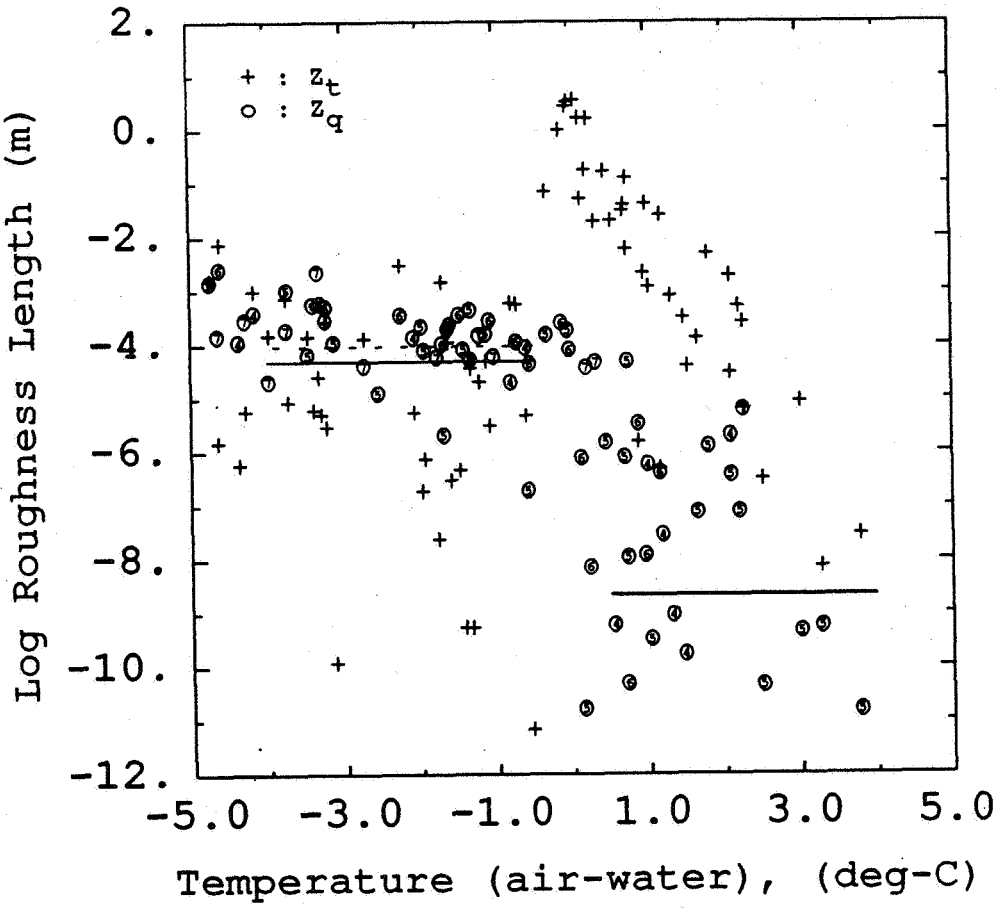

Figure 5.1.10: Surface roughness lengths, (+) z_t and (o) z_q, versus the air–water temperature difference. The numbers inside the circles indicate the approximate mean wind speed in m/s. The solid and dashed lines are the same as in Figure 5.1.9, but here their indicated range of validity may not be exact. The asymptotic behavior of z_t near zero temperature differences is due to measurement errors. With the isolation of these points, the similarity of z_t and z_q becomes more obvious in the unstable regime. Since both z_t and z_q are approaching to the lower solid line, their similarity may also be extended to the stable regime.

Pond (1982), the similarity of these two roughness scales may also be extended to the stable regime.

The results presented in Figures 5.1.9 and 5 1.10 yield $z_t = 1.1 \pm 2.2 \times 10^{-4}\ m$ and $z_q = 1.7 \pm 1.4 \times 10^{-4}\ m$ for the unstable regime. The three z_t and the three z_q values that were of the order of $\approx 10^{-2}$ were not included in these calculations. Large scatter in z_t is reflected by its standard deviation being twice as large as its mean (200% uncertainty). However, the similarity of the magnitudes of z_t and z_q is clear. No calculations were attempted for the stable regime.

Liu *et al* (1979) suggested that at low wind speeds the roughness lengths, z_t and z_q increase with increasing z_o; and then start decreasing when $U > 5\ m/s$ as a result of increased sheltering effects at the wave troughs. In order to test this theory, in Figure 5.1.11 $z_q u_*/\nu$ was plotted against roughness Reynolds number, $Rr = z_o u_*/\nu$ where ν is the viscosity of air. The solid line is the prediction by Liu *et al* (1979). The measurements indicate a slight increase with increasing Rr. The result of using the measured u_* with a constant value of $z_q = 9.5 \times 10^{-5}\ m$ (Large and Pond, 1982) are also illustrated. These findings do not support the theory of reduction in z_q and z_t due to increased sheltering effects in wave troughs. Since the bulk transfer coefficients, C_{HN} and C_{EN}, used in their model attain their maximum values of approximately 1.4×10^{-3} in the range of wind speeds considered in this study, the sensible and latent heat fluxes predicted by this model may be overestimated. This question is addressed in Section 5.4 where the bulk transfer coefficients are compared.

The results obtained from the above examinations indicate that the measured fluxes of momentum, sensible heat and latent heat are in general typical of other marine observations. However, quantitative evaluations based on the sensible and latent heat fluxes had to be restricted to the cases where air–sea temperature differences were not small.

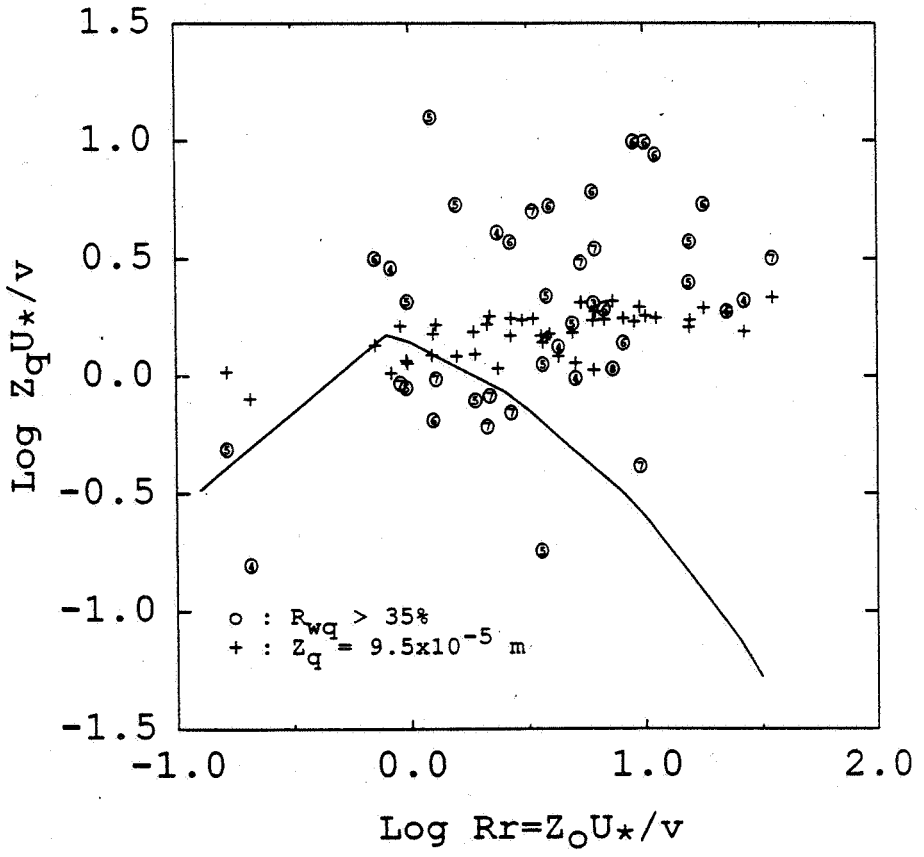

Figure 5.1.11: $z_q u_*/\nu$ against roughness Reynolds number, $Rr = z_0 u_*/\nu$ where ν is the viscosity of air. The solid line is the prediction by Liu *et al* (1979). (o) Measurements with the numbers inside the circles indicating the approximate mean wind speed in m/s. (+) Measured u_* with an assumed constant value of $z_q = 9.5 \times 10^{-5}$ m (Large and Pond, 1982).

5.2 Characteristics of the Long Wave Field

Measurements of long gravity waves were available and analyzed for all data sets. The wave information from periods corresponding to the selected runs (Section 5.1) were extracted and coupled with the results of atmospheric turbulence measurements. As mentioned in the previous section, all observations were made during periods when winds were from the NNW. Therefore, the fetch was fixed at $F = 7\ km$ for all runs. Therefore, the variations in the wave field were assumed to be due to different levels of atmospheric energy input and duration of the condition. Typical duration of a constant condition, i.e. wind speed range within $\pm 1\ m/s$ of the average value, was about 4 hrs. In this section, the nature of the observed long gravity waves are investigated.

Statistics of several long wave parameters were presented in Table 3.1. These can be summarized as follows. The periods of the dominant waves determined from the frequency, $f_p = \omega_p/2\pi$, of the spectral peak were $1/f_p \approx 2\ s$ long. Using the linear dispersion relation (Equation 2.1.31), the corresponding wavelength is found be $\lambda \approx 5\ m$. Maximum wavelength recorded was 8 m. As discussed in Chapter 2, when water surface waves are studied by a linear wave theory the error resulting from ignoring the nonlinear terms are of the order of the wave slope, ak, where a is the square root of the total variance of wave amplitude, $\overline{\zeta^2}$ (Equation 2.1.23) and $k = 2\pi/\lambda$ is the wavenumber. The root–mean–square (rms) wave slope, ak, is shown in Figure 5.2.1 against the wind forcing, U_{10}/C_p, where C_p is the phase speed of the dominant waves. As noted before, the wind speed, U_{10}, has been adjusted to the neutral stratification and 10 m height using the parameterization given by Large and Pond (1982). When wind and waves approach from different directions, the component of U_{10} in the direction of dominant waves should be taken (Donelan *et al*, 1985), but in this study, they were generally from the same direction. The wave slope was about 0.11 in the mean with a maximum of about 0.16, i.e. the error resulting from

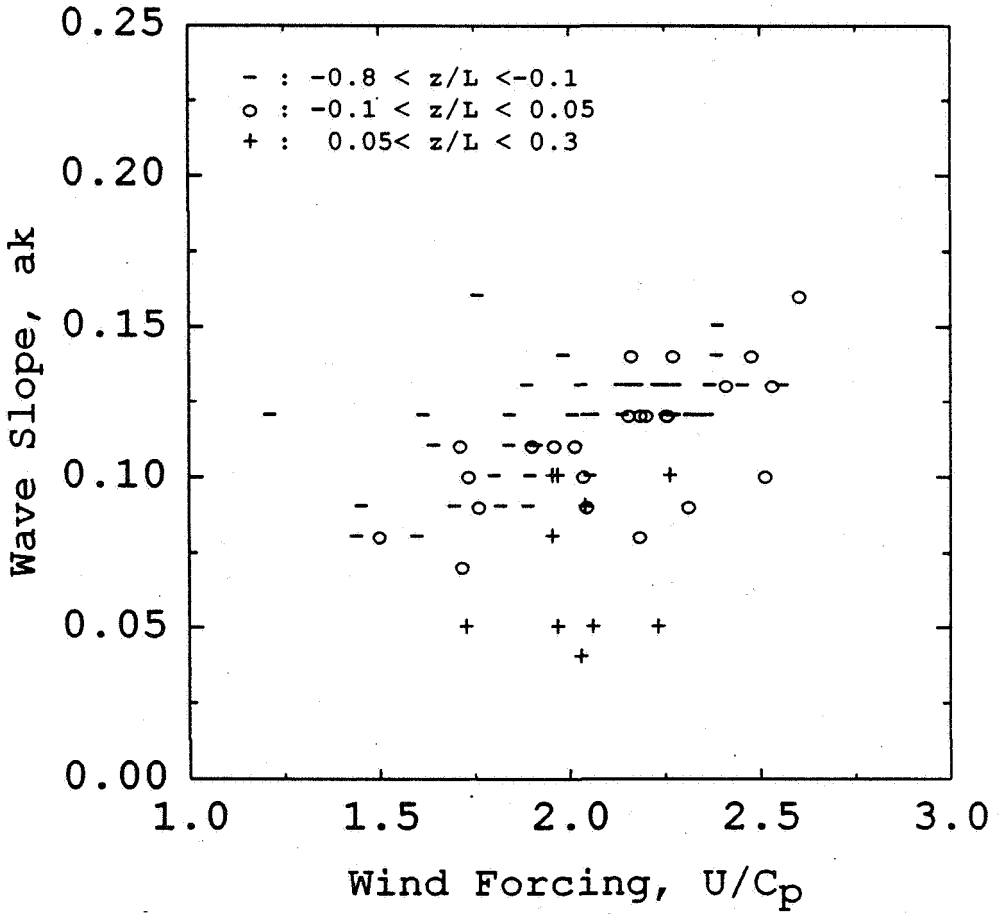

Figure 5.2.1: Long wave slope, ak, against the wind forcing, U_{10}/C_p. Larger slopes are primarily associated with stronger wind forcing. Effects of the atmospheric stratification is clearly brought out. During the periods corresponding to the lowest five points, occasionally wave damping by surface films were observed.

using a linear wave theory is roughly 10%–15% for these cases. The wave slopes increase with stronger wind forcing, large U_{10}/C_p. In other words, the young developing waves have steeper profiles. For fully developed waves, U_{10}/C_p is approximately unity. Stratification effects are noticable where much gentler slopes, $ak = 0.05$, are associated with stable conditions. Since the measurements had already been corrected for stratification effects on the wind profile (i.e. U_{10} and u_* can be used interchangebly), this observation is noteworthy. The lowest five points shown in Figure 5.2.1 represent periods in which wave damping by surface films was observed. The events were also pointed out in discussing z_o obtained from measured momentum fluxes (Figure 5.1.8) and will be considered in more depth in Section 5.5.

The study by Donelan *et al* (1985) showed that various features of water surface waves scale much better with U_{10}/C_p than with the nondimensional fetch, $\tilde{F} = gF/U_{10}^2$, suggested by Hasselmann *et al* (1973; JONSWAP experiment). Therefore, in Figure 5.2.2 the nondimensional wave height variance, $\tilde{V} = g^2\overline{\zeta^2}/U_{10}^4$, was plotted against U_{10}/C_p. The solid line describes the empirical fit, $\tilde{V} = 0.00274(U_{10}/C_p)^{-3.3}$, to the field data of Donelan *et al* (1985). The dashed line was obtained by shifting the solid line over our data points keeping the same slope. One notable feature is that except for the exceptional five data points the U_{10}/C_p scaling is also appropriate for our data sets. However, the absolute values of $\tilde{V}$ at a certain U_{10}/C_p are lower than the prediction of Donelan *et al* (1985). For the range considered here, the JONSWAP results are in good agreement with those of Donelan *et al* (1985). On the other hand, Kahma (1981) found that the nondimensional variance of surface elevations in his data were twice as high as those predicted by the JONSWAP model. Therefore, it can be concluded that these parameterizations of the nondimensional variance in terms of U_{10}/C_p or $\tilde{F}$ suggested by Donelan *et al* (1985) and Hasselmann *et al* (1973), respectively, are not complete. Since the evolution of a

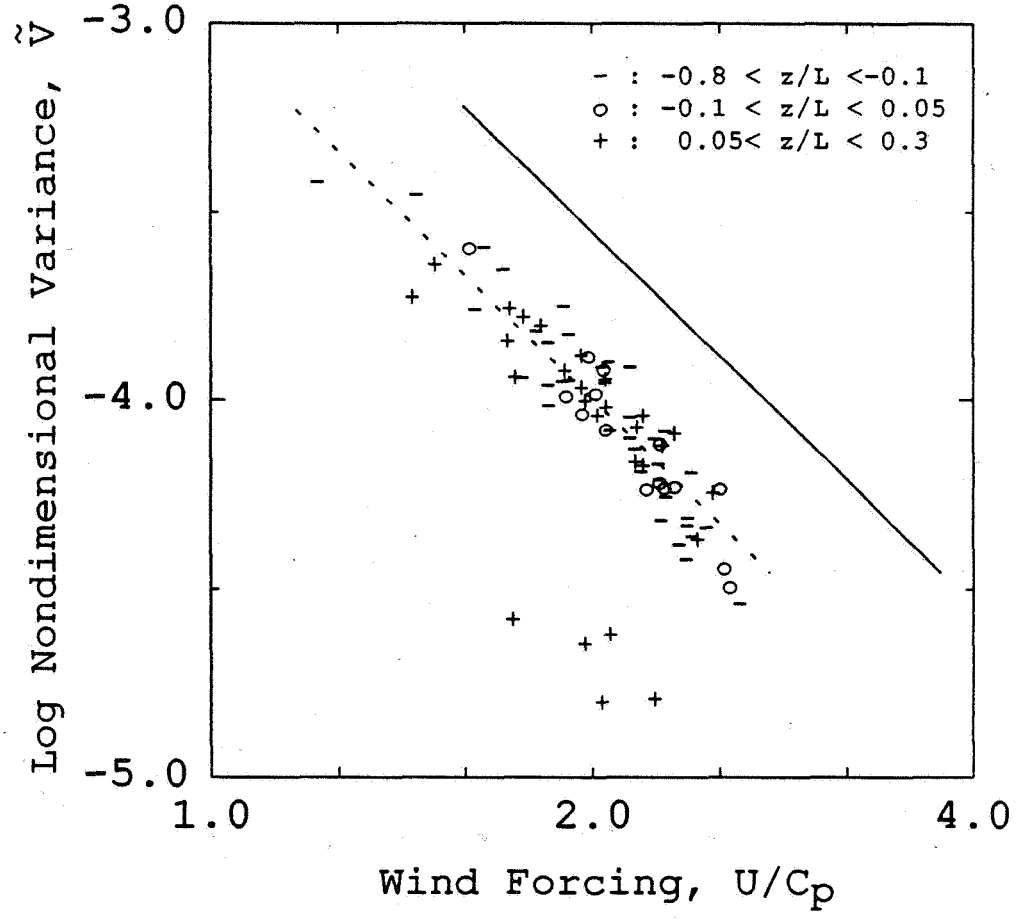

Figure 5.2.2: Nondimensional variance, $\tilde{V} = g^2\overline{\zeta^2}/U_{10}^4$, of wave elevation against the wind forcing, U_{10}/C_p. Except for the lowest five data points, $\tilde{V}$ scales with U_{10}/C_p satisfactorily. Solid line describes the empirical fit, $\tilde{V} = 0.00274(U_{10}/C_p)^{-3.3}$ given by Donelan *et al* (1985). Dashed line has the same slope as the solid one and indicates that the amplitudes of the observed waves were smaller than the values predicted by Donelan's *et al* (1985) parameterization.

wave field depends on the wind duration as well as wind speed and fetch, a general parameterization of $\tilde{V}$ must also include the effects the wind duration. In a recent publication, Hansen *et al* (1990) reported results (discussed in connection with Figure 5.2.6) based on measurements on Lake Washington that show good agreement with Donelan *et al* (1985). However, they did not have an absolute calibration for their wave gauge and the accuracy of their results may be questionable. Those data were also collected over a period of 6 hrs and at a different location on the lake where fetch and bottom conditions are somewhat different.

A similar systematic difference was also noticed in the relationship between the nondimensional fetch $\tilde{F}$ and U_{10}/C_p (Figure 5.2.3). The solid line corresponding to the empirical relationship given by Donelan *et al* (1985) is steeper than the dashed line describing the measurements on Lake Washington used in this study. This situation may be interpreted as follows. In this study, the variations in nondimensional fetch were only due to the change in wind speed. The data points below the solid line and $U_{10}/C_p \leq 1.6$, were obtained from cases of suddenly calming winds; the points above the solid line and $U_{10}/C_p > 2$ were from cases of suddenly rising winds. In either case, the waves have not yet adjusted to the present wind forcing: the phase speed C_p is "too large" for the former and "too small" for the latter case. This, in turn, implies that the empirical relationship between $\tilde{F}$ and U_{10}/C_p is not a useful one alone; and must be used with additional constraints on the steadiness of the winds and a minimum duration.

Despite the differences mentioned above between the measurements and the results of Donelan *et al* (1985), the shape of the frequency spectrum, $E(\omega)$, in the vicinity of the spectral peak was similar (Figure 5.2.4). The sample spectrum is from a case with $U_{10} = 6\ m/s$ and $U_{10}/C_p = 2.1$. The error bars indicate the 90% confidence intervals and have been plotted slightly to the right

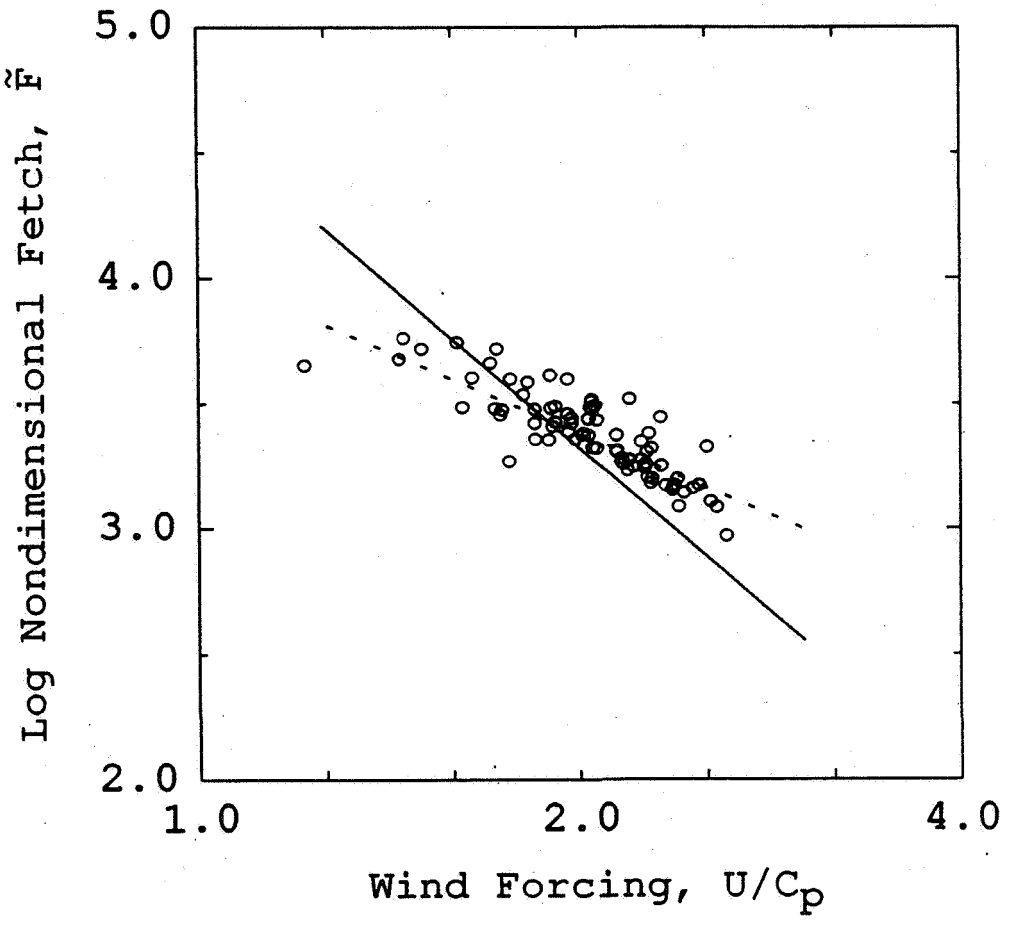

Figure 5.2.3: Nondimensional fetch, $\tilde{F} = gF/U_{10}^2$, against the wind forcing, U_{10}/Cp. Solid line describes the empirical fit, $U_{10}/C_p = 11.6\tilde{F}^{-0.23}$, given by Donelan *et al* (1985). Dashed line is an approximate fit to the measurements. Although the range of observed $\tilde{F}$ was limited, the difference in slopes is clearly visible.

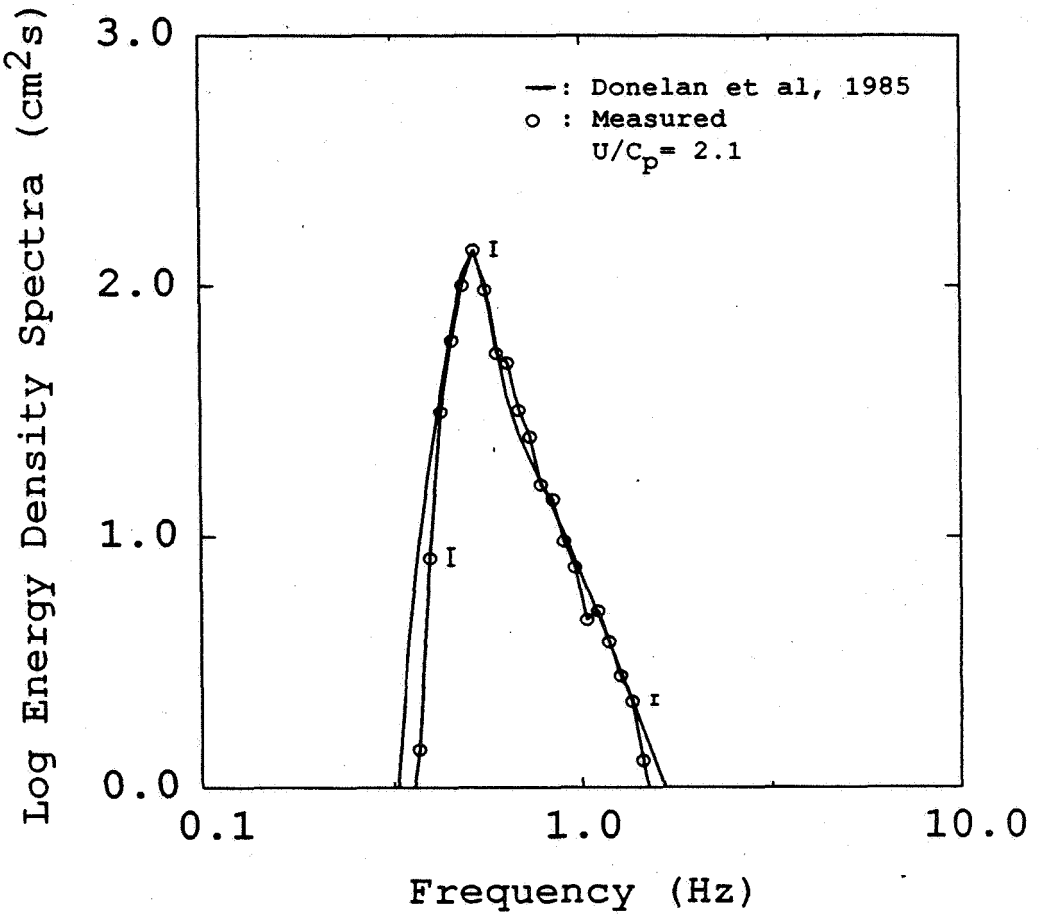

Figure 5.2.4: Comparison of a sample of measured frequency spectrum with the model of Donelan *et al* (1985). The error bars indicate the 90% confidence intervals and have been plotted slightly to the right of the actual frequency for clarity . The similarity in shape is remarkable hence, the present measurements are in support of the ω^{-4} proportionality in the range $1.5 < \omega/\omega_p < 3$. The measured spectrum (from run 16 in Table 3.1) is narrower below the peak frequency reflecting the differences in fetch between the two studies. To match the peak amplitudes, the model spectrum was multiplied by a factor of 0.7.

of the actual frequency for clarity. Parameters of the wave model which has an ω^{-4} dependency for $1.5 < \omega/\omega_p < 3$, are described by Equations 2.2.6–2.2.12. The width and enhancement of the spectral peak are in perfect agreement. However, to match the peak amplitudes, the model spectrum was multiplied by a factor of 0.7. At frequencies below that of the spectral peak, the model spectrum is slightly broader reflecting the differences in temporal and spatial scales between the two experiments. These low frequency components grow as a result of resonant wave–wave interactions, a weak process (Hasselmann, 1962), with time and length scales of the order of at least 100 times the dominat wave period and wavelength, respectively. Since the fetch over Lake Washington is much shorter than that over the experimental site (Lake Ontario) of Donelan *et al* (1985), the spectrum from the present study is narrower at low frequencies.

In order to illustrate the similarities in spectral slope between the present measurements and the model of Donelan *et al* (1985) at various levels of wind forcing, the energy density spectrum multiplied by ω^4 was normalized by the value of $\omega^4 E(\omega)$ averaged over $1.5 < \omega/\omega_p < 3.5$ and plotted against the nondimensional frequency ω/ω_p (Figure 5.2.5). The flatness of the nondimensional spectra indicate that a spectral slope of -4 is appropriate in the range $1.5 < \omega/\omega_p < 3$. This result holds irrespective of the value of U_{10}/C_p. At higher frequencies -5 is a better fit to the observed spectra (see Section 5.5).

The last parameterization to be tested is that of the equilibrium range value, $\alpha_D = 0.006(U_{10}/C_p)^{0.55}$ (Equation 2.2.12). In Figure 5.2.6, this empirical relationship given by Donelan *et al* (1985) is shown by the solid line. The dashed line was obtained from the same relationship using a different coefficient (0.006/2.2) to overlay the measurements. The dependence of the equilibrium range parameter from the present work on U_{10}/C_p has a trend similar to that predicted by Donelan *et al* (1985). Again the difference in absolute values are obvious. The equilibrium range parameters for the cases during which surface

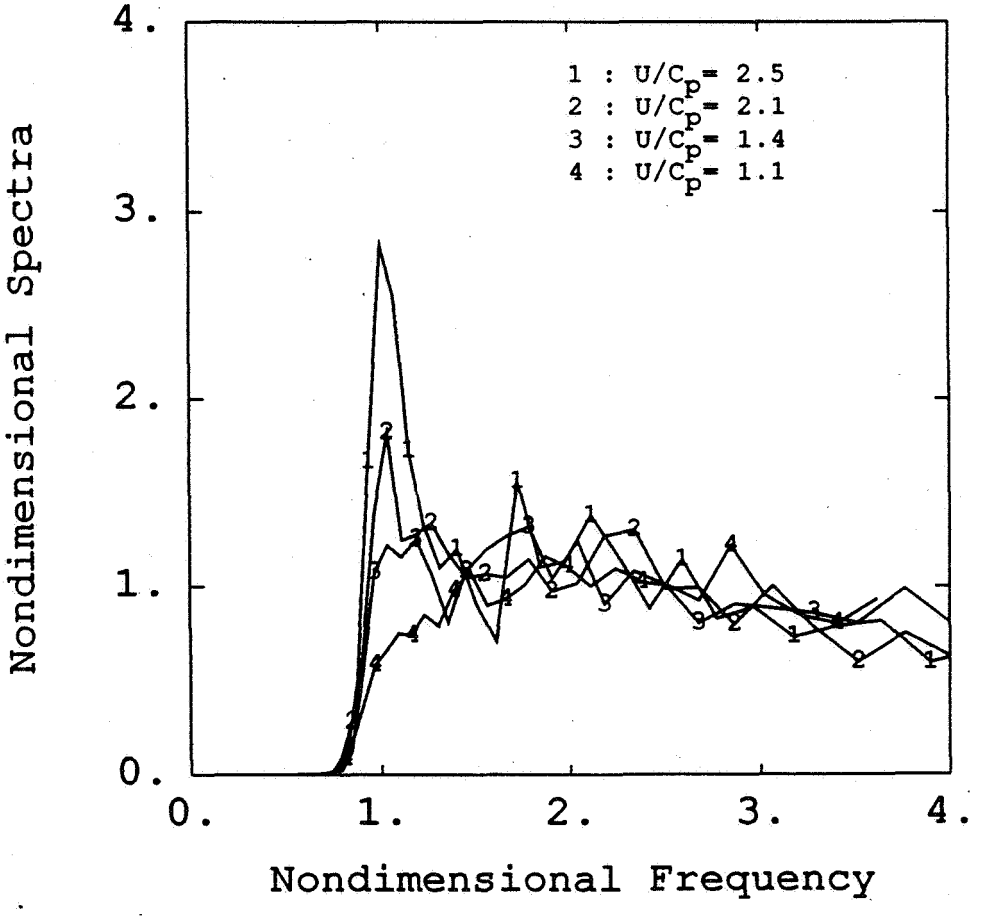

Figure 5.2.5: Nondimensional energy density spectra, $\omega^4 E(\omega)$ normalized by the value of $\omega^4 E(\omega)$ averaged over $1.5 < \omega/\omega_p < 3.5$, against the nondimensional frequency, ω/ω_p. The flatness of the nondimensional spectra irrespective of the level of wind forcing imply that a spectral slope of -4 is appropriate for $1.5 < \omega/\omega_p < 3$.

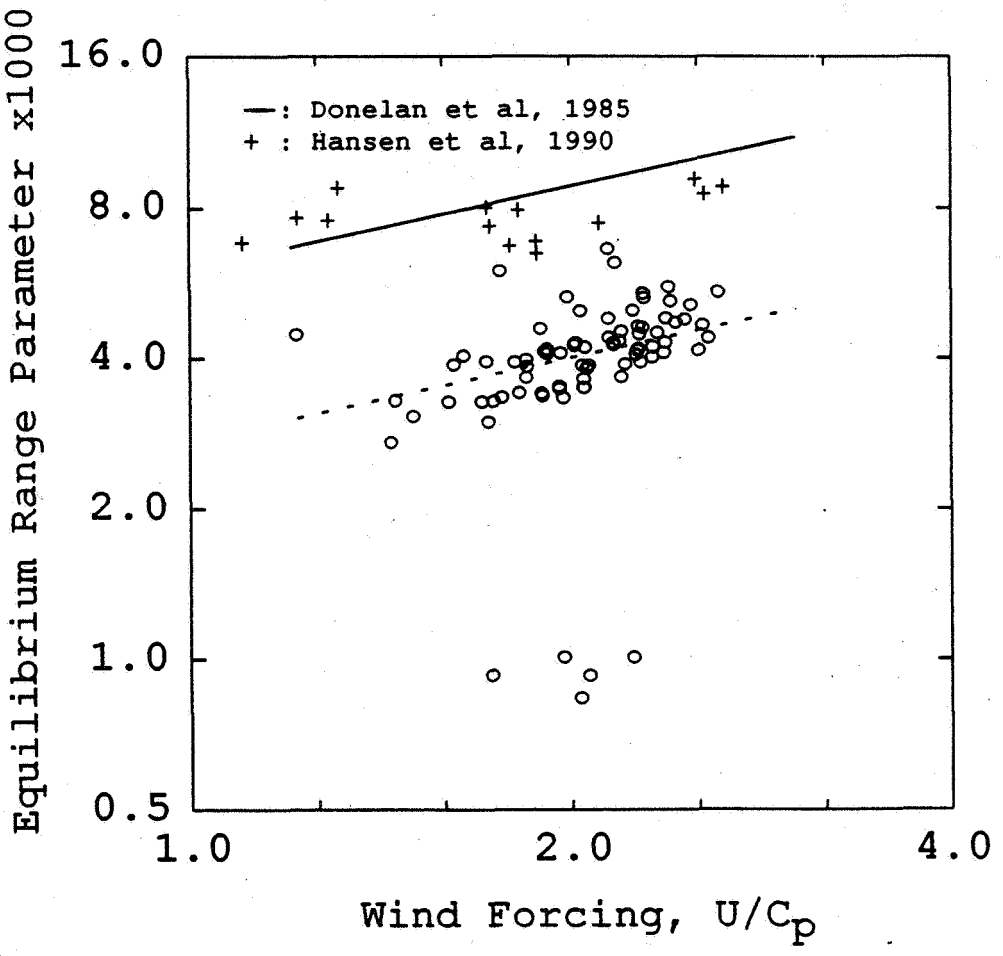

Figure 5.2.6: Equilibrium range parameter, α, against the wind forcing, U_{10}/C_p. (o) Results from this study; (–) $\alpha_D = 0.006(U_{10}/C_p)^{0.55}$ by Donelan *et al* (1985); (- -) Same as (–) except for the coefficient of (0.006/2.2); (+) Results by Hansen *et al* (1990) based on their measurements also on Lake Washington. Comparison with this study shows that the results by Hansen *et al* (1985) are different. Equilibrium range parameters from the present investigation show a systematic variation with U_{10}/C_p as suggested by Donelan *et al* (1985). However, the absolute values differ as indicated by the solid and dashed lines. The equilibrium range parameters for the cases during which surface slicks were observed, were much lower.

slicks were observed, were much lower. The data points reported by Hansen *et al* (1990, also from Lake Washington) are included for reference. The average value of their results is closer to that of Donelan *et al* (1985). However, as mentioned earlier, these results are based on an estimated calibration value for their wave gauge. Comparisons with present measurements and similar conditions suggest that their estimates of α_D could be off by about 50%, but their data set covers only a few hours. The less clear trend in their results may be due to noise in their limited data sets.

Discrepancies in the value of the equilibrium range parameter are not surprising. Values of the equilibrium range parameter from other experimental investigations (Kawai *et al*, 1977; Hasselmann *et al*, 1976; Mitsuyasu *et al*, 1980; Kahma, 1981; Forristal, 1981; Leykin and Rozenberg, 1984; Battjes *et al*, 1987; Toba *et al*, 1988) vary by a factor of 10. Conversions of these findings to a form suggested by Donelan *et al* (1985) require various approximations to relate u_* to U_{10} and $\tilde{F}$ to U_{10}/C_p. Also, in many cases ω_p has not been reported. Therefore, exact conversions were not attempted. However, these values would roughly scatter around the solid line in Figure 5.2.6 with the lowest values being comparable to the findings in this study.

In summary, the parameters of the observed gravity wave field were found to depend systematically on the wind forcing, U_{10}/C_p, as suggested by Donelan *et al* (1985). However, the nondimensional variance, $\tilde{V}$, of the surface elevations hence, the equilibrium range parameter, were smaller by about 50% than the predicted values for a given U_{10}/C_p. Considering the similar deviations between the results of Hasselmann *et al* (1973) and Kahma (1981) where parameterization was based on the nondimensional fetch, $\tilde{F}$, it can be concluded that $\tilde{V}$ may not be well defined by U_{10}/C_p or $\tilde{F}$ alone. Also, the relationship between the nondimensional fetch, $\tilde{F}$, and U_{10}/C_p for our data was found to differ from the

empirical form given by Donelan *et al* (1985) with our data showing a weaker dependence (flatter slope).

5.3 Estimate of Surface Roughness Length from Wave Data

In this section an estimate of the surface roughness length, $z_{o\zeta}$, is obtained from the long wave observations and is compared to z_o deduced from flux measurements and other suggested formulations. As discussed in Section 2.5, the surface roughness length is thought to be proportional to some wave related length scale weighted by a function that reflects the mobility of the surface roughness elements. Although the specific form of this relationship is controversial, there is an increasing support (see Section 2.5) for

$$gz_o/u_*^2 \propto z_o/\zeta_{rms} \propto f(C_p/U_{10})^m \propto f(C_p/u_*)^m, \quad m = -1, \tag{5.3.1}$$

where $\zeta_{rms} = \overline{\zeta^2}^{1/2}$ is the rms wave height. For the present purpose, i.e. to obtain $z_{o\zeta}$ using the wave data only, the formulation suggested by Donelan (1990) based on a large data set

$$z_o = 5.53 \times 10^{-4} \zeta_{rms} (U_{10}/C_p)^{2.66}, \tag{5.3.2}$$

was used. Since $\zeta_{rms} \propto (U_{10}/C_p)^{-1.65}$ (Donelan *et al*, 1985), the above formulation corresponds to the form given by Equation 5.3.1. Furthermore, the wind forcing term was replaced with the equilibrium range parameter, $\alpha_D = 0.006(U_{10}/C_p)^{0.55}$, since they were found to be strongly correlated (see Figure 5.2.6). The result is

$$z_{o\zeta} = 7.2 \times 10^{-3} \zeta_{rms} (\alpha_{Dm}/0.006)^{2.1}, \tag{5.3.3}$$

where the subscript m indicates that α_D was obtained from the measured wave spectra. The reason for this substitution is that although the variations in

wind speed during the selected periods were 20% of the mean or less, occasionally these periods were preceded by conditions of higher or lower average wind speeds. In a study of the response of wind–wave spectra to unsteady winds Toba *et al* (1988) found that the equilibrium range parameter shows a remarkable fluctuation on a time scale of the order of ten minutes, much faster than the time scale of growth of the dominant waves. Also, under strong wind forcing the waves become nonlinear with narrow high crests and wide shallow troughs (Stokes, 1847). Such a wave form requires the existence of a fundamental free wave and its bound harmonics with all components propagating at the phase speed of the free wave (Ramamonjiarisoa *et al*, 1978; also Section 2.1.2). In a Fourier analysis, these bound harmonics appear as secondary peaks at multiples of the peak frequency (e.g. Lake and Yuen, 1978; Komen, 1980) and can cause an increase in the equilibrium range parameter (Donelan *et al*, 1985). Therefore, by using the measured α_{Dm} rather than an average value of U_{10}/C_p, the estimated $z_{o\zeta}$ is allowed more freedom to vary with a changing relationship between wind and waves.

In Figure 5.3.1 estimates of $z_{o\zeta}$ determined according to Equation 5.3.3 from wave measurements are compared to z_o estimated from atmospheric flux measurements and flux–profile relations. Excluding the five data points from the slick cases for which $z_{o\zeta} \approx 10^{-6}$, variations in $z_{o\zeta}$ are approximately confined within one decade around its mean value of 10^{-4}. z_o has a similar mean value but its scatter is significantly large. As it will be seen in later discussions, the observed magnitudes of $z_{o\zeta}$ are very characteristic of the experimental conditions encountered and the extreme values of z_o are unreasonable. If these extreme values of z_o are masked, the agreement between the two estimates becomes more evident. The data points from measurements of surface fluxes that deviate significantly from wave related estimates are mainly the outliers. Such deviations may be caused by the intermittency in atmospheric turbulence,

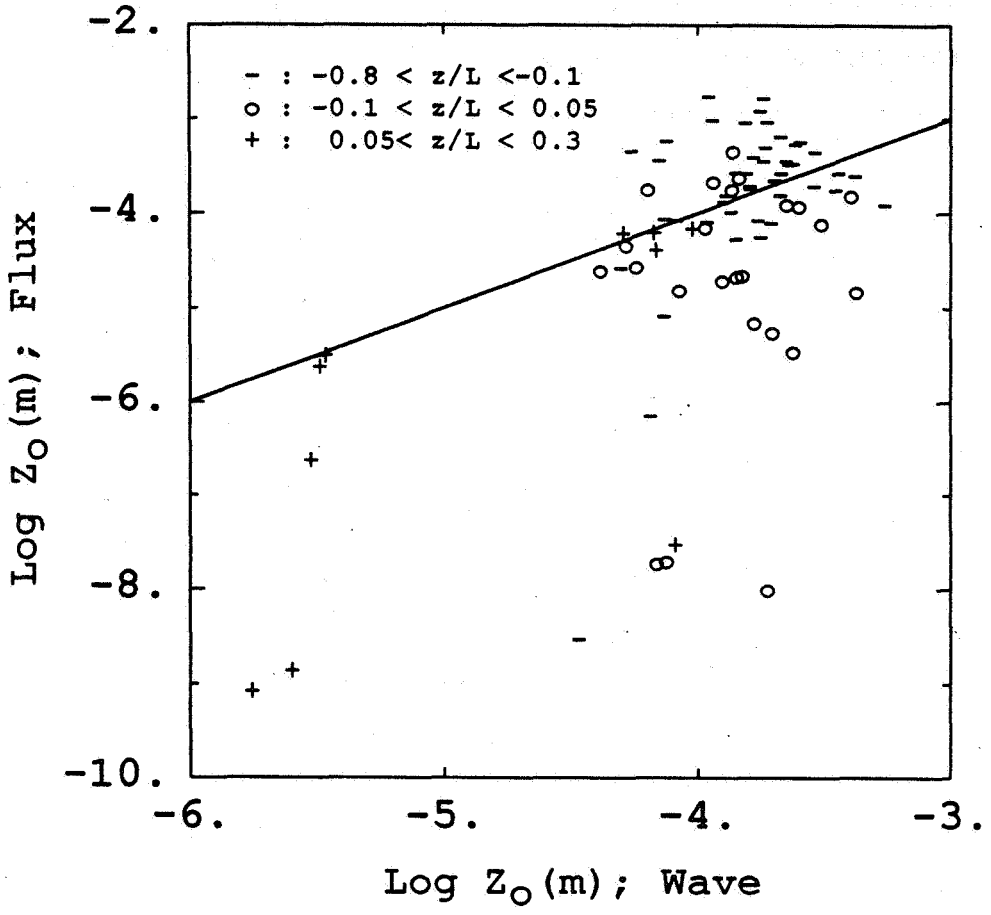

Figure 5.3.1: Comparison of the surface roughness length, z_0, estimated from atmospheric flux measurements to $z_{0\zeta}$ obtained from surface wave measurements. Five data points for which $z_{0\zeta} \approx 10^{-6}$ correspond to the slick cases. The rest of the observed magnitudes of $z_{0\zeta}$ are very characteristic of the experimental conditions encountered. The extreme values of z_0 that deviate significantly from wave related estimates are unreasonable. If these extreme values of z_0 are masked, the agreement between the two estimates becomes more evident. The straight line describes the ideal one–to–one correspondence between z_0 and $z_{0\zeta}$.

sampling variability arising from observations being conducted at one location and the low frequency atmospheric motions. The results obtained from the wave field are much more consistent, i.e. show less scatter, because the changes in the wave spectrum relevant to this study occur on long time and length scales. Hence, the observed wave spectra reflects the atmospheric energy input integrated over a large space.

$z_{o\zeta}$ from the present study is compared to the surface roughness lengths estimated from three model formulations in Figure 5.3.2. Note that the $z_{o\zeta}$ values obtained from wave spectra have the same trend as the points from Donelan (1990) as they should since both formulations are based on Donelan's *et al* (1985). Also, $z_{o\zeta}$ is smaller than the predictions as expected because the observed rms wave height and the equilibrium range parameter were smaller than the values suggested by Donelan *et al* (1985; see Figures 5.2.2 and 5.2.6). The estimates from Liu *et al* (1979) show good agreement with the wave–related results as well as with those predicted by Donelan (1990) at lower values of z_o, but they deviate systematically with increasing z_o. As mentioned before momentum fluxes, hence z_o, predicted by the Liu *et al* (1979) model are based on the results of Kondo (1975). In Section 5.1, comparisons of z_o from surface fluxes and from Kondo (1975) were presented (see Figure 5.1.8). There, it was noted that when plotted against the wind speed, predictions by Kondo (1975) were somewhat lower than the results from flux measurements. This is consistent with the findings in Figure 5.3.2. On the other hand, the predictions by Toba *et al* (1990; Equation 5.3.1 with $m = +1$) are overestimates in the full range of observations and their trend is similar to that of Liu *et al* (1979). Four $z_{o\zeta}$ values that lie above the predictions by Toba *et al* (1990) are from cases of suddenly calming winds and their magnitudes are in agreement with the expectations under such conditions (see Section 5.4).

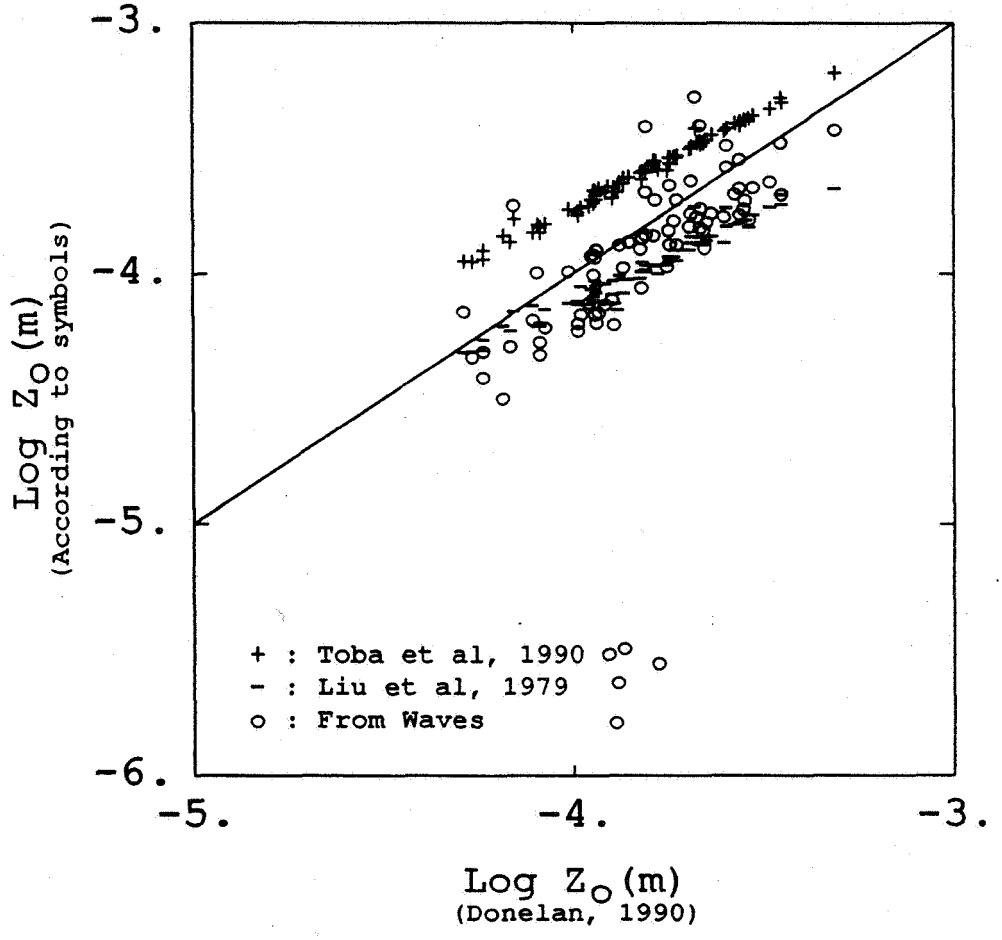

Figure 5.3.2: Comparisons of the surface roughness length, $z_{o\zeta}$, obtained from surface wave measurements to the estimates from three other formulations. $z_{o\zeta}$ values have a trend that is similar to those from Donelan (1990) but they are slightly lower as expected due to the differences in the magnitudes of the rms wave height and equilibrium range parameter between the observations and the predictions by Donelan *et al* (1985). The values predicted by Liu *et al* (1979) and Toba *et al* (1990) show similar trends but deviate from the others systematically with increasing z_o. The lowest five values of wave related estimates correspond to the cases for which surface slicks had been observed.

From the results illustrated in Figures 5.3.1 and 5.3.2 the success of the present approach in which the surface roughness length is determined using the equilibrium range parameter and the rms wave height obtained from the measured wave spectra is obvious. While the model predicted values of z_o show little variation, the wave related estimates, $z_{o\zeta}$, reflect the variability observed in flux–derived values (Figure 5.3.1) including those five cases when surface slicks had been observed occasionally.

The results obtained in this section show that the surface roughness length can be determined from the measurements of the equilibrium range parameter and the rms wave height with fine resolution. Consistency of the wave– and surface flux–derived roughness lengths, $z_{o\zeta}$ and z_o, respectively, indicate that parameterization of z_o according to Equation 5.3.1 with $m = -1$ is more appropriate than with $m = +1$ as proposed by Toba *et al* (1990). Also z_o obtained from surface fluxes is more likely to contain a sampling error than those obtained from wave spectra when temporal measurements at a fixed point are used.

5.4 Bulk Transfer Coefficients

In this section the bulk transfer coefficients are evaluated. The calculations were made according to the definitions given by Equation 2.5.10 in which these coefficients are expressed in terms of the characteristic roughness lengths, von Kármán constant, taken as 0.4, and 10 m height. The findings are compared to the values used by the surface flux model of Liu *et al* (1979) to test its applicability to the present observations.

Neutral drag coefficients, C_{DN}, for the selected cases are displayed in Figure 5.4.1. Overall average of C_{DN} calculated by using $z_{o\zeta}$ obtained from wave spectra can be described by $(1.29 \pm 0.14) \times 10^{-3}$. The mean value of C_{DN} from flux measurements is similar but the standard deviation is three times

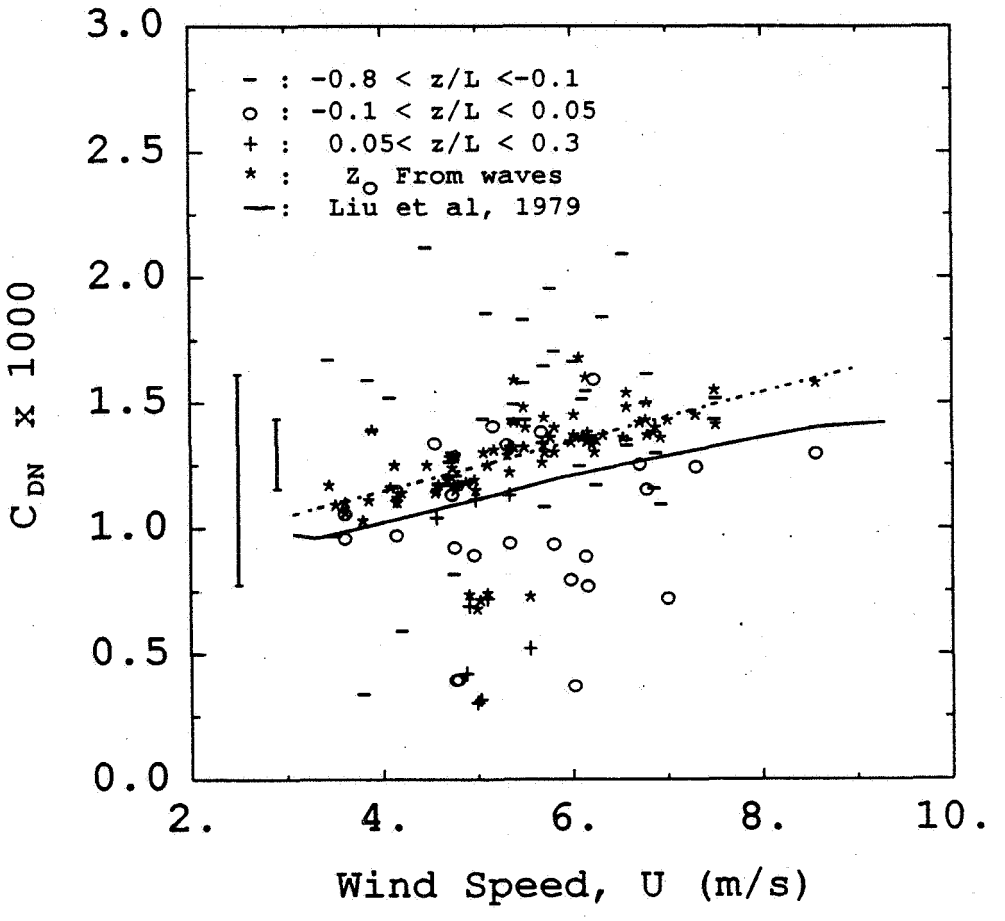

Figure 5.4.1: Neutral drag coefficient, C_{DN}, against the wind speed, U_{10}. The symbols indicating different atmospheric stratifications are associated with C_{DN} obtained from flux measurements. (*) indicates the values calculated using the surface roughness length, $z_{o\zeta}$, obtained from wave spectra. The dashed line which is a fit to the (*) values may be taken as representative of the ensemble average of experimental results. The long and short vertical bars with a total length of two standard deviations, are centered around the overall mean values of C_{DN} derived from measurements of fluxes and waves, respectively. The difference between the value predicted by Liu *et al* (1979, solid line) and the fit to the experimental results is systematic and is about 10% to 15%.

larger, $(1.19 \pm 0.42) \times 10^{-3}$. The large scatter of the data points obtained from measured fluxes manifests the variability of turbulent transport in light wind conditions. Considering that the wave–related data points nearly fall on a straight line and the atmospheric data points are almost symmetrically distributed around this line, the wave–related values may be taken as the ensemble average of the experimental results. A linear fit to the data points deduced from wave measurements yields

$$C_{DN} = (0.75 + 0.10U_{10}) \times 10^{-3}. \tag{5.4.1}$$

The above representation is useful for comparison purposes. The magnitudes of the wave–related C_{DN} and their variation with wind speed (Equation 5.4.1) are typical of numerous experimental investigations (see review by Geernaert, 1990). A widely used formulation of C_{DN} by Kondo (1975) also serves the model of Liu *et al* (1979) and is desribed by the solid line in the figure. The difference between the experimental values described by Equation 5.4.1 and those predicted by Kondo's (1975) formulation varies from 10% to 15%. The predicted values are lower for the wind speeds considered. Differences of this magnitude are generally within the range of experimental uncertainties as well as within the approximation of a constant flux layer. However, the observed deviations are systematic therefore, they must be accounted for.

The distribution with respect to z/L of C_{DN} deduced from surface fluxes may appear to indicate a dependency on atmospheric stratification. However, this appearance is not real as shown by the following arguments. Firstly, as seen in Figure 5.2.2 the total wave energy which is proportional to the total variance of surface elevations, does not reflect any dependence on stratification. Then, assuming that the fraction of the atmospheric energy input retained by the waves is the same for all the cases studied, it can be concluded that C_{DN}

obtained from surface fluxes should not depend on the atmospheric stratification either.

Secondly, the measurements have been adjusted to neutral atmospheric stratification using the Businger–Dyer formulation (Equations 2.5.5–2.5.7) and the same U_{10} has been used to calculate C_{DN} from surface fluxes and from wind–generated waves. Except for the five cases of stable stratification which will be discussed in the next section, C_{DN} from wave data increases with U_{10} in a consistent manner and unlike C_{DN} from surface fluxes they show little scatter irrespective of z/L. This is seen more clearly from Table 5.1 where samples of C_{DN} corresponding to the same periods of measurements of surface fluxes and of waves are compared for various U_{10} and z/L. The samples grouped in pairs have been obtained from consecutive periods of different runs except the one marked with (*) which is from a case with environmental conditions similar to those of the last pair. Comparisons show that C_{DN} obtained from surface fluxes varies by a large amount between two consecutive periods even under steady wind conditions. These large differences must be due to sampling variability because C_{DN} obtained from wave measurements shows no significant change for the same consecutive periods. Therefore, it can be concluded that the dependence of C_{DN} on z/L suggested by the distribution of the data points in Figure 5.4.1 is not real but it is due to the combination of large scatter of the data points and insufficient number of samples.

Another point to be noted in Table 5.1 is that some samples of C_{DN} were from periods of changing wind speeds. C_{DN} determined under such conditions may be in error due to the uncertainty in the mean wind speed assigned to the sampling period. However, the impact of this error on the overall results is not expected to be significant because selected runs were dominantly from periods of steady winds and also during cases when mean wind speed had an increasing

Table 5.1: Examples of C_{DN} showing that large variations in results obtained from surface flux measurements are due to sampling variability. This assumption is also supported by the values obtained from wave measurements which increase with wind speed in a consistent manner regardless of stratification. Each pair of C_{DN} has been obtained from consecutive periods of different runs except the one marked with (*) which is from a case similar to the last pair.

U_{10} (ms^{-1})	$C_{DN} \times 10^3$ (Flux)	$C_{DN} \times 10^3$ (Wave)	z/L	Wind trend
3.5	0.96	1.07	-0.51	Rising
3.8	0.33	1.01	-0.13	Rising
5.1	1.43	1.28	-0.28	Steady
4.5	2.11	1.23	-0.43	Calming
5.7	1.08	1.28	-0.27	Steady
5.5	1.83	1.30	-0.31	Steady
6.1	1.54	1.32	-0.19	Steady
5.1	1.85	1.23	-0.29	Calming
5.8	1.95	1.34	-0.24	Steady
6.1	1.51	1.34	-0.25	Steady
5.7	1.33	1.31	-0.15	Steady
6.5	2.09	1.34	-0.17	Rising
6.2	1.16	1.35	-0.12	Steady
6.3	1.84	1.35	-0.14	Steady
6.2	0.77	1.36	0.00	Rising
6.7	1.25	1.40	-0.05	Steady
6.0	0.37	1.35	0.03	* Steady

or decreasing trend, the variations in U_{10} in a particular sampling period were less than 2 m/s.

Large variations in the wind field can occur over much shorter time scales than those in the wave field. Therefore, during changing wind conditions the wave field may not have adjusted to the present winds. Under calming conditions this may result in a sea surface that is too rough for the present wind speed. Then, since C_{DN} is directly proportional to the surface roughness, it is expected to be larger during calming conditions than during steady state for the same wind speed. The opposite argument applies to the conditions of rising winds. Determination of the nature of the surface fluxes during rapidly changing environmental conditions such as in frontal zones are of utmost importance. However, little is known about this matter (e.g. Davidson, 1982; Geernaert *et al*, 1986; Geernaert, 1990; DeCosmo, 1991) due to the paucity of such data and to the limitations in the applicability of the common analysis techniques that rely on stationarity and horizontal homogeneity to such circumstances where these assumptions may not be valid.

A case study was conducted using the data, run number 16 in Table 3.1, when the winds showed the most dramatic variations in speed among the available data sets. The time series of U_{10} and C_{DN} for this period are illustrated in Figure 5.4.2. Light precipitation occurred during the period of 60–70 min when the gusty winds exceeded 10 m/s. The general agreement between the results based on Equation 5.4.1 and C_{DN} obtained from wave data is remarkably good. In accordance with the above expectations, C_{DN} from wave data were higher during calming winds by up to 23% (30–40 min and 85–110 min) and lower during increasing winds by up to 10% (25 min and 55 min) than the values from Equation 5.4.1 which is based on the steady state observations. On the other hand, C_{DN} from flux measurements varied approximately from 0.5×10^{-3} to 2×10^{-3} without any discernible relation to U_{10}. Review of the uw cospectra

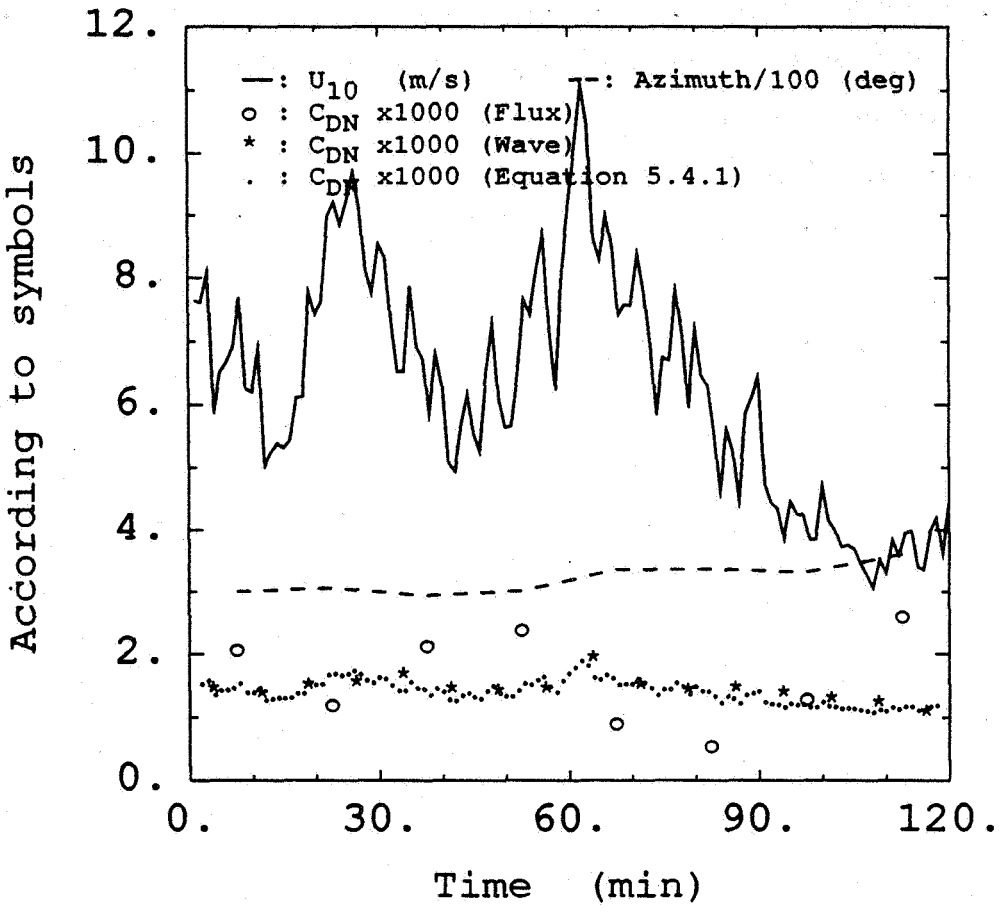

Figure 5.4.2: A case study of the neutral drag coefficient, C_{DN}, during rapidly changing wind speeds, U_{10}. Light precipitation occurred during the period between 60–70 *min*. The general agreement between the results based on Equation 5.4.1 and C_{DN} obtained from wave data is remarkable. Also, as expected C_{DN} from wave data are higher during calming winds (30–40 *min* and 85–110 *min*) and lower during increasing winds (25 *min* and 55 *min*) than the values from Equation 5.4.1 which is based on the steady state observations. On the other hand, C_{DN} from flux measurements varies approximately from 0.5×10^{-3} to 2×10^{-3} without any discernible relation to U_{10}. Review of the *uw* cospectra for this period showed that the inconsistent behavior of C_{DN} is largely due to the large variations in contributions to the total covariances from low frequency components.

for this period showed that the inconsistent behavior of C_{DN} is largely due to the large variations in contributions to the total covariances from low frequency components. These results clearly prove that the method of determination of C_{DN} from wind wave spectra devised in the present investigation has great potential for studies of transitional periods. With a better understanding of the response of the water surface waves to veering winds, the present approach may be improved or other methods may be constructed for applications to more complicated situations observed on open oceans.

The results on Stanton number, C_{HN}, obtained from measured fluxes are shown in Figure 5.4.3. The reason for plotting against z/L is to examine the behavior of C_{HN} in unstable and stable regimes as well as to isolate the data points corresponding to near neutral conditions. Due to large scatter and scarcity of the data points, a critical comparison of the Liu *et al* (1979) model to our measurements of sensible heat flux could not be made. (However, see the following discussions on C_{EN}.) Since there was no clear trend, the results were interpreted as C_{HN} being independent of wind speed. On the other hand, its average value varied with the atmospheric stratification as

$$C_{HN} = \begin{cases} (1.10 \pm 0.43) \times 10^{-3}, & \text{for -0.8}< z/L <\text{-0.1}, \\ (0.72 \pm 0.42) \times 10^{-3}, & \text{for 0.05}< z/L <0.3. \end{cases} \tag{5.4.2}$$

Considering that the change in the magnitudes of z_t and z_q are better characterized in terms of air–water temperature differences than in terms of the stratification parameter (see Figures 5.1.9 and 5.1.10), under near neutral conditions the bulk heat transfer coefficient should be selected according to this criterion, i.e. C_{HN} appropriate for unstable case when $T_a - T_s < 0$, and that appropriate for stable case otherwise. Since the mean values above are only one standard deviation apart, the confidence in this result is not great. However, these values are in good agreement with the reported values of 1.1×10^{-3} to

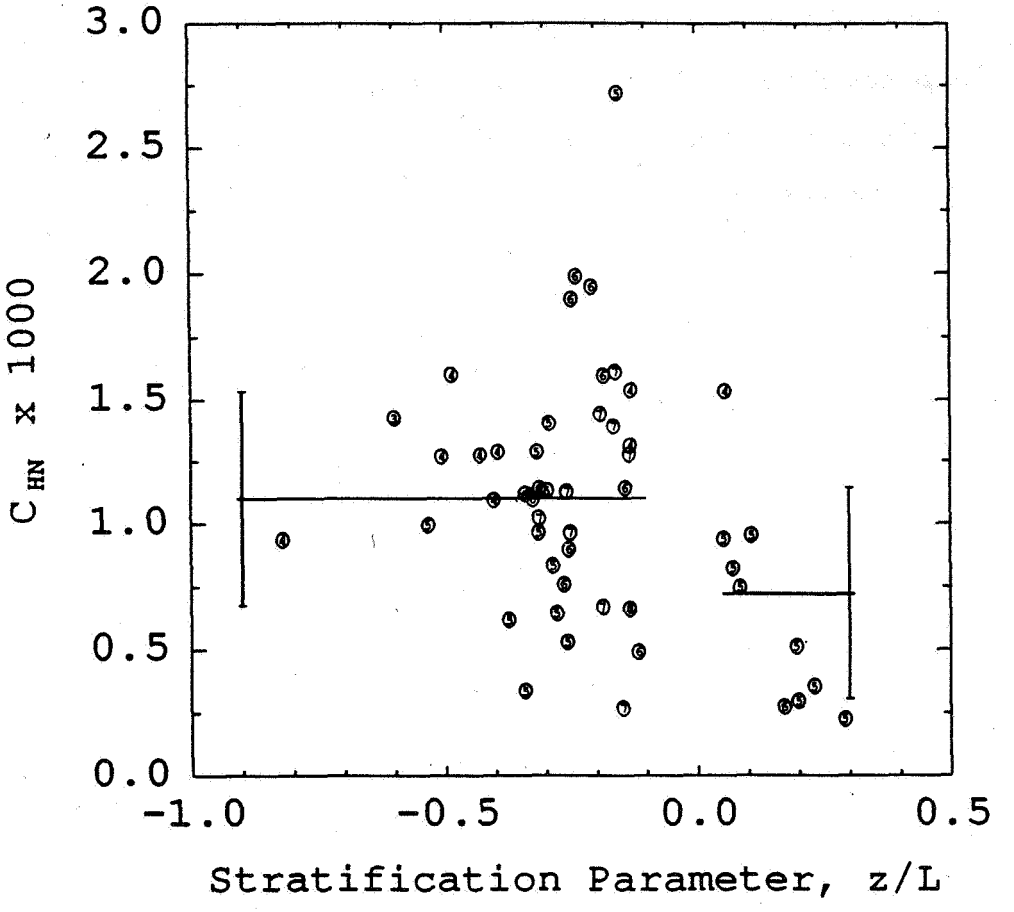

Figure 5.4.3: Stanton number, C_{HN}, against the stratification parameter, z/L. The results obtained from measurements of the sensible heat fluxes indicate that the Stanton number assumes different but constant values in the unstable and stable regimes and does not show any systematic variation with wind speed. The values corresponding to near neutral conditions have been omitted for clarity. Since the magnitudes of z_t and z_q are better characterized in terms of air–water temperature differences than of the stratification parameter (see Figures 5.1.9 and 5.1.10), under near neutral conditions C_{HN} should be selected according to this criterion, i.e. the value appropriate for unstable case when $T_a - T_s < 0$, and that appropriate for stable case otherwise. The vertical bars are centered at the experimental mean values and extend one standard deviation on each side. The horizontal lines indicate the range of validity for the given means. The numbers inside the circles correspond to the average wind speed for that run.

1.2×10^{-3} in the unstable regime (Smith, 1980; Anderson and Smith, 1981; Large and Pond, 1982; DeCosmo *et al*, 1988; DeCosmo, 1991) and 0.7×10^{-3} to 0.9×10^{-3} in the stable regime (Smith, 1980; Anderson and Smith, 1981; Large and Pond, 1982; Geernaert *et al*, 1987).

For Dalton number, C_{EN}, the situation was similar (Figure 5.4.4). The experimental data points suggest that the value of C_{EN} depends on the air–water temperature difference such that

$$C_{EN} = \begin{cases} (1.30 \pm 0.30) \times 10^{-3}, & \text{for } T_a - T_s < 0, \\ (0.70 \pm 0.23) \times 10^{-3}, & \text{for } 0 < T_a - T_s < 2.5. \end{cases} \tag{5.4.3}$$

Also, for $T_a - T_s > 2.5\ ^{\circ}C$, C_{EN} is seen to decrease further with increasing temperature difference. The results presented in the figure clearly indicate that this rapid change in the value of C_{EN} near $T_a = T_s$ cannot be described in terms of z/L. The reviews of published results by Smith (1989) and Geernaert (1990) show that the higher value of C_{EN} given in Equation 5.4.3 is commonly observed during unstable atmospheric stratification. These reviews also include a few cases where the reported magnitudes for stable stratification are low and similar to the present findings for $T_a - T_s > 0$. However, such low values have been suspected of instrumentational errors (see Smith, 1989). The adequacy of our instruments has been proved by the results from the HEXMAX field study (DeCosmo *et al*, 1988; DeCosmo, 1991). Therefore, this significant change (more than two standard deviations) in C_{EN} observed in the present and other investigations may deserve further attention.

One of the goals in this study is to evaluate the applicability of the surface flux model by Liu *et al* (1979) to the present observations. It was already demonstrated in Figure 5.4.1 that the model underestimates the neutral drag coefficient and hence, the momentum flux. For further comparisons, C_{EN} for $T_a - T_s < 0$ was plotted against U_{10} in Figure 5.4.5. Since the experimental results for $T_a - T_s > 0$ were much smaller than those for $T_a - T_s < 0$, they were

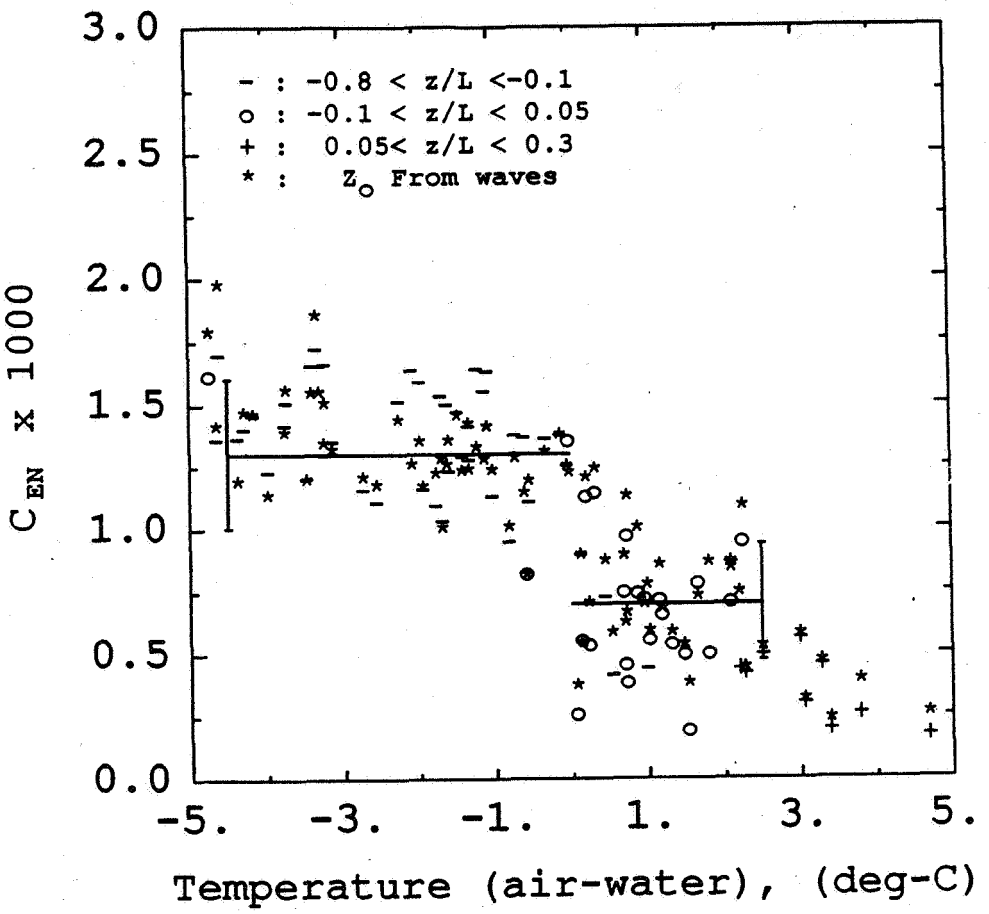

Figure 5.4.4: Dalton number, C_{EN}, against the air–water temperature difference. The symbols indicating different values of z/L are associated with the results obtained from measurements of the surface fluxes. The data points marked with (*) have been calculated using $z_{o\zeta}$ and show that some of the scatter in C_{EN} may be due to sampling error in atmospheric momentum fluxes. The experimental results may be interpreted as C_{EN} being constant for the wind speeds encountered with a characteristic value that depends on the air–water temperature difference. Note that the rapid transition in the value of C_{EN} cannot be described in terms z/L adequately. The vertical bars are centered at the experimental mean values and extend one standard deviation on each side. The horizontal lines indicate the range of validity for the given means.

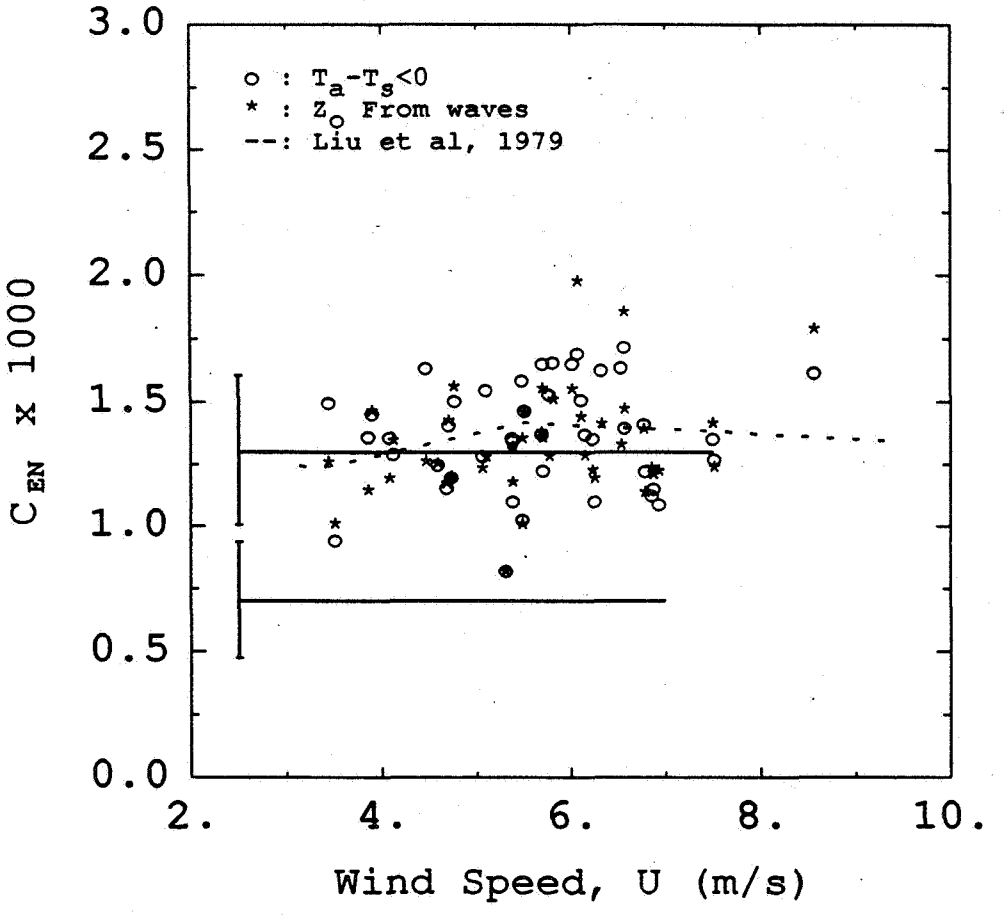

Figure 5.4.5: Dalton number, C_{EN}, against the wind speed, U_{10}. The upper and lower vertical bars are centered at the experimental mean values of C_{EN} for $T_a - T_s < 0$ and $T_a - T_s > 0$, respectively, and extend one standard deviation on each side. The horizontal lines indicate the range of validity for the given means. To avoid any possibility of causing a spurious dependence on U_{10}, only the data points for $T_a - T_s < 0$ are included. The values suggested by the Liu *et al* (1979) model are overestimates, particularly when $T_a - T_s > 0$. The symbol (o) indicates the results obtained from measurements of the surface fluxes. The data points marked with (*) have been calculated using $z_{o\zeta}$ and show that some of the highest values of C_{EN} may be due to sampling error in atmospheric momentum fluxes. The present results may be interpreted as C_{EN} being independent of wind speed with a characteristic value that depends on the air–sea temperature difference. The experimental results also show that the hypothesis of Liu *et al* (1979) about the variations in C_{EN} and C_{HN} due to shadowing effects in the wave troughs is not a valid one.

indicated only by their mean values to avoid any possibility of causing a spurious dependence on U_{10}. As seen in Figure 5.4.5, the values suggested by the Liu *et al* (1979) model are overestimates, particularly when $T_a - T_s > 0$. This is also true for Stanton number, beacuse of the similarity betweeen z_t and z_q (Figures 5.1.9 and 5.1.10) or between C_{HN} and C_{EN} (Figures 5.4.3 and 5.4.4). Also, the data points obtained using $z_{0\zeta}$ from wave measurements which mostly lie below the level of 1.5×10^{-3}, show that some of the highest values of C_{EN} may be due to sampling error in measured momentum fluxes. Therefore, the apparent increase in measured C_{EN} near $U_{10} = 6\ m/s$ is not significant. Together with the results presented in Figure 5.1.11 which suggested that the characteristic roughness scales for heat and moisture do not decrease with increasing roughness Reynolds number, it can be concluded that the hypothesis of Liu *et al* (1979) about the variations in C_{EN} and C_{HN} due to shadowing effects in the wave troughs is not a valid one.

As discussed in Section 5.1, in the present study z/L was estimated from the formulation of Large and Pond (1982). Now that the bulk transfer coefficients (Equations 5.4.1–5.4.3) from the field data were evaluated, the error introduced in z/L by using Large and Pond's (1982) formulation can be discussed. The heat exchange coefficients used in their formulation differ from the experimentally determined values only in C_{EN} for near neutral and stable conditions. Stratification corrections for near neutral conditions can be neglected. Only a few of the selected runs (10 out of 79) were from conditions of stable atmospheric stratification. During these cases the water surface temperatures were about 15 $^{\circ}C$ and the air–sea temperature differences varied from 2 to 5 $^{\circ}$. Contributions to z/L by the latent heat flux become important when the surface temperature is warm such as in the tropics or when there is a cold air outbreak over a marine surface. Hence, for the stable stratification cases encountered in this study such effects are not significant. The z/L formulation by Large and

Pond (1982) is based on a constant value of $C_{DN} = 1.2 \times 10^{-3}$ which corresponds to the experimental finding for $U_{10} = 4.5\ m/s$. Largest values of $|z/L|$ were also observed near this wind speed. At higher wind speeds, atmospheric stratification becomes closer to near neutral. At $U_{10} = 7\ m/s$ (above which there are four data points with two of them in near neutral conditions), the Large and Pond (1982) formulation underestimates the surface friction velocity by about 8%, well within the uncertainty of the experimentally determined values. Also the measurement heights for 70% of the selected runs were between 8 and 8.5 m, i.e. adjustments to the reference height of 10 m were negligible. Therefore, it can be concluded that although the z/L parameterization of Large and Pond (1982) is not the ideal one, the errors in the presented results introduced by this approximation are insignificant and do not affect the conclusions drawn.

In summary, the experimentally determined bulk transfer coefficients are generally in quantitative agreement with the findings from other investigations. However, the results obtained here indicate that the similarity of the turbulent exchange coefficients may not be restricted only to the unstable regime but may extend to the stable regime as well. These results also indicate that application of the Liu *et al* (1979) model to our observations may cause systematic errors in the estimated surface fluxes of momentum, sensible heat and water vapor. In particular, during stable stratification conditions, the predicted sensible and latent heat fluxes may be significantly overestimated.

5.5 Characteristics of the small scale waves

The purpose in this section is to investigate the response of the intrinsic frequency spectra of short gravity–capillary waves with wavelengths from 3 to 38 cm, to atmospheric energy input and surface films. This was attempted using the data sets collected in 1986 and 1987. This high frequency portion of the wave signal was not available in the data sets from 1988 and 1989.

The initial step in the analysis procedure was correction of Doppler shifts in the measured frequencies of small scale waves as described in Section 4.4. The next step was identification of the breaking events in the time series of short wave spectra so that they could be excluded from the ensemble averages. The detection scheme that we have developed earlier (Weissman *et al*, 1984), is based on the sudden increase in measured wave energy in a high frequency band (18–32 Hz) during wave breaking. However, the limits of the frequency band is not critical as long as the renewal time of the wave components corresponding to the selected band are short with respect to the long wave period. In the present study, the detection scheme was based on the wave energy in the 6–10 Hz band. The threshold criterion was determined by comparing the time of the detected event with the video recordings and good agreement was found. The portions of the data where the band energy exceeded its mean value by twelve standard deviations were found to be affected by the breaking waves and were not included in the following results. It was also noted that the increase in the band energy due to large scale breaking was about twenty standard deviations larger than the mean value. The breaking waves will be investigated in a later study.

The results of the above procedures on the wave spectra are illustrated in Figure 5.5.1 for the extreme cases of observed wind speeds, $U_{10} = 3.6\ m/s$ and 8.6 m/s. The atmospheric stratification during both of these runs was near neutral. The upper three curves are for $U_{10} = 8.6\ m/s$ and indicate the measured frequency spectrum and the intrinsic frequency spectra with breaking waves and without. The lower three curves are similar and are for $U_{10} = 3.6\ m/s$. The effects of Doppler frequency shifts on the average spectra at these frequencies (2–8 Hz) are about 5% and negligible. This is in agreement with the theoretical and experimental findings of Hansen *et al* (1990) based also on measurements from Lake Washington. The effects of wave breaking

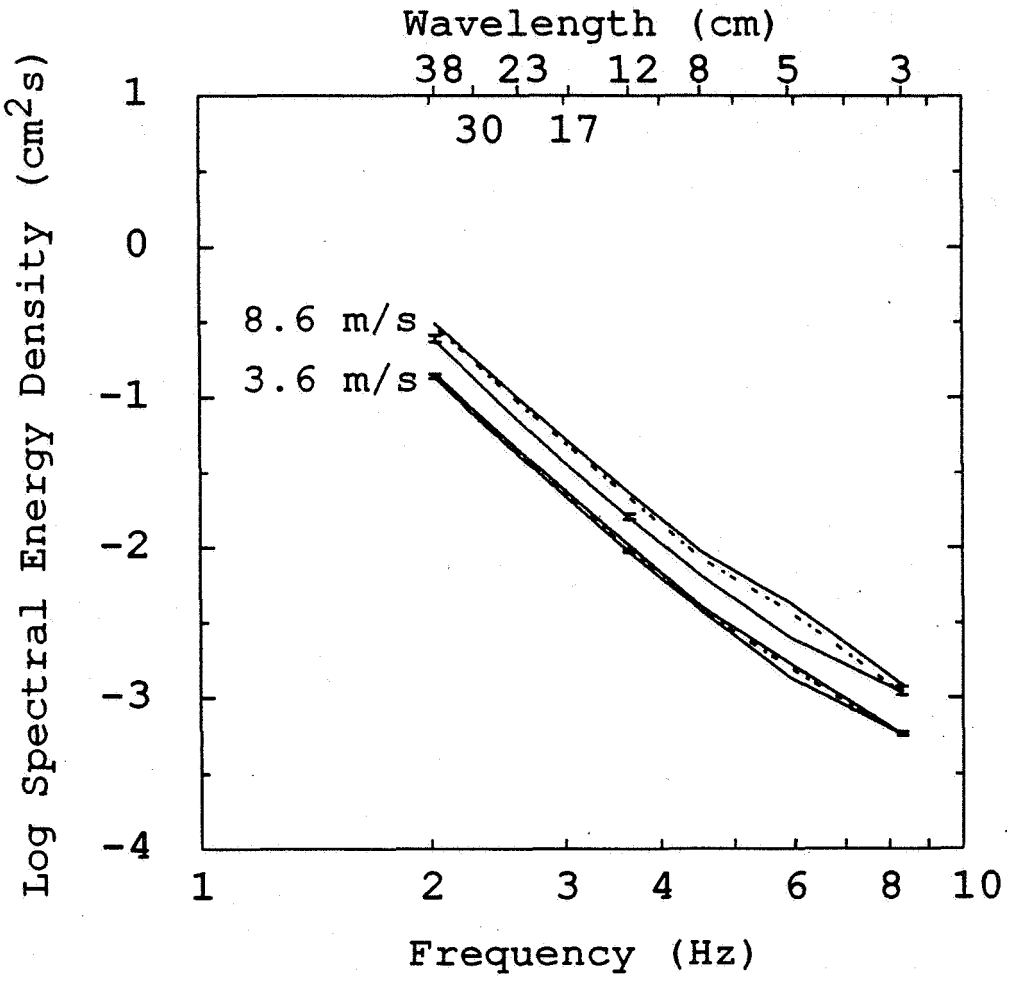

Figure 5.5.1: Energy density spectra, $E(f)$, versus the frequency, f. The upper three curves are for $U_{10} = 8.6\ m/s$ and indicate the measured frequency spectrum (top solid line) and the intrinsic frequency spectra with breaking waves (dashed) and without (lower solid line with 90% confidence interval marks). The lower three curves are similar and for $U_{10} = 3.6\ m/s$. At these frequencies (2–8 Hz), the effects of Doppler frequency shifts on the average spectra are negligible. Distortion of the spectra due to wave breaking is more significant in the higher wind speed case. Growth of the spectral energy densities with increasing wind speed is as expected.

on the spectra increase with wind speed. For $U_{10} = 8.6\ m/s$ these effects, that vary from 27% to 48%, are much stronger than those of Doppler shifts. Another point to be noted is the growth of the spectral energy densities with increasing wind speed. As wind speed increases from 3.6 to 8.6 m/s, the spectral energies of 38 and 3 cm long waves increase by 78% and 93%, respectively. These observed features are also consistent with the results of our previous studies (Ataktürk, 1984; Ataktürk and Katsaros, 1987) of small scale waves with intrinsic frequencies from 6 Hz to 17 Hz.

Composite frequency spectra for the selected runs from 1986 and 1987 data sets are displayed in Figure 5.5.2. Doppler shift corrected portions of the wave spectra are described by the curves in the frequency range from 2 Hz to 8 Hz. Consistent behavior of the composite spectra near $2Hz$ (marked by a gap) indicates that separation of the wave signal into low and high frequency portions by digital filtering was properly done. The most striking feature in Figure 5.5.2 is the presence of two family of curves. The lower set of curves correspond to run numbers 12–16 in Table 3.1. These periods of stable atmospheric stratification with $0.2 < z/L < 0.3$, had been previously noted for unusually low levels of measured momentum fluxes and for the wave field being underdeveloped for the observed wind speeds of $U_{10} \approx 5\ m/s$ (e.g. Figure 5.3.1). The term "underdeveloped" is in the sense of wave amplitude and not that of wavelength, because the spectral peak frequencies are typical of the conditions for $U_{10} \approx 5\ m/s$. These observed features can be interpreted as an indication of excessive dissipation of wave energy such as that due to surface films.

A smooth patch of water surface, generally attributed to the presence of surface films, was within the view of the video camera only once during these periods (after run 16). However, under identical conditions on the following day, three events were observed within a period of 2 hrs (not included in the selected runs). Therefore, it is probable that slicks were present upwind during

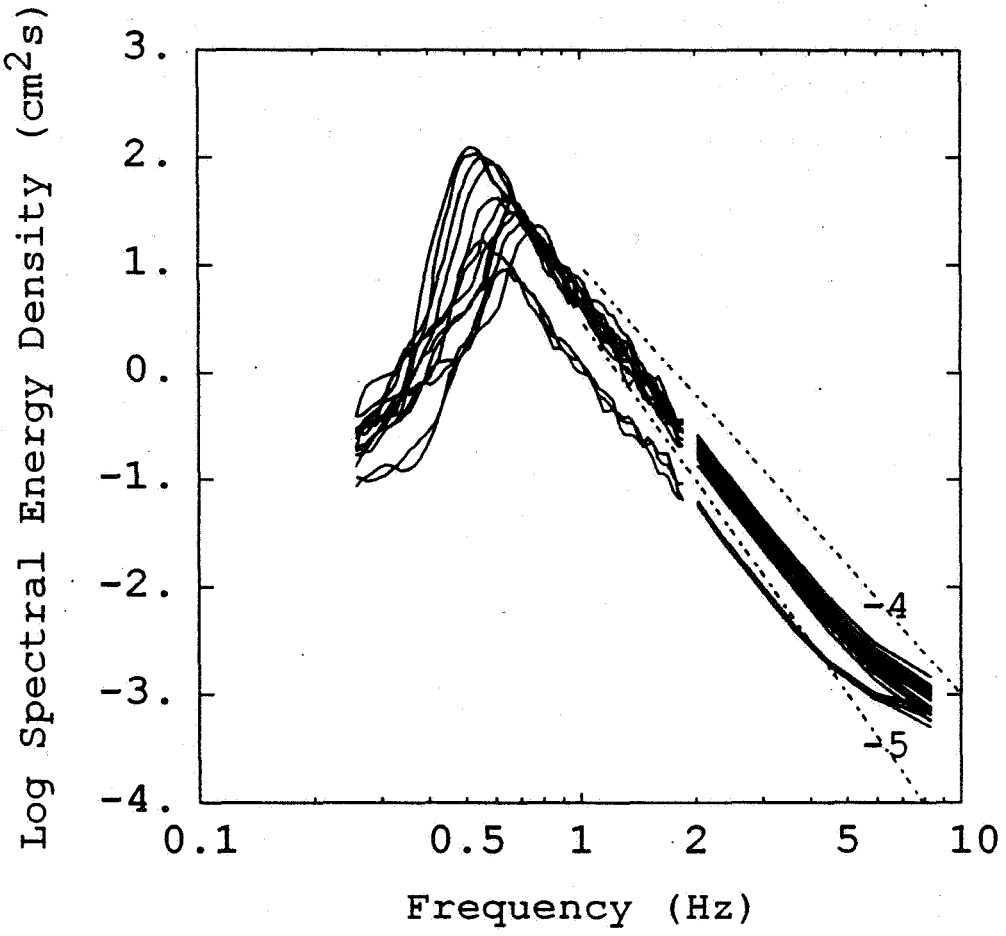

Figure 5.5.2: Composite energy density spectra, $E(f)$, versus the frequency, $f = \omega/2\pi$. The portion of the spectra above 2 Hz have been corrected for Doppler frequency shifts. Consistency of the composite spectra near 2 Hz (marked by a gap) indicates that separation of the wave signal into low and high frequency portions by digital filtering was properly done. The lower group of spectra correspond to the periods of stable atmospheric stratification with $0.2 < z/L < 0.3$, and had been previously noted for unusually low levels of measured momentum fluxes and for the wave field being underdeveloped for the observed wind speeds of $U_{10} \approx 5\ m/s$ (e.g. Figure 5.3.1).

runs 12–16 although they were not visually confirmed. These events lasted for about 2–7 *min*. Surface slicks, 1–4 *min* long in duration, were also observed during near neutral (run 3, $z/L = 0.01$) and unstable conditions of atmospheric stratification (run 23, $z/L = -0.49$) at lower wind speeds, $U_{10} \approx 3.5\ m/s$. However, the wave spectra corresponding to these cases are buried within the upper family of curves.

The above situation may be explained by the following hypothesis. Momentum flux from air to sea under stable atmospheric stratification occurs intermittently (Businger, 1973). During periods of less atmospheric activity, surfactants can form monomolecular films on the water surface that lead to suppression of existing waves through the Marangoni effect (Section 2.4). Consequently, the surface becomes smoother which, in turn, causes a reduction in the momentum flux in the next active period. This negative feedback results in a wave field that is subject to less atmospheric input and increased dissipation, such as those characterized by the lower family of curves in Figure 5.5.2. On the other hand, during near neutral and unstable conditions, steady action of the wind stress prevents the formation of surface films or quickly destroys those formed during low wind speed periods. Hence, the resulting effects on the wave field is not as dramatic.

The current investigation also provides information about the influence of natural surface films on intrinsic frequency spectra of wind waves. Such data which can be interpreted readily, are invaluable but also extremely scarce. (However, see Katsaros *et al* [1989] which includes some results from this work.) Analysis by Katsaros *et al* (1989) at the same site indicate that the naturally–formed surface films consist of biogenic materials with some petroleum residues also present, and deviations of surface tensions from that of clean water are typically less than 3 mN/m. This is also supported by the present study (see Section 3.2.5). The effects of surface films on the performance and calibration

of a resistance wave gauge do not pose a problem (Lobemeier, 1978). The observed "slicks of opportunity" were not large: 30–50 m long and 10–20 m wide. They were advected by the surface currents, and passed by the wave gauge within 1–7 min. Due to the small dimensions and short duration of these slicks, attention was focused on small–scale waves that are affected directly by the surface films. The attenuation of long gravity waves is an indirect result of the combined effects of reduced atmospheric input, enhanced dissipation and redistribution of the wave energy between wave components through nonlinear wave–wave interactions (Section 2.4). The time and length scales for the long wave attenuation are much larger than those of the observed slicks.

Attenuation of the short gravity–capillary waves in the presence of surface films are illustrated in Figure 5.5.3. The time next to each pair of spectra shows the duration of the observed slicks. For clarity, the spectra marked with 1,2 and 3 have been multiplied by a factor of 10^3,10^2 and 10, respectively. Wind speed during these periods was between 3.5 and 4 m/s. Spectra number 2 and 4 were from stable, number 1 from near neutral and, number 3 from unstable conditions of atmospheric stratification. In the figure, the lowest and highest frequencies correspond to the wavelengths of 38 and 3 cm, respectively, and the 90% confidence intervals are for the 5 cm long waves. The results show that 3 to 5 cm long waves are affected by the surface films first and in a very short period of time. Influence on longer waves becomes apparent with increasing duration. Attenuations experienced by the shortest waves, $\lambda = 3$ and 5 cm, varied between 24% and 46%. Attenuation of the longest waves, $\lambda = 38$ cm, ranged from zero to 26%. Degree of attenuation at a wavelength, $\lambda = k/2\pi$, was calculated from the Doppler corrected spectra as;

$$R = 100 \times [E - E_s]/E, \tag{5.5.1}$$

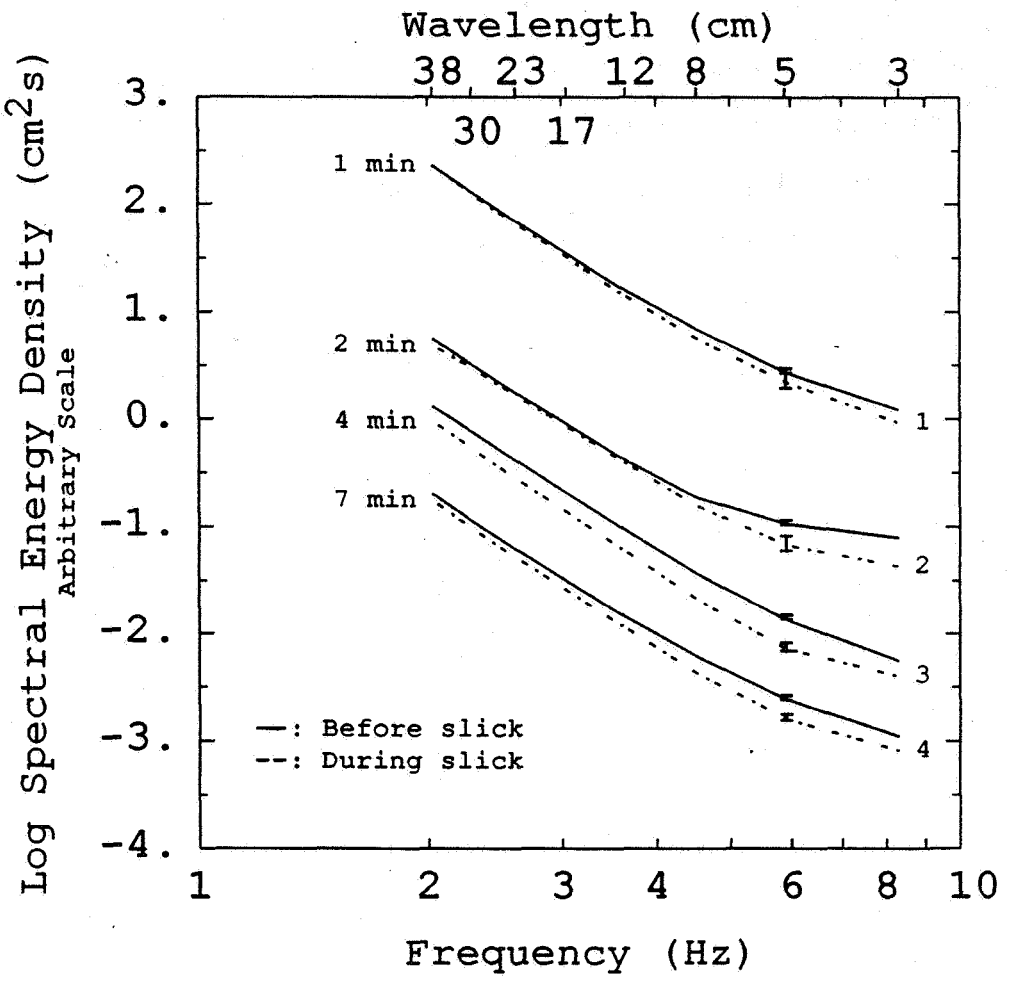

Figure 5.5.3: Energy density spectra, $E(f = \omega/2\pi)$, versus the intrinsic frequency, $f = \omega/2\pi$ showing the observed suppression of small scale waves by surface films. The indicated times are the durations of the slicks. Wave components at the highest frequencies (λ = 3 to 5 cm) are attenuated first and by 24% to 46% on the average. The attenuation at the lowest frequency ($\lambda = 38$ cm) occurs over longer duration and varies from zero to 26%. At still higher frequencies (not shown in the figure), the degree of attenuation decreases (see Katsaros *et al*, 1989).

where E and E_s are the average spectral energy density before and during slick, respectively.

The percentage attenuations given above are the averages over the duration of the slicks. In our previous study (Katsaros *et al*, 1989), the maximum attenuations for wave components from 4 to 17 Hz were found to be about 80%–90%, i.e. twice as high as the average values calculated here. Also, in that study we found that the attenuations decrease at frequencies above 10 Hz or wavelengths smaller than 2 cm. These findings at high frequencies had been attributed to the limited resolution of the wave gauge. However, the theoretical and experimental results obtained by Lombardini *et al* (1989) and the conclusions drawn from the reanalysis of available data by Wu (1989) show that the suppression of water surface waves by surface films are most effective for wavelengths between 2 and 40 cm (10 and 2 Hz, respectively) with maximum suppression occurring at wavelengths of 4–5 cm ($\approx$ 5 Hz) depending on the chemical composition and the thickness of the surface film. Therefore, the observed decrease in wave suppression at high frequencies reported by Katsaros *et al* (1989) are verified here.

In Section 5.2 it was seen that the spectral slope in the equilibrium range, $1.5 < \omega/\omega_p < 3$, is $\propto \omega^{-4}$ (Figure 5.2.5). Comparisons to the dashed lines in Figure 5.5.2 indicate that the spectral slope at higher frequencies, say up to about 4 Hz, is close to -5. At the highest frequencies, the spectral slope is seen to become gentler. Since a spectral slope of -5 cannot continue indefinitely, such a transition is expected. In our earlier studies of high frequency wave components (Ataktürk, 1984; Ataktürk and Katsaros, 1987), the spectral slope above 10 Hz was found to be approximately -3.3 which is in good agreement with -3.5 reported by Leykin and Rozenberg (1984) based on observations in the Caspian Sea over much wider ranges of wind speeds and sea states.

Zakharov and Filonenko (1966) originally suggested that the shape of the spectrum in the high frequency range is governed by the energy flux from the range of input to the range of dissipation, or from near the spectral peak to the high frequency tail of the spectrum (Zakharov and Zaslavskii, 1982, 1983; Kitaigorodskii, 1983; Leykin and Rozenberg, 1984; Phillips, 1985; Hansen *et al*, 1990). Also, the spectra at high frequencies are distorted due to the angular spreading of wave components that depends on the distance from the spectral peak (Banner, 1990; Section 2.2). Therefore, the composite wave spectra were nondimensionalized as in Figure 5.2.5 and were replotted (Figure 5.5.4). The results show that in this nondimensional form the spectral slope in the equilibrium range is about -4, but at higher frequencies it is not well defined and varies between -4 and -5. Since the highest frequency for all spectra was 8 Hz, the maximum nondimensional frequency extent of a spectrum in the figure depends on the peak frequency. Thus, as the peak frequency decreases the spectral slopes become larger and transition to much gentler slopes occur at higher nondimensional frequencies. Similar observations about the nonuniqueness of the spectral slopes have also been reported by Leykin and Rozenberg (1984) and Liu (1989) using large data sets. Although they did not make an explicit comment, such variations are also present in the results of Hansen *et al* (1990) based on the measurements also on Lake Washington. This subject requires further investigation.

In summary, it has been shown that the intrinsic frequency spectra of short gravity–capillary waves grow with increasing wind speed. Therefore, the energy density spectra of water surface waves at frequencies above the spectral peak cannot be satisfactorily represented by the simple form, $E(\omega) = \beta g^2 \omega^{-5}$ where β is a constant, as suggested by Phillips (1958). However, determination of the proper spectral form requires further investigation. When effective surface drift is taken to be that at a wavelength related depth, for the wavelengths

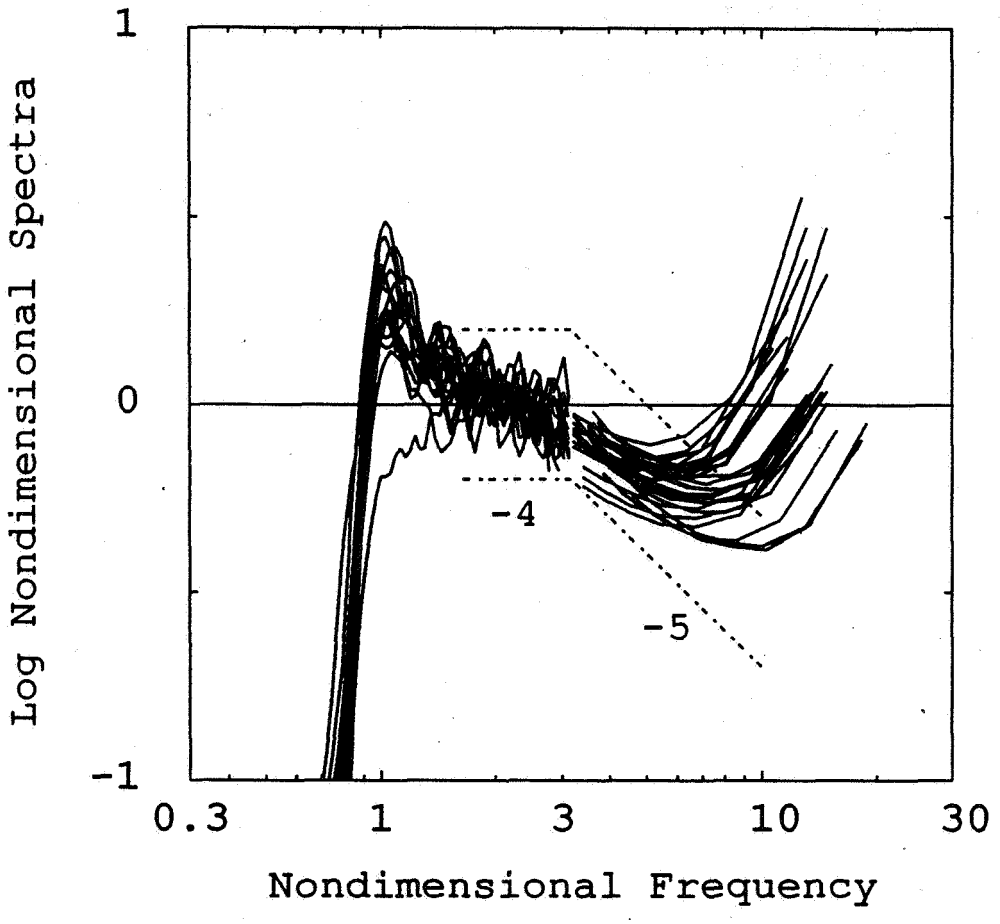

Figure 5.5.4: Nondimensional energy density spectra, $\omega^4 E(\omega)$ normalized by the value of $\omega^4 E(\omega)$ averaged over $1.5 < \omega/\omega_p < 3.5$, against the nondimensional frequency, ω/ω_p. A spectral slope of -4 is appropriate for $1.5 < \omega/\omega_p < 3$, but above the equilibrium range it is not well defined and varies from -4 to -5. With decreasing peak frequency, i.e. increasing dominant wavelength, the spectral slopes become larger and transition to gentler slopes occur at higher nondimensional frequencies. The dashed lines with slopes of zero and -1, correspond to spectral slopes of -4 and -5, respectively, in a dimensional representation.

considered, 3 *cm* to 38 *cm*, distortion of the wave spectra due to Doppler frequency shifts was found negligible. Much stronger effects on short wave spectra were found to be due to wave breaking. Together with the results from our previous study (Katsaros *et al*, 1989), attenuation of short gravity–capillary waves were found to be most effective for the wavelengths considered, 3–38 *cm*, and maximum for the wavelengths of 4–5 *cm*. A hypothesis was suggested to explain the observed underdeveloped amplitudes of the wave field during conditions of stable stratification when surface films were present.

CHAPTER 6: CONCLUSIONS

The analysis of the selected portions of the data sets collected over the years of 1986 through 1989 from a mast on Lake Washington provided further insight into the physical interactions between air and sea. Experimental conditions encountered at this site are highly repeatible. Also, the field data are free of the complications that may result from the presence of swell and tidal currents. The data sets analyzed clearly demonstrate the high degree of variability in air–sea interaction processes that are observed in a natural environment during light wind conditions.

6.1 Brief Summary of Results and Conclusions

Conclusions based on the experimental results and the uncertainties in these findings can be summarized as follows.

1) Under the conditions of light winds and nonneutral atmospheric stratification, various turbulence statistics were found to show large deviations from the values observed at higher wind speeds. The scatter in these statistics may result from inadequate averaging of the effects of the large scale eddies and the intermittent nature of the atmospheric turbulence as well as from methods used in removing the trend from the time series. Such statistics could not provide an estimate of the surface fluxes to an accuracy of better than 50%. Therefore, they may be useful only for qualitative description of the experimental conditions.

2) Measurements of the fluctuating components of wind, temperature and specific humidity were corrected for errors caused by the limited frequency response of the flux measuring system. After these corrections, surface fluxes were determined by the eddy correlation technique with an estimated uncertainty of 10% or 20% at most. For similar environmental conditions, the measured

fluxes of momentum, sensible heat and latent heat were found to vary by as much as $\pm 35\%$, $\pm 60\%$ and $\pm 30\%$, respectively. These large deviations from the overall means were mainly due to the sampling variability associated with our one–point measurements. Such variability in the experimental results may be reduced by spatial averaging.

3) A technique was devised to estimate the surface roughness length parameter and the neutral drag coefficient from the wave height spectra. The approach was based on the empirical relationships suggested by Donelan *et al* (1985) and Donelan (1990). On the average, the estimates obtained by this method were in good agreement with those determined through the measurements of surface fluxes. These results showed that $gz_o/u_*^2 \propto f(C_p/u_*)^m$ with $m = -1$. The wave–related estimates of the surface roughness length and the neutral drag coefficient were significantly more consistent than those obtained from atmospheric turbulence measurements. This was because variations in a wave field in response to changes in atmospheric input occur gradually. The response time for the observed waves were of the order of 10 *min*. For the same reason, z_o and C_{DN} determined from the measured wave spectra were higher (lower) during periods of rapidly decreasing (increasing) winds than during steady state conditions for a given U_{10} (Figure 5.4.2).

4) Characteristic roughness lengths for temperature and specific humidity were found to be similar in stable and unstable stratification. A slight difference in their magnitudes in the unstable regime with $z_q > z_t$ is in agreement with the results from other studies. However, establishing their observed similarity in the stable regime requires further investigation. It was also shown that z_t and z_q can be treated as constants with a value that depends on the atmospheric stratification. They do not vary with sea state due to shadowing effects in the wave troughs as suggested by Liu *et al* (1979).

5) Neutral bulk transfer coefficients determined from this study are generally in good agreement with the results from numerous studies conducted over the marine environment. However, significantly lower values of the exchange coefficient for latent heat flux obtained from near neutral and stable conditions may deserve further investigation. It is also suggested that the values of the exchange coefficients for heat fluxes in near neutral stratification should be selected with respect to air–water temperature differences and not with respect to z/L.

6) Under the conditions of light winds, estimates of the stratification parameter, z/L, based on the measured fluxes may be in large error due to the sampling variabilities mentioned in (1) and (2). Uncertainties in z/L may be reduced by using an estimate obtained from a verified bulk formulation. In the present study, z/L was estimated from the formulation of Large and Pond (1982).

7) Various parameters of the observed long gravity waves were found to depend systematically on the ratio, U_{10}/C_p, as suggested by Donelan *et al* (1985). However, for a given U_{10}/C_p the nondimensional variance of the surface elevations and the equilibrium range parameter were smaller by about 50% than the values given by Donelan *et al* (1985). Also, the relationship between the nondimensional fetch and U_{10}/C_p for our data was found to differ from their empirical form with our data showing a weaker dependence. The reason for these discrepancies may be that the present formulations do not include the effects of the wind duration.

8) The energy density spectrum of gravity waves in the nondimensional frequency range $0.85 < \omega/\omega_p < 3.5$ can be adequately represented by the model suggested by Donelan *et al* (1985), though care must be taken of the absolute magnitudes (see 7).

9) It was shown that the energy densities in the intrinsic frequency spectra of short gravity–capillary waves increase with increasing wind speed. Therefore, the energy density spectra of water surface waves at frequencies above the spectral peak cannot be satisfactorily represented by the simple form, $E(\omega) = \beta g^2 \omega^{-5}$, where β is a constant, as suggested by Phillips (1958). Determination of the proper spectral form requires further investigation.

10) When effective surface drift is taken to be that at a wavelength related depth, for the wavelengths considered (3 *cm* to 38 *cm*) distortion of the wave spectra due to Doppler frequency shifts was found to be negligible. Much stronger effects on short wave spectra were found to be due to wave breaking.

11) Short gravity–capillary waves with wavelengths from 3 *cm* to 38 *cm* were observed to be strongly attenuated by the surface films. Together with the results from our previous study (Katsaros *et al*, 1989), maximum attenuation was found to occur for the wavelengths of about 4–5 *cm*. A hypothesis based on the intermittency of the momentum flux during conditions of stable stratification and the increased likelihood of formation of surface films under such circumstances was suggested to explain the observed underdeveloped amplitudes of the wave field.

6.2 Recommedations for Future Research

Following is a list of research efforts that are needed to extend these ideas and results.

1) Intermittent nature of the turbulent transfer during conditions of stable atmospheric stratification needs to be quantitatively characterized. Neglecting this effect may cause large errors in the surface fluxes estimated from bulk formulations.

2) Dependency of the latent heat flux on atmospheric stratification needs to be clarified. Also, further evidence is needed to determine whether the

magnitudes of the bulk transfer coefficients for heat fluxes correlate better with the air–sea temperature difference or the atmospheric stratification parameter, z/L. In such efforts, fast response instruments should be used to reduce the uncertainty in the experimental results.

3) The wave height variance is not adequately parameterized in terms of fetch or U_{10}/C_p alone. Further efforts are needed to obtain a complete parameterization. Since evolution of a wave field depends not only on fetch and wind speed but also on the wind duration, the present formulations may be improved by including the effects of the wind duration.

4) The approach of determining the surface roughness length and the neutral drag coefficient from wave spectra, used in this investigation, was shown to be a powerful tool for studying the interaction between air and sea during unsteady wind speed conditions. The application of this approach to open ocean observations during which wind field may be changing both in speed and direction, such as in frontal zones, should be explored. For such applications, the approach followed here should be modified to include the response of the water surface waves to veering winds which is another not–well–understood aspect of air–sea interaction.

5) Breaking waves of different scales play a major role in air–sea exchanges of momentum, heat and matter. Despite their importance, the theory of wave breaking is far from being complete. Further progress in the area requires more experimental evidence.

REFERENCES

Adam, N.K., 1937: A rapid method for determining the lowering of tension of exposed water surface with some observations of surface tension of the sea and inland waters. *Proc. Royal Soc. (B)*, **122**, 134–139.

Alofs, D.J. and R.L. Reisbig, 1972: An experimental evaluation of oil slick movement caused by waves. *J. Phys. Oceanogr.*, **2**, 439–443.

Alpers, W. and K. Hasselmann, 1978: The two–frequency microwave technique for measuring ocean–wave spectra from an airplane or satellite. *Bound. Layer Meteorol.*, **13**, 215–230.

Alpers, W., 1983: Imaging ocean surface waves by synthetic aperture radar – a review. In *Satellite Microwave Remote Sensing*, T.D. Allan, Ed., John Wiley & Sons, NY, pp. 107–119.

Anderson, R.J. and S.D. Smith, 1981: Evaporation coefficient for the sea surface from eddy flux measurements. *J. Geophys. Res.*, **86**, 449–456.

Ataktürk, S.S., 1984: Intrinsic frequency spectra of small scale wave amplitude measured in a lake. M.Sc. thesis, Univ. of Wash., Seattle, 96 pp.

Ataktürk, S.S. and K.B. Katsaros, 1987: Intrinsic frequency spectra of short gravity–capillary waves obtained from temporal measurements of wave height on a lake. *J. Geophys. Res.*, **92**, 5131–5141.

Ataktürk, S.S. and K.B. Katsaros, 1989: The K–Gill: A twin propeller–vane anemometer for measurements of atmospheric turbulence. *J. Atmos. Ocean. Tech.*, **6**, 509–515.

Banner, M.L., 1986: A comparison of the wave–induced momentum flux to breaking and nonbreaking waves. In *Wave Dynamics and Radio Probing of the Ocean Surface*, O.M. Phillips and K. Hasselmann, Eds., Plenum Press, New York, pp. 321–334.

Banner, M.L., 1990a: The influence of wave breaking on the surface pressure distribution in wind–wave interactions. *J. Fluid Mech.*, **211**, 463–495.

Banner, M.L., 1990b: Equilibrium spectra of wind–waves. *J. Phys. Oceanogr.*, **20**, 966–984.

Banner, M.L. and W.K. Melville, 1976: On the separation of air–flow over water waves. *J. Fluid Mech.*, **77**, 825–842.

Banner, M.L. and O.M. Phillips, 1974: On the incipient breaking of small scale waves. *J. Fluid Mech.*, **65**, 647–656.

Banner, M.L. and E.H. Fooks, 1985: On the microwave reflectivity of small–scale breaking water waves. *Proc. R. Soc. Lond.*, A **399**, 93–109.

Banner, M.L., I.S.F. Jones, and J.C. Trinder, 1989: Wavenumber spectra of short gravity waves. *J. Fluid Mech.*, **198**, 321–344.

Barber, N.F., 1963: The directional resolving power of an array of wave recorders. In *Ocean Wave Spectra*, Englewood Cliffs, N.J., Prentice–Hall, Inc., pp. 137–150.

Barnett, T.P. and K.E. Kenyon, 1975: Recent advances in the study of wind–waves. *Rep. Prog. Phys.*, **38**, 667–729.

Bass, F.G., I.M. Fuks, A.E. Kalmykov, I.E. Ostrovsky, and A.D. Rosenberg, 1968: Very high frequency radiowave scattering by a disturbed sea surface. *IEEE Trans.*, **AP–16**, 554–568.

Battjes, J.A., T.J. Zitman, and L.H. Holthuijsen, 1987: A reanalysis of the spectra observed in JONSWAP. *J. Phys. Oceanogr.*, **17**, 1288–1295.

Beal, R.C,. P.S. DeLeonibus, and I. Katz, 1981: *Spaceborne Synthetic Aperture Radar for Oceanography*. Johns Hopkins Press, 215 pp.

Blanc, T.V., 1985: Variation of bulk–derived surface flux, stability, and surface roughness results due to the use of different transfer coefficient schemes. *J. Phys. Oceanogr.*, **15**, 650–669.

Blanc, T.V., 1987: Accuracy of bulk–method–determined flux, stability, and sea surface roughness. *J. Geophys. Res.*, **92**, 3867–3876.

Blanchard, D.C. and A.H. Woodcock, 1957: Bubble formation and modification in the sea and its meteorological significance. *Tellus*, **9**, 145–158.

Bortkovskii, R.S., 1987: *Air–Sea Exchange of Heat and Moisture during Storms*, D. Reidel Publ. Co., Dordrecht, The Netherlands, 194 pp.

Brigham, E.O., 1974: *The Fast Fourier Transform*, Prentice–Hall, Inc., Eaglewood Cliffs, N.J., 252 pp.

Brown, G.S., 1978: Backscattering from a gaussian–distributed perfectly conducting rough surface. *IEEE Trans.*, bf AP–26, 472–482.

Brown, R.A., 1980: Longitudinal instabilities and secondary flows in the planetary boundary layer: A review. *Rev. of Geophys. and Space Phys.*, **18**, 683–697.

Brown, R.A. and W.T. Liu, 1982: An operational large–scale marine planetary boundary layer model. *J. Appl. Meteorol.*, **21**, 261–269.

Brown, R.A., 1983: On a satellite scatterometer as an anemometer. SEASAT II. Scientific results. *J. Geophys. Res.*, **88**, 1663–1673.

Brown, R.A., 1986: On satellite scatterometer capabilities in air–sea interaction. *J. Geophys. Res.*, **91**, 2221–2232.

Bunker, A.F., 1976: Computations of surface energy flux and annual air–sea interaction cycles of the North Atlantic Ocean. *Mon. Wea. Rev.*, **104**, 1122–1140.

Busch, N.E., 1973: On the mechanics of atmospheric turbulence. In *Workshop on Micrometeorology*, D.A. Haugen, Eds., Am. Meteorol. Soc., Boston, Mass., pp. 1–65.

Businger, J.A., 1973: Turbulent transfer in the atmospheric surface layer. In *Workshop in Micrometeorology*, D.A. Haugen, Ed., Am. Meteorol. Soc., Boston, Mass., pp. 67–100.

Businger, J.A., J.C. Wyngaard, Y. Izumi, and E.F. Bradley, 1971: Flux–profile relationships in the atmospheric surface layer. *J. Atmos. Sci.*, **28**, 181–189.

Bye, J.A.T, 1967: The wave–drift current. *J. Mar. Res.*, **25**, 95–102.

Byrne, H.M., 1982: The variation of the drag coefficient in the marine surface layer due to temporal and spatial variations in the wind sea state. Ph.D. dissertation, Univ. of Wash., Seattle.

Cavaleri, L., J.A. Ewing, and N.D. Smith, 1978: Measurement of the pressure and velocity field below surface waves. In *Turbulent Fluxes Through the Sea Surface, Wave Dynamics, and Prediction*, A. Favre and K. Hasselmann, Eds., Plenum Press, New York, pp. 257–272.

Chang, M.S., 1969: Mass transport in deep–water long–crested random gravity waves. *J. Geophys. Res.*, **74**, 1515–1536.

Charnock, H., 1955: Wind stress on a water surface. *Q. J. R. Meteorol. Soc.*, **81**, 639–640.

Charnock, H., 1958: A note on empirical wind–wave formulae. *Q. J. R. Meteorol. Soc.*, **84**, 443–447.

Cooley, J.W. and M.T. Dolan, 1979: Fast Fourier transform subroutines. In *Programs for Digital Signal Processing*, IEEE press, pp 1.0.1–12.

Davidson, K.L., 1982: Preliminary results of drag coefficients measured during STREX. Manuscript, Presented at *The Annual Meeting, AGU*, San Francisco, CA, December, 1982.

Davies, J.T. and R.W. Vose, 1965: On the damping of capillary waves by surface films. *Proc. Roy. Soc.*, **286**, 218–234.

Davis, R.E. and L.A. Regier, 1977: Methods for estimating directional wave spectra from multi–element arays. *J. Mar. Res.*, **35**, 453–457.

Deardorff, J.W., 1967: Aerodynamic theory of wave growth with constant wave steepness. *J. Oceanogr. Soc. Japan*, **23**, 278–297.

Deardorff, J.W., 1968: Dependence of air–sea transfer coefficients on bulk stability. *J. Geophys. Res.*, **73**, 2549–2557.

Decosmo, J., 1991: Exchange of momentum, heat, and water vapor over whitecap sea states. Ph.D. dissertation, Univ. of Wash., Seattle, in preparation.

DeCosmo, J., K.B. Katsaros, and R.J. Lind, 1988: Surface layer measurements during HEXMAX by the University of Washington. In *Proceedings of the NATO Advanced Workshop, Humidity Exchange Over the Sea Main Experiment (HEXMAX), Analysis and Interpretation*, W.A. Oost, S.D. Smith, and K.B. KAtsarso, Eds., Dellenhove, Epe, The Netherlands, April 25–29, 1988, 29–39.

Dobson, F.W., 1971: Measurements of atmospheric pressure on wind–generated sea waves. *J. Fluid Mech.*, **48**, 91–127.

Dobson, F.W. and J.A. Elliott, 1978: Wave–pressure correlation measurements over growing sea waves with a wave follower and fixed–height pressure sensors. In *Turbulent Fluxes Through the Sea Surface, Wave Dynamics, and Prediction*, A. Favre and K. Hasselmann, Eds., Plenum Press, New York, pp. 421–432.

Donelan, M.A., 1978: Whitecaps and momentum transfer. In *Turbulent Fluxes Through the Sea Surface, Wave Dynamics, and Prediction*, A. Favre and K. Hasselmann, Eds., Plenum Press, New York, pp. 273–287.

Donelan, M.A., 1982: The dependence of the aerodynamic drag coefficient on wave parameters. In *First International Conference on Meteorology and Air–Sea Interaction of the Coastal Zone*, Am. Meteorol. Soc., Boston, Mass., pp. 381–387.

Donelan, M.A., 1990: Air–sea interaction. In *The Sea*, Vol. bf 9, B. LeMehaute and D. Hanes, Eds., Wiley–Interscience, N.Y., (in press).

Donelan, M.A. and W.J. Pierson, 1983: The sampling variability of estimates of spectra of wind–generated gravity waves. *J. Geophys. Res.*, **88**, 4381–4392.

Donelan, M.A. and W.J. Pierson, 1984: Does the scatterometer see wind speed or friction velocity? Proceedings of the International Union of Radio Scientists Meeting, May 14–23, Shoresh, Israel, N.A.S.A. *Conf. Publ.*, 2303.

Donelan, M.A. and W.J. Pierson, 1987: Radar scattering and equilibrium ranges in wind–generated waves with application to scatterometry. *J. Geophys. Res.*, **92**, 4971–5029.

Donelan, M.A., J. Hamilton, and W.H. Hui, 1985: Directional spectra of wind–generated waves. *Phil. Trans. R. Soc. Lond.*, A **315**, 509–562.

Dyer, A.J., 1974: A review of flux–profile relationships. *Bound. Layer Meteorol.*, **7**, 363–372.

Elliott, J.A., 1972: Microscale pressure fluctuations near waves being generated by the wind. *J. Fluid Mech.*, **54**, 427–448.

Ermakov, S.A., A.M. Zujkova, A.R. Panchenko, S.G. Salashin, T.G. Talipova, and V.I. Titov, 1986: Surface film effect on short wind waves. *Dyn. Atmos. Oceans*, **10**, 31–50.

Evans, D.D. and O.H. Shemdin, 1980: An investigation of the modulation of capillary and short gravity waves in the open ocean. *J. Geophys. Res.*, **85**, 5019–5024.

Fairall, C.W., J.B. Edson, and M.A. Miller, 1990: Heat fluxes, whitecaps, and sea spray. In *Surface Waves and Fluxes: Volume 1– Current Theory*, G.L. Geernaert and W.J. Plant, Eds., Kluwer Academic Press, Dordrecht, The Netherlands, pp. 173–208.

Forristal, G.Z., 1981: Measurements of a saturated range in ocean wave spectra. *J. Geophys. Res.*, **86**, 8075–8084.

Friehe, C.A. and K.F. Schmitt, 1976: Parameterization of air–sea interface fluxes of sensible heat and moisture by the bulk aerodynamic formulas. *J. Phys. Oceanogr.*, **6**, 801–809.

Garratt, J.R., 1975: Limitations of the eddy–correlation technique for the determination of turbulent fluxes near the surface. *Bound. Layer Meteorol.*, **8**, 255–259.

Garratt, J.R., 1977: Review of drag coefficients over oceans and continents. *Mon. Wea. Rev.*, **105**, 915–928.

Garratt, J.R. and P. Hyson, 1975: Vertical fluxes of momentum, sensible heat anf water vapour during the air mass transformation experiment (AMTEX) 1974. *J. Meteorol. Soc. Japan*, **53**, 149–160.

Garrett, C., and J. Smith, 1976: On the interaction between long and short surface wave. *J. Phys. Oceanogr.*, **6**, 925–930.

Garrett, J., 1970: Field observations of frequency domain statistics and nonlinear effects in wind–generated ocean waves. Thesis, Univ. of British Columbia, 196 pp.

Garrett, W.D., 1967: Damping of capillary waves at the air–sea interface by oceanic surface–active material. *J. Marine Res.*, **25**, 279–291.

Garrett, W.D., 1986; The physicochemical effects of organic films at the sea surface and their role in the interpretation of remotely sensed imagery. *ONRL Report on the Role of Surfactant Films on the Interface Properties of the Sea Surface*, F.L. Herr and J. Williams, Ed. Office of Naval Research, London, Rep. C–11–86, 11–17.

Geernaert, G.L., 1990: Bulk parameterizations for the wind stress and heat fluxes. In *Surface Waves and Fluxes: Volume 1– Current Theory*, G.L. Geernaert and W.J. Plant, Eds., Kluwer Academic Press, Dordrecht, The Netherlands, pp 91–172.

Geernaert, G.L. and K.B. Katsaros, 1986: Incorporation of stratification effects on the oceanic roughness length in the derivation of the neutral drag coefficient. *J. Phys. Oceanogr.*, **16**, 1580–1584.

Geernaert, G.L., K.B. Katsaros, and K. Richter, 1986: Variation of the drag coefficient and its dependence on sea state. *J. Geophys. Res.*, **91**, 7667–7679.

Geernaert, G.L., K.L. Davidson, S.E. Larsen, and T. Mikkelsen, 1988: Wind stress measurements during the Tower Ocean Wave and Radar Dependence Experiment. *J. Geophys. Res.*, **93**, 13913–13923.

Geernaert, G.L., S.E. Larsen, and F. Hansen, 1987: Measurements of the wind stress, heat flux, and turbulence intensity during storm conditions over the North Sea. *J. Geophys. Res.*, **92**, 13127–13139.

Gill, G.C., 1967: On the dynamic response of meteorological sensors and recorders. *Proc. First Canadian Conf. Micrometeorology, Part I*, Can. Dept. of Transport, Meteorol. Br., Toronto, 1–27.

Gill, G.C., 1975: Development and use of the UVW anemometer. *Bound. Layer Meteorol.*, **8**, 475–495.

Gloersen, P. and F.T. Barath, 1977: A scanning multichannel radiometer for Nimbus–G and SeaSat–A. *IEEE J. Ocean. Eng.*, Vol. **OE–2**, No. **2**, 172–178.

Gottifredi, J.C. and G.J. Jameson, 1968: The suppression of wind–generated waves by a surface film. *J. Fluid Mech.*, **32**, 609–618.

Gotwols, B.L. and G.B. Irani, 1980: Optical determination of the phase velocity of short gravity waves. *J. Geophys. Res.*, **85**, 3964–3970.

Graf, W.H., N. Merzi, and C. Perrinjaquet, 1984: Aerodynamic drag measured at a nearshore platform on Lake of Geneva. *Arch. Met. Geophys. Bioklim.*, **A33**, 151–173.

Grose, P.L., K.L. Warsh, and M. Garstang, 1972: Dispersion relations and wave shapes. *J. Geophys. Res.*, **77**, 3902–3906.

Hamilton, J., W.H. Hui, and M.A. Donelan, 1979: A statistical model for groupiness in wind waves. *J. Geophys. Res.*, **84**, 4875–4884.

Hansen, C., K.B. Katsaros, S.A. Kitaigorodskii, and S.E. Larsen, 1990: The dissipation range of wind–wave spectra observed on a lake. *J. Phys. Oceanogr.*, **20**, 1264–1277.

Hasse, L., 1971: The sea surface temperature deviation and the heat flow at the air–sea interface. *Bound. Layer Meteorol.*, **1**, 368–379.

Hasse, L., M. Grünewald, and D.E. Hasselmann, 1978a: Field observations of air flow above the waves. In *Turbulent Fluxes through the Sea Surface, Wave Dynamics and Prediction*, A. Favre and K. Hasselmann, Eds., Plenum Press, pp. 483–494.

Hasse, L., M. Grünewald, J. Wucknitz, M. Dunckel, and D. Schriever, 1978b: Profile derived turbulent fluxes in the surface layer under disturbed and undisturbed conditions during GATE. *Meteor–Forschungsergebnisse*, **13**, 24–40.

Hasselmann, D.E., M. Dunckel, and J.A. Ewing, 1980: Directional wave spectra observed during JONSWAP 1973. *J. Phys. Oceanogr.*, **10**, 1264–1280.

Hasselmann, D.E., J. Bösenberg, M. Dunckel, K. Richter, M. Grünewald, and H. Carlson, 1986: Measurements of wave induced pressure over surface gravity waves. in *Wave Dynamics and Radio Probing of the Ocean Surface*, edited by O.M. Phillips and K. Hasselmann, Plenum, New York, pp. 353–368.

Hasselmann, K., 1960: Grundgleichungen der Seegangsvorhersage. *Schiffstechnik*, **7**, 191–195.

Hasselmann, K., 1962: On the non–linear energy transfer in a gravity–wave spectrum. Part 1. General Theory. *J. Fluid Mech.*, **12**, 481–500.

Hasselmann, K., 1963a: On the non–linear energy transfer in a gravity–wave spectrum. Part 2. Conservation theorems; wave–particle analogy; irreversibility. *J. Fluid Mech.*, **15**, 273–281.

Hasselmann, K., 1963b: On the non–linear energy transfer in a gravity–wave spectrum. Part 3. Evaluation of the energy flux and swell–sea interaction for a Neumann spectrum. *J. Fluid Mech.*, **15**, 385–398.

Hasselmann, K., and W. Alpers, 1986: The response of synthetic aperture radar to ocean surface waves. In *Wave Dynamics and Radio Probing of the Ocean Surface*, O.M. Phillips and K. Hasselmann, Eds., Plenum Press, New York, pp. 393–402.

Hasselmann, K., T.P. Barnett, E. Bouws, H. Carlson, D.E. Cartwright, K. Enke, J.A. Ewing, H. Gienapp, D.E. Hasselmann, P. Kruseman, A. Meerburg, P. Müller, D.J. Olbers, K. Richter, W. Sell, and H. Walden, 1973: Measurements of wind–wave growth and swell decay during the North Sea Wave Project (JONSWAP). *Dtsch. Hydrogr. Z.*, **A8**, 95 pp.

Hasselmann, K., D.B. Ross, P. Müller, and W. Sell, 1976: A parametric wave prediction model. *J. Phys. Oceanogr.*, **6**, 200–228.

Hasselmann, S., and K. Hasselmann, 1985: Computations and parameterizations of the nonlinear energy transfer in a gravity–wave spectrum. Part 1: A new method for efficient computations of the exact nonlinear transfer integral. *J. Phys. Oceanogr.*, **15**, 1369–1377.

Hasselmann, S., K. Hasselmann, J.H. Allender, and T.P. Barret, 1985: Computations and parameterizations of the nonlinear energy transfer in a gravity–wave spectrum. Part 2: Parameterizations of the nonlinear energy transfer for application in wave models. *J. Phys. Oceanogr.*, **15**, 1378–1391.

Hasselmann, D., J. Bösenberg, M. Dunckel, K. Richter, M. Grünewald, and H. Carlson, 1986: Measurements of wave–induced pressure over surface gravity waves. In *Wave Dynamics and Radio Probing of the Ocean Surface*, O.M. Phillips and K. Hasselmann, Eds., Plenum Press, New York, pp. 353–368.

Hatori, M., 1984: Nonlinear properties of laboratory wind waves at energy contaning frequencies. Part 1. Probability density distribution of surface elevation. *J. Oceanogr. Soc. Japan*, **40**, 12–18.

Hicks, B.B., 1972: Propeller anemometers as sensors of atmospheric turbulence. *Bound. Layer Meteorol.*, **3**, 214–228.

Hino, M., S. Kataoka, and D. Kaneko, 1969: Experriment of surface film effect on wind–wave generation. *Coastal Engineering in Japan*, **12**, 1–8.

Hollinger, J., R. Lo, G. Poe, R. Savage, and J. Pierce, 1987: Special sensor microwave/imager user's guide. Report, Nav. Res. Lab., Washington, D.C.

Holmes, R.M., G.C. Gill, and H.W. Carson, 1964: A propeller–type vertical anemometer. *J. Appl. Meteorol.*, **3**, 802–804.

Hsiao, S.V., and O.H. Shemdin, 1983: Measurements of wind velocity and pressure with a wave follower during MARSEN, *J. Geophys. Res.*, **88**, 9841–9849.

Hsu, C.T., E.Y. Hsu, and R.L. Street, 1981: On the structure of turbulent flow over progressive water wave: Theory and experiment in a transformed, wave–following co–ordinate system. *J. Fluid Mech.*, **105**, 87–117.

Hsu, C.T., H.Y. Wu, E.Y. Hsu, and R.L. Street, 1982: Momentum and energy transfer in wind generation of waves. *J. Phys. Oceanogr.*, **12**, 929–951.

Hsu, H.P., 1970: *Fourier analysis*. R. Mehra, Ed., Simon and Schuster Tech Outlines, New York, 274 pp.

Hsu, S.A., 1974: A dynamic roughness equation and its application to wind stress determination at the air–sea interface. *J. Phys. Oceanogr.*, **4**, 116–120.

Hsu, S.A., 1986: A mechanism for the increase of wind stress (drag) coefficient with wind speed over water waves: A parametric model. *J. Phys. Oceanogr.*, **16**, 144–150.

Huang, N.E., 1979: On surface drift currents in the ocean. *J. Fluid Mech.*, **91**, 191–208.

Huang, N.E. and S.R. Long, 1980: An experimental study of the surface elevation, probability distribution, and statistics of wind generated waves. *J. Fluid Mech.*, **101**, 179–200.

Huang, N.E., S.R. Long, and L.F. Bliven, 1986b: An experimental study of the statistical properties of wind–generated gravity waves. In *Wave Dynamics and Radio Probing of the Ocean Surface*, O.M. Phillips and K. Hasselmann, Eds., Plenum Press, New York, pp. 129–144.

Huang, N.E., L.F. Bliven, S.R. Long, and P.S. DeLeonibus, 1986a: A study of the relationship among wind speed, sea state, and the drag coefficient for a developing wave field. *J. Geophys. Res.*, **91**, 7733–7742.

Huang, N.E., S.R. Long, C.C. Tung, Y. Yuen, and L.F. Bliven, 1981: A unified two–parameter wave spectral model for a general sea state. *J. Fluid Mech.*, **112**, 203–224.

Hui, W.H. and G. Tenti, 1982: A new approach to steady flows with free surfaces. *J. Appl. Math. Phys.*, **33**, 569–589.

Hui, W.H. and G. Tenti, 1985: Nonlinear water wave theory via pressure formulation. In *The Ocean Surface: Wave Breaking, Turbulent Mixing and Radio Probing*, Y.Toba and H. Mitsuyasu, Eds., D. Reidel Publishing Co., Dordrecht, Holland, pp. 17–24.

Hühnerfuss, H. and W.D. Garrett, 1981: Experimental sea slicks: Their practical applications and utilization for basic studies of air–sea interactions. *J. Geophys. Res.*, **86**, 439–447.

Hühnerfuss, H., P.A. Lange, and W. Walter, 1985a: Relaxation effects in monolayers and their contribution to water wave damping, I, Wave induced phase shifts. *J. Colloid Interface Sci.*, **108**, 430–441.

Hühnerfuss, H., P.A. Lange, and W. Walter, 1985b: Relaxation effects in monolayers and their contribution to water wave damping, II, The Marangoni phenomenon and gravity wave attenuation. *J. Colloid Interface Sci.*, **108**, 442–450.

Hühnerfuss, H., W. Walter, P.A. Lange, and W. Alpers, 1987: Attenuation of wind waves by monomolecular sea slicks and the Marangoni effect. *J. Geophys. Res.*, **92**, C4, 3961–3963.

Hühnerfuss, H., W. Alpers, W.D. Garrett, P.A. Lange, and S. Stolte, 1983: Attenuation of capillary and gravity waves at sea by monomolecular organic surface films. *J. Geophys. Res.*, **88**, C14, 9809—9816.

Hühnerfuss, H., W. Alpers, W.L. Jones, P.A. Lange, and K. Richter, 1981: The damping of ocean surface waves by a monomolecular film measured by wave staffs and microwave radars. *J. Geophys. Res.*, **86**, C1, 429–438.

Irani, G.B., B.L. Gotwols, and A.W. Bjerkaas, 1986: The 1978 Ocean Wave Dynamics Experiment, Optical and in situ measurement of the phase velocity of wind waves. In *Wave Dynamics and Radio Probing of the Ocean Surface*, O.M. Phillips and K. Hasselmann, Eds., Plenum Press, New York, pp. 165–179.

Janssen, P.A.E.M., 1989: Wave–induced stress and the drag of air flow over sea waves. *J. Phys. Oceanogr.*, **19**, 745–754.

Jähne, B., and K.S. Riemer, 1990: Two–dimensional wave number spectra of small–scale water surface waves. *J. Geophys. Res.*, **95**, 11531–11546.

Jones, I.S.F. and B.C. Kenney, 1977: The scaling of velocity fluctuations in the surface mixed layer. *J. Geophys. Res.*, **82**, 1392–1396.

Kahma, K.K., 1981: A study of the growth of the wave spectrum with fetch. *J. Phys. Oceanogr.*, **11**, 1503–1515.

Kahma, K.K. and M.A. Donelan, 1988: A laboratory study of the minimum wind speed for wind wave generation. *J. Fluid Mech.*, **192**, 339–364.

Kaimal, J.C., J.C. Wyngaard, Y. Izumi, and O.R. Coté, 1972: Spectral characteristics of surface layer turbulence. *Quart. J. Roy. Meteorol. Soc.*, **98**, 563–589.

Kusaba, T. and A. Masuda, 1988: The roughness height and drag law over the water surface based on the hypothesis of local equilibrium. *J. Oceangr. Soc. Jap.*, **44**, 200–214.

Katsaros, K.B., 1977: The sea surface temperature deviation at very low wind speeds; is there a limit? *Tellus*, **29**, 229–239.

Katsaros, K.B., H. Gucinski, S.S. Ataktürk, and R. Pincus, 1989: Effects of reduced surface tension on short waves at low wind speeds in a fresh water

lake. In *Radar Scattering from Modulated Wind Waves*, G.J. Komen and W.A. Oost, Eds., Kluwer Academic Publishers, Norwell, MA, pp. 61–74.

Kawai, S., 1979: Generation of initial wavelets by instability of a coupled shear flow and their evolution to wind waves. *J. Fluid Mech.*, **93**, 661–703.

Kawai, S., K. Okuda, and Y. Toba, 1977: Field data support of three–seconds power law and $gu_*\sigma^{-4}$ spectral form for growing wind waves. *J. Oceanogr. Soc. Japan*, **33**, 137–150.

Keller, W.C. and J.W. Wright, 1975: Microwave scattering and the straining of wind–generated waves. *Radio Sci.*, **10**, 139–147.

Keller, W.C., W.J. Plant, and G.R. Valenzuela, 1986: Observation of breaking ocean waves with coherent microwave radar. In *Wave Dynamics and Radio Probing of the Ocean Surface*, O.M. Phillips and K. Hasselmann, Eds., Plenum Press, New York, pp. 285–294.

Keller, W.C., W.J. Plant, and D.E. Weissman, 1985: The dependence of X–band microwave sea return on atmospheric stability and sea state. *J. Geophys. Res.*, **90**, 1019–1029.

Kenyon, K.E., 1969: Stokes drift for random gravity waves. *J. Geophys. Res.*, **74**, 6991–6994.

Keulegan, G.H., 1951: Wind tides in small closed channels. *J. Res., Nat. Bur. Stand.*, **46**, 358–381.

Kinsman, B., 1965: *Wind Waves: Their Generation and Propagation on the Ocean Surface.* Dover Publications edition, 1984, N.Y., 676 pp.

Kitaigorodskii, S.A., 1968: On the calculation of the aerodynamic roughness of the sea surface. *Izv. Acad. Sci. USSR, Atmos. Ocean. Phys.*, 4, No. 8.

Kitaigorodskii, S.A., 1973: *The Physics of Air–Sea Interaction.* Translated from Russian by A. Baruch, Israel Programs for Scientific Translations, Jerusalem, 237 pp.

Kitaigorodskii, S.A., 1983: On the theory of the equilibrium range in the spectrum of wind–generated gravity waves. *J. Phys. Oceanogr.*, **13**, 816–827.

Kitaigorodskii, S.A. and Y.A. Volkov, 1965: On the roughness parameter of the sea surface and the calculation of the momentum flux in the near water layer of the atmosphere. *Izv. Atmos. Ocean Phys.*, **1**, 973–988.

Kitaigorodskii, S.A., O.A. Kuznetsov, and G.N. Panin, 1973: Coefficients of drag, sensible heat, and evaporation in the atmosphere over the surface of the sea. *Izv. Acad. Sci. USSR, Atmos. Ocean. Phys.*, Engl. Transl., **9**, 644–647.

Kitaigorodskii, S.A., V.P. Krasitskii, and M.M. Zaslavskii, 1975: On Phillips' theory of equilibrium range in the spectra of wind–generated gravity waves. J. Phys. Oceanogr., **5**, 410–420.

Komen, G.J., 1980: Nonlinear contributions to the frequency spectrum of wind–generated water waves. *J. Phys. Oceanogr.*, **10**, 779–790.

Komen, G.J., S. Hasselmann, and K. Hasselmann, 1984: On the existence of a fully developed wind–sea spectrum. *J. Phys. Oceanogr.*, **14**, 1271–1285.

Kondo, J., 1975: Air–sea bulk transfer coefficients in diabatic conditions. *Bound. Layer Meteorol.*, **9**, 91–112.

Kondo, J., Y. Fujinawa, and G. Naito, 1973: High–frequency components of ocean waves and their relation to the aerodynamic roughness. *J. Phys. Oceanogr.*, **3**, 197–202.

Lake, B.M. and H.C. Yuen, 1978: A new model for nonlinear wind waves. Part I. Physical model and experimental evidence. *J. Fluid Mech.*, **88**, 33–62.

Lamb, H., 1932: *Hydrodynamics*, 6th ed., Cambridge University Press, New York, 738 pp.

Lange, P. and H. Hühnerfuss, 1978: Drift response of monomolecular slicks to wave and wind action. *J. Phys. Oceanogr.*, **8**, 142–150.

Large, W.G. and S. Pond, 1981: Open ocean momentum flux measurements in moderate to strong winds. *J. Phys. Oceanogr.*, **11**, 324–336.

Large, W.G. and S. Pond, 1982: Sensible and latent heat flux measurements over the ocean. *J. Phys. Oceanogr.*, **12**, 464–482.

Larson, T.R., and J.W.right, 1975: Wind–generated gravity–capillary waves: Laboratory measurements of temporal growth rates using microwave backscatter. *J. Fluid Mech.*, **70**, 417–436.

Leykin, I.A. and A.D. Rozenberg, 1984: Sea–tower measurements of wind–wave spectra in the Caspian Sea. *J. Phys. Oceanofgr.*, **14**, 168–176.

Lighthill, J., 1978: *Waves in Fluids.* Cambridge University Press, Cambridge, 504 pp.

Liu, H.T. and J.T. Lin, 1979: Effects of oil slick on wind waves. *Proc. Oil Spill Conf.*, Los Angeles, CA, 665–674.

Liu, H.T., K.B. Katsaros, and M.A. Weissman, 1982: Dynamic response of thin–wire wave gauges. *J. Geophys. Res.*, **87**, 5686–5698.

Liu, P.C., 1989: On the slope of the equilibrium range in the frequency spectrum of wind waves. *J. Geophys. Res.*, **94**, 5017–5023.

Liu, W.T., K.B. Katsaros, and J.A. Businger, 1979: Bulk parameterizations of air–sea exchanges of heat and water vapor including the molecular constraints at the interface. *J. Atmos. Sci.*, **36**, 1722–1735.

Lobemeier, P., 1978: Entwicklung eines Seegangsmeßsystem zur Untersuchung des kurzwelligen Seegangs. *FWG–Ber.* 1978–3, Forschungsanst. der Bundeswehr für Wasserschall– und Geophys., Kiel, Fed. Rep. of Germany.

Lombardini, P.P., B. Fiscella, P. Trivero, C. Cappa, and W.D. Garrett, 1989: Modulation of the spectra of short gravity waves by sea surface films: slick detection and characterization with a microwave probe. *J. Atmos. Ocean. Tech.*, **6**, 882–890.

Long, R.B., 1980: The statistical evaluation of directional spectrum estimates derived from pitch/roll buoy data. *J. Phys. Oceanogr.*, **10**, 944–952.

Long, R.B. and K. Hasselmann, 1979: A variational technique for extracting directional spectra from multi–component wave data. *J. Phys. Oceanogr.*, **9**, 373–381.

Longuet–Higgins, M.S., 1962: The statistical geometry of random surfaces. In *Hydrodynamic Instability.* AMS, Providence, R.I., pp. 105–144.

Longuet–Higgins, M.S., 1963: The generation of capillary waves by steep gravity waves. *J. Fluid Mech.*, **16**, 138–159.

Longuet–Higgins, M.S., 1969a: On wave breaking and the equilibrium spectrum of wind–generated waves. *Proc. Roy. Soc.*, A **310**, 151–159.

Longuet–Higgins, M.S., 1969b: A non–linear mechanism for the generation of sea waves. *Proc. Roy. Soc.*, A **311**, 371–389.

Longuet–Higgins, M.S., 1978a: Some new relations between Stokes's coefficients in the theory of gravity waves. *J. Inst. Maths. Applics.*, **22**, 261–273.

Longuet–Higgins, M.S., 1978b: The instabilities of gravity waves of finite amplitude in deep water. Part I. Superharmonics. *Proc. Roy. Soc.*, A **360**, 471–488.

Longuet–Higgins, M.S., 1980: On the distribution of the heights of sea waves: Some effects of nonlinearity and finite bandwidth. *J. Geophys. Res.*, **88**, 1519–1523.

Longuet–Higgins, M.S., 1985a: A new way to calculate steep gravity waves. In *The Ocean Surface: Wave Breaking, Turbulent Mixing and Radio Probing*, Y.Toba and H. Mitsuyasu, Eds., D. Reidel Publishing Co., Dordrecht, Holland, pp. 1–15.

Longuet–Higgins, M.S., 1985b: Accelerations in steep gravity waves. *J. Phys. Oceanogr.*, **15**, 1570–1579.

Longuet–Higgins, M.S. and E.D. Cokelet, 1978: The deformation of steep surface waves on water II. *Proc. R. Soc. Lond.*, A **364**, 1–28.

Longuet–Higgins, M.S. and R.W. Stewart, 1960: Changes in the form of short gravity waves on long waves and tidal currents. *J. Fluid Mech.*, **8**, 565–583.

Longuet–Higgins, M.S., D.E. Cartwright, and N.D. Smith, 1963: Observations of the directional spectrum of sea waves using the motions of a floating buoy. In *Ocean Wave Spectra*, Englewood Cliffs, N.J., Prentice–Hall, Inc., pp. 111–136.

Lucassen–Reynders, E.H. and J. Lucassen, 1969: Properties of capillary waves. *Adv. Colloid Interface Sci.*, **2**, 347–395.

Lucassen, J., 1981: Effect of surface–active material on the damping of gravity waves: A Reappraisal. *J. Colloid Interface Sci.*, **85**, 52–58.

Maat, N., C. Kraan, and W.A. Oost, 1990: The roughness of wind waves. 31 pp. (Unpublished manuscript.)

Miche, M., 1951: Action of the swell. *Ann. Ponts Chaussees*, **121**, 285–319.

Monahan, E.C. and G.M. Niocaill, 1986: *Oceanic Whitecaps*, Eds. E.C. Monahan and G. Mac Niocaill, D. Reidel Publishing Company, 294 pp.

Monahan, E.C., C.W. Fairall, K.L. Davidson, and P.J. Boyle, 1983: Observed inter–relation between 10–m winds, ocean whitecaps and marine aerosols. *Quart. J. Roy. Meteorol. Soc.*, **109**, 379–392.

Monin, A.S. and A.M. Obukhov, 1954: Basic laws of turbulent mixing in the ground layer of the atmosphere. *Tr. Acad. Nauk SSSR Geofiz., Inst.*, **151**, 163–187.

Monin, A.S. and A.M. Yaglom, 1971: *Statistical Fluid Mechanics, Mechanics of Turbulence: Volume 1*. The MIT Press, 769 pp.

Masagutov, T.F., 1981: Calculation of vertical turbulent fluxes in the near–water layer of the ocean in tropical latitudes. *Meteorol. Gidrol*, **12**, In Russian, 61–68. (Also, Naval Intelligence Support Center, Translation No. 7084, Washington, DC.)

Masuda, A. and T. Kusaba, 1987: On the local equilibrium of winds and wind–waves in relation to surface drag. *J. Oceangr. Soc. Jap.*, **43**, 28–36.

McBean, G.A., 1971: The variations of the statistics of wind, temperature and humidity fluctuations with stability. *Bound. Layer Meteorol.*, **1**, 438–457.

McBean, G.A., 1972: Instrument requirements fo eddy correlation measurements. *J. Appl. Meteorol.*, **11**, 1078–1084.

McLean, J.W., 1982: Instabilities of finite amplitude water waves. *J. Fluid Mech.*, **114**, 315–330.

McLeish, W. and G.E. Putland, 1975: Measurements of wind–driven flow profiles in the top milimeter of water. *J. Phys. Oceanogr.*, **5**, 516–518.

McLeish, W., D. Ross, R.A. Schuchman, P.G. Teleki, S.V. Hsiao, O.H. Shemdin, and W.E. Brown, Jr., 1980: Synthetic aperture radar imaging of ocean surface waves: comparison with wave measurements. *J. Geophys. Res.*, **85**, 5003–5011.

McNamee, B.P., B.B. Sharp, and L.K. Stevens, 1983: Measurement of water particle velocities in waves. *Appl. Ocean Res.*, **5**, No. 1, 49–53.

Melville, W.K., 1982: The instability and breaking of deep–water waves. *J. Fluid Mech.*, **115**, 165–185.

Melville, W.K., 1983: Wave modulation and breakdown. *J. Fluid Mech.*, **128**, 489–506.

Melville, W.K., R.J. Rapp, and E. Chan, 1985: Wave breaking, turbulence and mixing. In *The Ocean Surface: Wave Breaking, Turbulent Mixing and Radio Probing*, Y.Toba and H. Mitsuyasu, Eds., D. Reidel Publishing Co., Dordrecht, Holland, pp. 413–418.

Merzi, N. and W.H. Graf, 1988: Wind stress over water waves: Field experiments on Lake of Geneva. *Meteorol. Atmos. Phys.*, **39**, 14–24.

Miles, J.W., 1957: On the generation of surface waves by shear flows. *J. Fluid Mech.*, **3**, 185–204.

Mitsuyasu, H., 1968: On the growth of the spectrum of wind–generated waves. 1. *Rep. Res. Inst. Appl. Mech.*, **16**, 459–465.

Mitsuyasu, H., 1969: On the growth of the spectrum of wind–generated waves. 2. *Rep. Res. Inst. Appl. Mech.*, **17**, 235–243.

Mitsuyasu, H., 1985: A note on the momentum transfer from wind to waves. *J. Geophys. Res.*, **90**, 3343–3345.

Mitsuyasu, H., and T. Honda, 1982: Wind–induced growth of water waves. *J. Fluid Mech.*, **123**, 425–442.

Mitsuyasu, H., Y.Y. Kuo, and A. Masuda, 1979: On the dispersion relation of random gravity waves. Part 2. An experiment. *J. Fluid Mech.*, **92**, 731–749.

Mitsuyasu, H., F. Tasai, T. Suhara, S. Mizuno, M. Ohkuso, T. Honda, and K. Rikiishi, 1975: Observations of the directional spectrum of ocean waves using a cloverleaf buoy. *J. Phys. Oceanogr.*, **5**, 750–760.

Mitsuyasu, H., F. Tasai, T. Suhara, S. Mizuno, M. Ohkuso, T. Honda, and K. Rikiishi, 1980: Observation of the power spectrum of ocean waves using a cloverleaf buoy. *J. Phys. Oceanogr.*, **10**, 286–296.

Miyake, M., R.W. Stewart, and R.W. Burling, 1970: Spectra and cospectra of turbulence over water. *Quart. J. Roy. Meteor. Soc.*, **96**, 138–143.

Monin, A.S. and A.M. Yaglom, 1971: *Statistical Fluid Mechanics: Mechanics of Turbulence*. The MIT Press, 769 pp.

O'Brien, J.J. *et al*, 1982: *Scientific Opportunities Using Satellite Wind Stress Measurements over the Ocean.* Report of the Satellite Surface Stress Working Group, N.A.S.A., Nova Univ./N.Y.I.T. Press, Fort Lauderdale, Florida, 153 pp.

Obukhov, A.M., 1946: Turbulence in an atmosphere with a non–uniform temperature. *Tr. Akad. Nauk SSSR Inst. Teoret. Geofiz.*, **1** (Trans. in *Bound. Layer Meteorol.*, **2**, 7–29).

Okuda, K., 1982: Internal flow structure of short wind waves, Part I. On the internal vorticity structure. *J. Oceanogr. Soc. Jap.*, **38**, 28–42.

Okuda, K., S. Kawai, and Y. Toba, 1977: Measurement of skin friction distribution along the surface of wind waves. *J. Oceanogr. Soc. Jap.*, **33**, 190–198.

Ó Muircheartaigh, I.G. and E.C. Monahan, 1986: Statistical aspects of the relationship between oceanic whitecap coverage, wind speed and other environmental factors. In *Oceanic Whitecaps*, Eds. E.C. Monahan and G. Mac Niocaill, D. Reidel Publishing Company, pp. 125–128.

Pawka, S.S., S.V. Hsiao, O.H. Shemdin, and D.L. Inman, 1980: Comparisons between wave directional spectra from SAR and pressure sensor arrays. *J. Geophys. Res.*, **85**, 4987–4995.

Panofsky, H.A. and J.A. Dutton, 1984: *Atmospheric Turbulence: Models and Methods for Engineering Applications.* Wiley, 397 pp.

Paulson, C.A., 1970: The mathematical representation of wind speed and temperature profiles in the unstable atmospheric surface layer. *J. Appl. Meteorol.*, **9**, 857–861.

Phillips, O.M., 1957: On the generation of waves by turbulent wind. *J. Fluid Mech.*, **2**, 417–495.

Phillips, O.M., 1958: The equilibrium range in the spectrum of wind–generated ocean waves. *J. Fluid Mech.*, **24**, 426–434.

Phillips, O.M., 1977: *The Dynamics of the Upper Ocean.* Cambridge University Press, 336 pp.

Phillips, O.M., 1981a: Wave interactions – the evolution of an idea. *J. Fluid Mech.*, **106**, 215–227.

Phillips, O.M., 1981b: The dispersion of short wavelets in the presence of a dominant long wave. *J. Fluid Mech.*, **107**, 465–485.

Phillips, O.M., 1981c: The structure of short gravity waves on the ocean surface. In *Spaceborne Synthetic Aperture Radar for Oceanography*, Beal, DeLeonibus, and Katz, Eds., Johns Hopkins Press, pp. 24–31.

Phillips, O.M., 1985: Spectral and statistical properties of the equilibrium range in wind–generated gravity waves. *J. Fluid Mech.*, **156**, 505–531.

Phillips, O.M., 1988: Radar returns from the sea surface – Bragg scattering and breaking waves. *J. Phys. Oceanogr.*, **18**, 1065–1074.

Phillips, O.M. and M.L. Banner, 1974: Wave breaking in the presence of wind drift and swell. *J. Fluid Mech.*, **66**, 625–640.

Pierson, W.J., 1983: Highlights of the SEASAT–SASS program: A review. In *Satellite Microwave Remote Sensing*, T.D. Allan, Ed., John Wiley & Sons, NY, pp. 69–86.

Pierson, W.J. and L. Moskowitz, 1964: A proposed spectral form for fully developed wind seas based on the similarity theory of S.A. Kitaigorodskii. *J. Geophys. Res.*, **69**, 5181–5190.

Plant, W.J., 1988: The modulation transfer function: concept and applications. In *Radar Scattering from Modulated Wind Waves*, G.J. Komen and W.A. Oost, Eds., Kluwer Academic Publishers, Norwell, MA, pp. 155–174.

Plant, W.J., 1990: Bragg scattering of electromagnetic waves from the air/sea interface. In *Surface Waves and Fluxes: Volume 2–Remote Sensing*, G.L. Geernaert and W.J. Plant, Eds., Kluwer Academic Press, Dordrecht, The Netherlands, pp. 41–108.

Plant, W.J. and J.W. Wright, 1977: Growth and equilibrium of short gravity waves in a wind–wave tank. *J. Fluid Mech.*, **82**, 767–793.

Plant, W.J. and J.W. Wright, 1980: Phase speeds of upwind and downwind traveling short gravity waves. *J. Geophys. Res.*, **85**, 3304–3310.

Plant, W.J., W.C. Keller, and A. Cross, 1983: Parametric dependence of ocean wave–radar modulation transfer function. *J. Geophys. Res.*, **88**, 9747–9756.

Rabiner, L.R. and B. Gold, 1975: *Theory and Application of Digital Signal Processing.* Prentice–Hall, Inc., Englewood Cliffs, N.J.

Ramamonjiarisoa, A., S. Baldy, and I. Choi, 1978: Laboratory studies on wind–wave generation, amplification, and evolution. In *Turbulent Fluxes through the Sea Surface, Wave Dynamics and Prediction*, A. Favre and K. Hasselmann, Eds., Plenum Press, pp. 403–420.

Reece, A.M., 1978: Modulation of short waves by long waves. *Bound. Layer Meteorol.*, **13**, 203–214.

Reisbig, R.L., D.J. Alofs, R.C. Shah, and S.K. Banerjee, 1973: Measurement of oil spill drift caused by the coupled parallel effects of winds and waves. *Mém. Soc. Roy. Sci. Liège*, **6**, 67–77.

Richter, K. and W. Rosenthal, 1986: Energy distribution of waves above 1 Hz on long wind waves. In *Wave Dynamics and Radio Probing of the Ocean Surface*, O.M. Phillips and K.Hasselmann, Eds., Plenum Press, New York, pp. 75–93.

Rice, S.O., 1951: Reflection of electromagnetic waves from slightly rough surfaces. *Comm. Pure Appl. Math.*, 4, 351–378.

Russell, R.C.H. and J.D.C. Osorio, 1958: An experimental investigation of drift profiles in a closed channel. *Proc. of the Sixth Conference on Coastal Engineering, Council on Wave Research*, Univ. of California, Berkeley, 171–183.

Sano, Y. and Y. Mitsuta, 1968: Dynamic response of the hygrometer using fine thermocouple psychrometer. *Spec. Contr. Geophys. Inst., Kyoto Univ.*, **8**, 61–70.

Schlichting, H., 1968: *Boundary Layer Theory.* 6th ed., McGraw–Hill, N.Y., 747 pp.

Scott, J.C., 1972: The influence of surface–active contamination on the initiation of wind waves. *J. Fluid Mech.*, **56**, 591–606.

Scott, J.C., 1978: The historical development of theories of wave-calming using oil. *History of Technology*, **3**, 163–186.

Scott, J.C., 1979: *Oil on Troubled Waters: A Bibliography on the Effects of Surface-Active Films on Surface Wave Motions.* Multi-Science Publ. Co, Ltd., London, UK, 82 pp.

Scott, J.C., 1986: The effect of organic films on water surface motions. In *Oceanic Whitecaps*, Eds. E.C. Monahan and G. Mac Niocaill, D. Reidel Publishing Company, pp. 159–165.

Shaw, W.J. and J.E. Tillman, 1980: The effect of and correction for different wet–bulb and dry–bulb response in thermocouple psychrometry. *J. Appl. Meteorol.*, **19**, 90–97.

Shemdin, O.H., 1972: Wind–generated current and phase speed of wind waves. *J. Phys. Oceanogr.*, **2**, 411–419.

Shemdin, O.H., H.M. Tran, and S.C. Wu, 1988: Directional measurements of short ocean waves with stereophotography. *J. Geophys. Res.*, **93**, 13891–13901.

Sinitsyn, Y.A., I.A. Leykin, and A.D. Rozenberg, 1973: The space–time characteristics of ripple in the presence of long waves. *Izv. Acad. Sci. USSR, Atmos. Ocean. Phys.*, Engl. Transl., **9**, 511–519.

Smith, J.A., 1986: Short surface waves with growth and dissipation. *J. Geophys. Res.*, **91**, 2616–2632.

Smith J.A., 1990: Modulation of short wind waves by long waves. In *Surface Waves and Fluxes: Volume 1- Current Theory*, G.L. Geernaert and W.J. Plant, Eds., Kluwer Academic Press, Dordrecht, The Netherlands, pp 247–284.

Smith, S.D., 1980: Wind stress and heat flux over the ocean in gale force winds. *J. Phys. Oceanogr.*, **10**, 709–726.

Smith, S.D., 1988: Coefficients for sea surface wind stress, heat flux, and wind profiles as a function of wind speed and temperature. *J. Geophys. Res.*, **93**, 15467–15472.

Smith, S.D., 1989: Water vapor flux at the sea surface. *Bound. Layer Meteorol.*, **47**, 277–293.

Smith, S.D., K.B. Katsaros, and W.A. Oost, 1983: HEXOS – Humidity exchange over the sea: Scientific plan. Can. Tech. Report on Hydrog. and Ocean Sciences, No. 21, Bedford Inst. Oceanogr., P.O. Box 1006, Dartmouth, Nova Scotia.

Snyder, R.L. and R.M. Kennedy, 1983: On the formation of whitecaps by a threshold mechanism. Part I: Basic formalism. *J. Phys. Oceanogr.*, **13**, 1482–1492.

Snyder, R.L., F.W. Dobson, J.A. Elliott, and R.B. Long, 1981: Array measurements of atmospheric pressure fluctuations above surface gravity waves. *J. Fluid Mech.*, **102**, 1-59.

Starr, V.P., 1945: Water transport of surface waves. *J. Meteorol.*, **2**, 129–131.

Stewart, R.H., 1974: The air–sea momentum exchange. *Bound. Layer Meteorol.*, **6**, 151–167.

Stewart, R.H. and J.W. Joy, 1974: HF radio measurements of surface currents. *Deep Sea Res.*, **21**, 1039–1049.

Stewart, R.W., 1961: The wave drag of wind over water. *J. Fluid Mech.*, **10**, 189–194.

Stolte, S., 1984: Modulation of short waves by long wind waves and wind. Ph.D. dissertation, Univ. of Hamburg, 199 pp.

Stolte, S., 1989: Short wave modulation and breaking, experimental results. wind speeds in a fresh water lake. In *Radar Scattering from Modulated Wind Waves*, G.J. Komen and W.A. Oost, Eds., Kluwer Academic Publishers, Norwell, MA, pp. 201–210.

Stokes, G.G., 1847: On the theory of oscillatory waves. *Trans. Camb. Phil. Soc.*, **8**, 441–455. (Also in *Mathematical and Physical Papers*, Vol. I., Cambridge University Press, London, pp. 197–229.)

Stokes, G.G., 1880: Supplement to a paper on the theory of oscillatory waves. In *Mathematical and Physical Papers*, Vol. I., Cambridge University Press, London, pp. 314–326.

Su, M.Y. and A.W. Green, 1986: Experimental studies of strong nonlinear interactions of deep–water gravity waves. In *Wave Dynamics and Radio Probing of the Ocean Surface*, O.M. Phillips and K.Hasselmann, Eds., Plenum Press, New York, pp. 231–253.

Su, M.Y., M. Bergin, P. Marler, and T. Myrick, 1982: Experiments on nonlinear instabilities and evolution of steep gravity wave trains. *J. Fluid Mech.*, **124**, 45–72.

Sverdrup, H.U., M.W. Johnson, and R.H. Flemming, 1942: *The Oceans, Their Physics, Chemistry, and General Biology*. Englewood Cliffs, Prentice–Hall, Inc., N.J., 1087 pp.

Tayfun, M.A., 1980: Narrow band nonlinear sea waves. *J. Geophys. res.*, **85**, 1548–1552.

Tennekes, H. and J.L. Lumley, 1972: *A First Course in Turbulence*. The MIT Press, 300 pp.

Thorpe, S.A., 1982: On the clouds of bubbles formed by breaking wind–waves in deep water, and their role in air–sea gas transfer. *Phil. Trans. R. Soc. Lond.*, A **304**, 155–210.

Toba, Y., 1973: Local balance in the air–sea boundary processes. III. On the spectrum of wind waves. *J. Oceanogr. Soc. Japan*, **29**, 209–220.

Toba, Y., 1979: Study on wind waves as a strongly nonlinear phenomenon. *Twelfth Symp. on Naval Hydrodynamics*, Natl. Acad. of Sci., Washington, DC, 529–540.

Toba, Y. anf M. Koga, 1986: A parameter describing overall conditions of wave breaking, whitecapping, sea–spray production and wind stress. In *Occeanic Whitecaps*, E.C. Monahan and G. Mac Niocaill, Eds., D. Reidel, 37–47.

Toba, Y., K. Okada, and I.S.F. Jones, 1988: The response of wind–wave spectra to changing winds. Part I: Increasing winds. *J. Phys. Oceanogr.*, **18**, 1231–1240.

Toba, Y., N. Ebuchi, 1990: Multiple regimes in wave–dependent wind stress: A working hypothesis. Manuscript, Presented at *The Robert W. Stewart Symp.*, Victoria, B.C., 25–26 May, 1990, 16 pp.

Toba, Y., N. Iida, H. Kawamura, N. Ebuchi, and I.S.F. Jones, 1990: Wave dependence of sea–surface wind stress. *J. Phys. Oceanogr.*, **20**, 705–721.

Trizna, D.B., R.W. Bogle, J.C. Moore, and C.M. Howe, 1980: Observation by H.F. radar of the Phillips resonance mechanism for generation of wind waves. *J. Geophys. Res.*, **85**, 4946–4956.

Tsahalis, D.T., 1979: Theoretical and experimental study of wind– and wave–induced drift. *J. Phys. Oceanogr.*, **9**, 1243–1257.

Tsukamoto, O., 1986: Dynamic response of the fine wire psychrometer for direct measurement of water vapor flux. *J. Atmos. Ocean. Tech.*, **3**, 453–461.

Tyler, G.L., C.C. Teague, R.H. Stewart, A.M. Peterson, W.H. Munk, and J.W. Joy, 1974: Wave directional spoectra from synthetic aperture observatations of radio scatter. *Deep Sea Res.*, **21**, 986–1016.

Ulaby, F.T., R.K. Moore, and A.K. fung, 1981: *Microwave Remote Sensing, Active and Passive, Vol I.* Addison–Wesley Publ. Co., Reading, Mass., 456 pp.

Unlüata, Ü. and C.C. Mei, 1970: Mass transport in water waves. *J. Geophys. Res.*, **75**, 7611–7618.

Valenzuela, G.R., 1976: The growth of gravity–capillary waves in a coupled shear flow. *J. Fluid Mech.*, **76**, 229–250.

van Dorn, W.G., 1953: Wind stress on an artificial pond. *J. Mar. res.*, **12**, 249–276.

van Gastel, K., P.A.E. Janssen, and G.J. Komen, 1985: On phase velocity and growth rate of wind induced gravity–capillary waves. *J. Fluid Mech.*, **161**, 199–216.

Walsh, E.J., D.W. Hancock III, D.E. Hines, R.N. Swift, and J.F. Scott, 1989: An observation of the directional wave spectrum evolution from shoreline to fully developed. *J. Phys. Oceanogr.*, **19**, 670–690.

Weissman, M.A., S.S. Ataktürk, and K.B. Katsaros, 1984: Detection of breaking events in a wind–generated wave field. *J. Phys. Oceanogr*, **14**, 1608–1619.

Weseley, M.L., G.W. Thurtell, and C.B. Tanner, 1970: Eddy correlation measurements of sensible heat flux near the earth's surface. *J. Appl. Meteorol.*, **9**, 45–50.

Willebrandt, J., 1975: Energy transport in a nonlinear and inhomogeneous random gravity wave field. *J. Fluid Mech.*, **70**, 113–126.

Wisler, M.M. and J.P. Hollinger, 1977: *Estimation of marine environmental parameters using microwave radiometric remote sensing systems.* NRL memo report, 3661.

Wright, J.W., 1968: A new model for sea clutter. *IEEE Trans.*,, **AP–16**, 217–223.

Wright, J.W., 1978: Detection of ocean waves by microwave radar; the modulation of short gravity–capillary waves. *Bound. Layer Meteorol.*, **13**, 87–105.

Wright, J.W., W.J. Plant, W.C. Keller, and W.L. Jones, 1980: Ocean wave radar modulation transfer functions from the West Coast Experiment. *J. Geophys. Res.*, **85**, 4957–4966.

Wu, J., 1975: Wind–induced drift currents. *J. Fluid Mech.*, **68**, 49–70.

Wu, J., 1980: Wind stress coefficients over the sea surface near neutral conditions – A revisit. *J. Phys. Oceanogr.*, **10**, 727–740.

Wu, J., 1983: Sea–surface drift curents induced by wind and waves. *J. Phys. Oceanogr.*, **13**, 1441–1451.

Wu, J., 1984: Viscous sublayer below a wind–disturbed water surface. *J. Phys. Oceanogr.*, **14**, 138–144.

Wu, J., 1988: On nondimensional correlation between roughness length and wind–friction velocity.*J. Oceanogr. Soc. Jap.*, **44**, 254–260.

Wu, J., 1989: Suppression of oceanic ripples by surfactant–spectral effects deduced from sun–glitter,wave–staff and microwave measurements, *J. Phys. Oceanogr.*, **19**, 238–245.

Wyngaard, J.C., 1973: On surface–layer turbulence. In *Workshop on Micrometeorology*, D.A. Haugen, Eds., Am. Meteorol. Soc., Boston, Mass., pp. 101–149.

Wyngaard, J.C., O.R. Coté, and Y. Izumi, 1971: Local free convection, similarity, and the budgets of sheer stress and heat flux. *J. Atmos. Sci.*, **28**, 1171–1182.

Yefimov, V.V., Y.P. Solov'yev, and G.N. Khristoforov, 1972: Observational determination of the phase velocities of spectral components of wind waves. *Izv. Acad. Sci. USSR, Atmos. Ocean. Phys.*, Engl. Transl., **8**, 435–446.

Yefimov, V.V. and Y.P. Solov'yev, 1979: Dispersion relation and frequency angular spectra of wind waves. *Izv. Acad. Sci. USSR, Atmos. Ocean. Phys.*, Engl. Transl., **15**, 818–825.

Yermakov, S.A., A.R. Panchenko, T.G. Talipova, 1986: Damping of high–frequency wind waves by artificial surfactant films. *Izv. Atmos. Oceanic Phys.*, **21**, 54–58.

Zakharov, V.E. and N.N. Filonenko, 1966: The energy spectrum for random surface waves. *Dokl. Acad. Sci., USSR*, **170**, 1291–1295.

Zakharov, V.E. and M.M. Zaslavskii, 1982: The kinetic equation and Kolmogorov spectra in the weak turbulence theory of wind waves. *Izv. Atmos. Ocean. Phys.*, **18**, 747–753.

Zakharov, V.E. and M.M. Zaslavskii, 1983: Shape of the spectrum of energy–carying components of a water surface in the weak turbulence theory of wind waves. *Izv. Atmos. Ocean. Phys.*, **19**, 207–212.

Zhang, S.F., 1988: A critical evaluation of the von Karman constant from a new atmospheric surface layer experiment. Ph.D. dissertation, Univ. of Wash., Seattle.

Zhang, S.F., S.P. Oncley, and J.A. Businger, 1988: A critical evaluation of the von Karman constant from a new atmospheric surface layer experiment. Preprints, *Eigth Symposium on Turbulence and Diffusion*, April 26–29, 1988, San Diego, CA. Am. Meteorol. Soc., Boston, MA, 148–150.

VITA

Serhad Sabri Ataktürk, son of Ali Rıza and Hediye Ataktürk, was born in [redacted], on [redacted]. After attending public schools in his home town, he graduated from Edirne High School in June, 1970. He received a B.S. degree in Physics from the Middle East Technical University, Ankara, Turkey, in April, 1978. Then, he attended the newly established department of Marine Sciences of the same university in Içel. During the next two years, he was involved in numerous scientific cruises and was a member of the scuba diving team. Receiving a M.S. degree in Physical Oceanography in July, 1980, he became one of the early graduates of the department. In 1980, he started his studies at the department of Atmospheric Sciences, the University of Washington, Seattle, Washington, which he had visited in 1979 with the financial support from NATO, to attend a course on air–sea interaction. In his first year, he was supported by a NATO Grant for Visiting Scholar. He earned his second M.S. degree in Atmospheric Sciences in June, 1984. During the past decade, he participated in numerous field experiments on air–sea interaction and acoustic and electromagnetic backscatter from the water surface conducted at the MS–MAST facility at Lake Washington and the research platforms in the North Sea (Forschungsplatform Nordsee, Federal Republic of Germany, 1985; the HEXMAX experiment, Meetpost Noordwijk, The Netherlands, 1986).

He is married to Jane J. Hunter since 1984 and is the happy father of Kyle Erhan and Katelyn Rahşan, 3 years and 8 months old, respectively.

PUBLICATIONS:

Ataktürk, S.S., 1980: Atmospheric variability and air–sea interactions in the northern margins of Cilician Basin. M.S. thesis, Middle East Technical University, Marine Sciences, Içel, Turkey, 84 pp.

Weissman, M.A., S.S. Ataktürk, and K.B. Katsaros, 1984: Detection of breaking events in a wind–generated wave field. *J. Phys. Oceanogr*, **14**, 1608–1619.

Ataktürk, S.S., 1984: Intrinsic frequency spectra of small scale wave amplitude measured in a lake. M.Sc. thesis, Univ. of Wash., Seattle, 96 pp.

Ataktürk, S.S. and K B. Katsaros, 1987: Intrinsic frequency spectra of short gravity–capillary waves obtained from temporal measurements of wave height on a lake. *J. Geophys. Res.*, **92**, 5131–5141.

Ataktürk, S.S. and K.B. Katsaros, 1989: The K–Gill: A twin propeller–vane anemometer for measurements of atmospheric turbulence. *J. Atmos. Ocean. Tech.*, **6**, 509–515.

Katsaros, K.B., H. Gucinski, S.S. Ataktürk, and R. Pincus, 1989: Effects of reduced surface tension on short waves at low wind speeds in a fresh water lake. In *Radar Scattering from Modulated Wind Waves*, G.J. Komen and W.A. Oost, Eds., Kluwer Academic Publishers, Norwell, MA, pp. 61–74.